8-18-2016 12:00 AM

Insights into Chibby's structural elements and their interplay in Wnt signaling protein-protein interactions

Ryan C Killoran
The University of Western Ontario

Supervisor
Dr. James (Wing-Yiu) Choy
The University of Western Ontario

Graduate Program in Biochemistry
A thesis submitted in partial fulfillment of the requirements for the degree in Doctor of Philosophy

Abstract

The Wnt/β-catenin signaling pathway is critical to embryonic development and adult tissue homeostasis. Mutations to Wnt signaling components can cause dysregulation of the pathway, leading to various human diseases such as cancer. The partially disordered protein Chibby (Cby) is a conserved nuclear protein that acts as an antagonist in the Wnt/β-catenin signaling pathway. Cby's antagonism is accomplished via two mechanisms. First, by competing with the Tcf/Lef family of transcription factors, Cby abrogates the β-catenin-mediated transcription of Wnt signaling genes. Moreover, upon phosphorylation on serine 20 by the kinase Akt, Cby forms a complex with the protein 14-3-3 to facilitate the nuclear export of β-catenin. Structurally, Cby is composed of an unstructured N-terminal half, while its C-terminal half harbours a coiled-coil domain. Cby's N-terminal half comprises a 14-3-3 binding motif, while its C-terminal half mediates the interaction with β-catenin, as well as TC-1, an antagonist of Cby. In this thesis, the molecular details of Cby's structural elements and its interactions with the Wnt signaling components 14-3-3, β-catenin and TC-1 were investigated. The Cby/14-3-3 interaction was studied by using a combined approach of nuclear magnetic resonance (NMR) spectroscopy, isothermal titration calorimetry (ITC) and X-ray crystallography. While the solved crystal structure revealed a canonical 14-3-3 binding mode, NMR spectroscopy and ITC revealed that residues flanking Cby's 14-3-3 binding motif are involved in the interaction. Next, hydrogen-deuterium exchange mass spectrometry revealed that in addition to Cby's disordered N-terminus, Cby contains a disordered C-terminal extension. ITC and NMR experiments demonstrate that the disordered N-terminus negatively regulates target binding between TC-1 and Cby's coiled-coil domain. Lastly, mutagenesis studies suggest that Cby's coiled-coil domain utilizes differing binding modes when interacting with β-catenin and TC-1, with Cby binding as a monomer to β-catenin and as a dimer to TC-1. In conclusion, this thesis demonstrates how Cby's structural

elements collectively mediate protein-protein interactions in the Wnt signaling pathway.

Keywords

Chibby; 14-3-3; β-catenin; TC-1; Wnt signaling pathway; coiled-coil; protein-protein interactions; phosphorylation; X-ray crystallography; NMR spectroscopy; isothermal titration calorimetry; circular dichroism spectroscopy

Co-Authorship Statement

Chapter 1 - Figure 1.1 is adapted from Clevers H, Nusse R (2012) Cell 149: 1192-1205. Figure 1.7 is adapted from Gall C, Xu H, Brickenden A, Ai X, Choy WY (2007) Protein Science 16: 2510-2518.

Chapter 2 - This chapter contains an expanded version of the published manuscript Ryan C. Killoran, Jingsong Fan, Daiwen Yang, Brian H. Shilton and Wing-Yiu Choy Plos One 10(4): e0123934. J. Fan and D. Yang collected NMR data required for NMR backbone assignment data on 14-3-3ΔC12 construct. B.H. Shilton performed X-ray crystallography data collection and assisted with solving the 14-3-3/Chibby crystal structure. Cα distance matrices used to calculate distance-based RMSDs in Figure 2.4 were generated by W.Y. Choy. Susanna George assisted with protein purifications and isothermal titration calorimetry experiments involving all 14-3-3 isoforms. All other experiments, ITC, NMR backbone assignment and titrations were conducted and analyzed by R.C. Killoran. Manuscript was written by R.C. Killoran, B.H. Shilton and W.Y. Choy.

Chapter 3 - This chapter contains an expanded version of the published manuscript Ryan C. Killoran, Modupeola A. Sowole, Mohammad A. Halim, Lars Konermann and Wing-Yiu Choy Protein Science. doi:10.1002/pro.2936 (ahead of print). M. A. Sowole performed hydrogen-deuterium exchange mass spectrometry (HDX-MS) experiments, analyzed the HDX-MS data and designed Figure 3.1 and Figure 3.2. M.A. Halim performed preliminary HDX-MS experiments on Chibby. R.C. Killoran performed all other experiments involving

circular dichroism and NMR spectroscopy and their analysis. The initial manuscript was written by R.C. Killoran, followed by revisions from L. Konermann and W.Y. Choy.

Chapter 4 - Figure 4.1 is adapted from Mokhtarzada S, Yu C, Brickenden A, Choy WY (2011) Biochemistry 50: 715-726. Cameron Harper assisted in the mutagenesis of the C-Cby L84A/L98A construct and helped develop the purification protocol of this mutant. All circular dichroism and NMR spectroscopy experiments were performed and analyzed by R.C. Killoran.

Dedication

For my parents, Liane and Calvin Killoran,

and in memory of my grandparents, Annette and Leo Lauzon.

Acknowledgments

I would like to thank my supervisor, Dr. James Wing-Yiu Choy, for his support and insight throughout my studies. I feel very fortunate to have started in the Choy lab as a summer student during my undergraduate degree in 2010 and have continually enjoyed working under Dr. Choy's supervision.

To my advisory committee, Dr. Gary Shaw and Dr. Brian Shilton, thank you for your guidance and constructive suggestions.

Thanks to members of the Choy lab, past and present, for your thoughtful discussions. Special thanks to our lab technician, Anne Brickenden, for going above and beyond everyday to help us grad students.

I would like to thank Lee-Ann Briere for teaching and advising me on several biophysical techniques. To members of the department, past and present, thanks for making my time here so enjoyable.

To my partner Chelsea and to my parents, thanks for the love and support throughout this journey.

Table of Contents

List of Tables

List of Figures

List of Abbreviations

AANAT	Serotonin-N-acetyltransferase
Akt/PKB	Protein Kinase B
APC	Adenomatous polyposis coli
β-TrCP	F box/WD-repeat β-transducin repeat-containing protein
C-Cby	C-terminal Cby (residues 67-126)
Cby	Chibby
CD	Circular Dichroism
CEP164	Centrosomal protein of 164 kDa
CHOP	C/EBP homologous protein
CK1	Casein kinase Ia
Coil-Cby	Coiled-coil domain of Cby (residues 67-104)
CRM-1	Chromosome Region Maintenance-1
CtBP	C-terminal binding protein
DSS	2,2-dimethyl-2-sila-pentane-5-sulfonic acid
DTT	Dithiothreitol
Dvl	Dishevelled
FAP	Familial adenomatous polyposis
FoxM1	Forkhead box M1
Fz	Frizzled
GM130	Golgi matrix 130
GSK3β	Glycogen synthase kinase 3β
HDAC	Histone deacetylase
HDX-MS	Hydrogen-deuterium exchange mass spectrometry
HSQC	Heteronuclear Single Quantum Coherence
ICAT	Inhibitor of β-catenin and Tcf4
IPTG	Isopropyl-β-D-Thiogalactopyranoside
ITC	Isothermal titration calorimetry
JNK2	c-Jun N-terminal kinase 2
LRP 5/6	Low-density lipoprotein receptor-related protein 5/6

MBP	Maltose Binding Protein
N-Cby	N-terminal Cby (residues 1-63)
NBPF1	Neuroblastoma breakpoint family member 1
NES	Nuclear export signal
NLS	Nuclear localization signal
NMR	Nuclear magnetic resonance
NOESY	Nuclear Overhauser effect spectroscopy
Par-4	Prostate apoptosis response factor 4
PCP	Planar cell polarity pathway
PDB	Protein Data Bank
TC-1	Thyroid cancer-1
Tcf/Lef	T cell factors/ lymphoid enhancer factor
TEV	Tobacco etch virus
TROSY	Transverse Relaxation Optimized Spectroscopy

Ala (A)	Alanine
Arg (R)	Arginine
Asn (N)	Asparagine
Asp (D)	Aspartic Acid
Cys (C)	Cysteine
Gln (Q)	Glutamine
Glu (E)	Glutamic Acid
Gly (G)	Glycine
His (H)	Histidine
Ile (I)	Isoleucine
Leu (L)	Leucine
Lys (K)	Lysine
Met (M)	Methionine
Phe (F)	Phenylalanine
Pro (P)	Proline
Ser (S)	Serine
Thr (T)	Threonine
Trp (W)	Tryptophan
Tyr (Y)	Tyrosine
Val (V)	Valine
pS/pT	phosphoserine / phosphothreonine

Chapter 1

1 Introduction

1.1 Introduction to Wnt Signaling

Signaling pathways are critical systems utilized across animal life to coordinate cell-to-cell communication and regulate cellular functions. A cell's ability to recognize and respond to signaling molecules in the extracellular environment is crucial for development, tissue repair, immunity and homeostasis. Strict regulation of these pathways is critical, as errors from signal transduction can lead to developmental defects or disease.

The Wnt signaling proteins are involved in multiple developmental events in embryogenesis including body axis patterning and cell proliferation, and have been implicated in stem-cell control and adult cell homeostasis [1,2,3]. The Wnt proteins are part of a family of growth factors that are associated with three downstream pathways: the Wnt/β-catenin pathway, the Wnt/Ca^{2+} pathway (reviewed in [4]) and the planar cell polarity pathway (PCP) [5]. Each pathway has its own set of specific genes that are targeted upon stimulation [6,7]. Over the past three decades, the most heavily focused Wnt pathway in this field of study has been the β-catenin-dependent Wnt signaling pathway, also referred to as canonical Wnt signaling. Here, the transcriptional co-activator β-catenin is a downstream component of the pathway, responsible for the activation of the pathway's target genes [8].

A simplified view of canonical Wnt signaling is illustrated in Figure 1.1 A. In unstimulated conditions (-Wnt signal), cytoplasmic β-catenin exists as part of a large

protein complex, commonly referred to as the destruction complex, which contains the scaffolding proteins adenomatous polyposis coli (APC) and Axin [2,9]. β-catenin is phosphorylated on Ser/Thr residues on its N-terminus by serine/threonine kinases glycogen synthase kinase 3β (GSK3β) and casein kinase Iα (CK1) [10]. Phosphorylated β-catenin is subsequently recognized by the F box/WD-repeat β-transducin repeat-containing protein (β-TrCP) and targeted for ubiquitin-dependent degradation by the proteasome [11]. Through this mechanism, cytoplasmic β-catenin levels are kept low, preventing this protein from entering the nucleus. In the nucleus, the T-cell factor (Tcf) / Lymphoid enhancing factor (Lef) transcription factors, necessary for the expression of Wnt-specific target genes, interact with the transcriptional repressors Groucho, histone deacetylase (HDAC) and C-terminal binding protein (CtBP) [12,13].

In the activated Wnt pathway, the Wnt proteins interact with the family of frizzled (Fz) receptors, which are members of the G-protein coupled receptor family, and the low-density lipoprotein receptor-related protein 5/6 (LRP5/6) receptors [14]. The activated receptors lead to the stabilization and accumulation of β-catenin in the cytosol. β-catenin that is free from the destruction complex is able to translocate to the nucleus where it binds to the Tcf/Lef transcription factors to activate Wnt signaling genes [15,16,17].

A defined cellular mechanism by which β-catenin is stabilized has continually been developed and refined over the past two decades. In a commonly presented model, the activated receptor complex promotes the recruitment of the cytoplasmic phosphoprotein Dishevelled (Dvl), a known interactor of Axin. Dvl mediates the formation of LRP5/6 Wnt signalosomes through its multimerization [18], as well as

promotes the CK1 phosphorylation of the cytoplasmic domains of LRP5/6. Dvl and the phosphorylated LRP5/6 collectively recruit Axin to the membrane [19]. The sequestration of Axin to the cell membrane effectively dissolves the destruction complex, leading to the stabilization of β-catenin.

The collection of studies that have jointly developed models to describe β-catenin's stabilization have generally used over-expression strategies to study the destruction complex. A recent study, conducted by Li *et al*. [20], which looked at the endogenous complex, proposed a different model. This study suggests that β-catenin is not released from the destruction complex upon Wnt signaling. Instead, Wnt signaling suppresses β-catenin's ubiquitination by promoting the dissociation of β-TrCP, causing the destruction complex to be saturated with phosphorylated β-catenin at the membrane. At this point, any newly synthesized, non-phosphorylated β-catenin is free to translocate to the nucleus and activate Wnt target genes. This new model is illustrated for comparison in Figure 1.1 B.

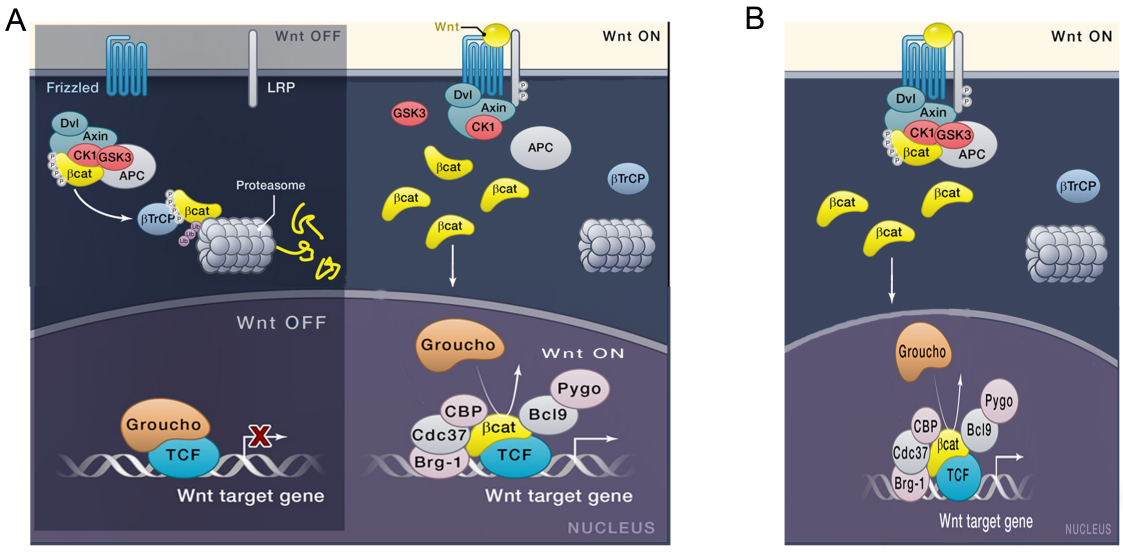

Figure 1.1 Wnt signaling models

A. A simplified model of the Wnt/β-catenin signaling pathway. In the absence of a Wnt signal, the destruction complex is intact and β-catenin is targeted for ubiquitination by β-TrCP, followed by degradation by the proteasome. Upon activation, Axin is recruited to the membrane, leading to the dissolution of the destruction complex. Stabilized β-catenin can then translocate to the nucleus and activate Wnt target genes. **B.** A new Wnt/β-catenin signaling model based on a study looking at endogenous destruction complex proteins [20]. Wnt activation recruits the intact destruction complex to the membrane and blocks the ubiquitination of β-catenin. Any newly synthesized β-catenin proceeds to activate target genes. Figure was adapted from figures generated by Clevers and Nusse [3].

1.2 Wnt/β-catenin signaling in human disease and therapeutic development

Mutations to proteins involved in Wnt signaling that lead to aberrant activation of the pathway are frequently observed in human cancers. Germline mutations in the APC gene lead to a hereditary cancer syndrome called familial adenomatous polyposis (FAP) [21,22]. These patients carry heterozygous APC mutations, with the second allele frequently lost in individual cells during adulthood, leading to colon adenomas (polyps) [23]. Global-exome sequencing projects have shown that the majority of colorectal cancers carry inactivating APC mutations [24]. The loss of APC function causes stabilization of cytosolic β-catenin, where it can then constitutively interact with Tcf/Lef. In some rare cases of colorectal cancer where no APC mutations exist, Axin2 is mutated [25], or activating point mutations to the regulatory Ser/Thr residues of β-catenin's N-terminus are discovered [26].

Mutations to Wnt pathway components are not limited to colorectal cancers. For example, oncogenic β-catenin mutations have been observed in hepatocellular carcinomas, melanoma, Wilms tumour and liver, endometrial ovarian and prostate cancers (reviewed in [27]). Outside of cancer, the Wnt signaling pathway has been linked to type II diabetes, with the identification of specific single nucleotide polymorphisms (SNPs) to the Wnt proteins WNT5B [28], and WNT10B [29] as well as TCF7L2 [30]. Moreover, aberrant Wnt signaling has been implicated in bone-density syndromes [31] as well as in Alzheimer's disease [32].

With an expanding association to various human diseases, modulation or disruption of Wnt signaling through the discovery of small molecules has received extensive research efforts [33]. Presently, the frizzled and LRP receptors that bind to Wnt proteins have proven to be difficult to target pharmacologically as no effective small-molecule inhibitors currently exist. However, the development of a biologic agent, a humanized antibody to the frizzled receptor named Vantictumab, has entered several clinical trials (https://clinicaltrials.gov/ct2/results?term=omp18R5&Search=Search). Small molecule screening for Wnt signaling modulators has yielded some success when targeting upstream components. For instance, Axin stability is regulated by its poly-ADP ribosylation, a process catalyzed by the enzyme tankyrase [34]. Inhibition of tankyrase by molecules like IWR [35] and XAV939 [34] lead to elevated Axin levels which then destabilizes β-catenin. Next, small-molecule inhibitors of the enzyme Porcupine represent one of the most specific Wnt signaling disruptors discovered to date [35]. Porcupine mediates the attachment of palmitoleate, a 16-carbon monounsaturated fatty acid, to the Wnt proteins [36]. Wnt proteins that lack lipids are not secreted and as such, inactive Porcupine cannot produce active Wnt proteins. A compound named IWP2 [35] has been shown to inactivate Porcupine with high selectivity and has been effectively used in cell culture experiments to knock down Wnt signaling [37].

The most attractive drug target of canonical Wnt signaling is the Tcf/Lef and β-catenin complex as it operates downstream of the pathway. However, disruption of the β-catenin/Tcf or Lef complex may have undesired consequences; outside of Wnt signaling, β-catenin is a central component of adhesion junctions. Here, β-catenin links cadherins at the plasma membrane to α-catenin [38,39]. As Tcfs and Lefs share a common binding

site with E-cadherin [40], inhibitors that dislodge the β-catenin/Tcf or Lef complex may disrupt cell adhesions as well.

Dislodging the β-catenin/Tcf or Lef complex by small molecules is a significant challenge, as the binding interface between these transcription factors and β-catenin extends over a large surface of β-catenin (Tcf, for example, buries over ~ 4800 Å of surface area [41]). While a few compounds have been suggested to disrupt complex formation, such as 2,4-diamino-quinazolines [42] or the molecules PKF115-854 and CGP049090 (screened by Lepourcelet *et al*. [43]), their specificity and efficacy have not been reported.

1.3 Regulation of β-catenin in Wnt signaling

Multiple regulatory strategies employed by the cell focus on various stages of the Wnt pathway; from the cell membrane to the nucleus. Not surprisingly, β-catenin is a focal point. Many proteins are found to direct its subcellular localization or impede its transcription of target genes. First, several regulatory mechanisms are in place to control the nuclear import and export of β-catenin. For instance, the forkhead box M1 (FoxM1) transcription factor, whose cellular levels are elevated by Wnt induction, efficiently promotes the nuclear localization of β-catenin (which it interacts directly with) through its functional nuclear localization signal (NLS) [44]. Another example comes from the work of Wu *et al*. [45], which demonstrated that the activation of Rac1/JNK2 is fundamental to the Wnt-mediated nuclear localization of β-catenin. This study reveals that Wnt stimulation increases Rac1 activation, followed by JNK2 activation. JNK2 then phosphorylates β-catenin on residues Ser191 and Ser605, which promotes β-catenin's

nuclear localization. Last, in addition to playing roles in the destruction complex, both Axin and APC harbour a NLS and NES (nuclear export signal), enabling them to shuttle in and out of the nucleus along with bound β-catenin [46,47,48].

Several proteins that antagonize the β-catenin/Tcf or Lef complex as a means of modulating Wnt signaling have been reported. These proteins include inhibitor of β-catenin and Tcf4 (ICAT) [49], the chromatin remodeling enzymes HDAC1 and HDAC2 [50], the transcriptional repressor Kaiso [51] and the cell cycle regulator p15RS [52]. Interestingly, the protein Chibby (Cby), first reported for its role in Wnt signaling by Takemaru *et al*. [53], represses β-catenin-mediated expression of Wnt target genes by the two mechanisms discussed above; it competes with the Tcf/Lef transcription factors for binding to β-catenin [53], and regulates β-catenin's nuclear translocation in conjunction with the 14-3-3 proteins [54,55].

1.4 The Wnt signaling antagonist Chibby

Cby is a 126-residue, 14.5 kDa protein that is evolutionarily conserved from human to fly (Figure 1.2). Structurally, the protein's N-terminal half (residues 1-63) is intrinsically disordered [56] while its C-terminal half (residues 64-126) harbors a coiled-coil domain that promotes the protein's dimerization [56,57]. The two structural halves of Cby work together to perform Cby's function as an antagonist to the Wnt pathway. First, pulldown assays have demonstrated that Cby's C-terminal half alone is sufficient for binding to β-catenin [53]. Meanwhile, Cby phosphorylation at residue serine 20 by the kinase Akt promotes Cby's interaction with the scaffolding protein 14-3-3 [54]. This

Figure 1.2 Cby Multiple Sequence Alignment

Multiple sequence alignment of Cby from human, mouse (*Mus musculus*), bovine (*Bos Taurus*), frog (*Xenopus tropicalis*), zebrafish (*Danio rerio*) and fly (*Drosophila melanogaster*). Alignment was generated using T-Coffee [58] and figure was made using BoxShade. Sequence features are labeled.

Cby/14-3-3 interaction promotes the nuclear exclusion of β-catenin and thus represses the transcriptional coactivator's activity [54,55].

A study by Li *et al*. [55] demonstrated that Cby actively shuttles between the nucleus and cytoplasm via its NLS and NES. Cby's NLS is found at its very C-terminus (residues 123-126) and mediates binding with isoforms of the importin-α family, which are nuclear transport proteins. Cby's NES is found within its N-terminal half (residues 21-29) and interacts with nuclear export transporter chromosomal maintenance 1 (CRM1). Cby's nuclear-cytoplasmic shuttling affects the subcellular distribution and signaling activity of β-catenin; immunofluorescence microscopy experiments [55] reveal that deletion of Cby's NLS leads to cytoplasmic sequestration of β-catenin while loss-of-function mutations to Cby's NES lead to nuclear retention of β-catenin. TOPFLASH assays (a Tcf/Lef reporter kit used to measure Wnt signaling activity in cultured cells) were used to demonstrate that mutations to Cby's NLS effectively repressed β-catenin signaling by trapping β-catenin in the cytoplasm. Conversely, mutations to the NES caused Cby to have markedly reduced ability to antagonize β-catenin signaling, presumably due to their failure in translocating β-catenin to the cytoplasm.

The protein 14-3-3 stimulates the cytoplasmic sequestration of both Cby and β-catenin through an unclear mechanism. However, the study by Li *et al*. [55] provides some evidence that the 14-3-3/Cby interaction promotes Cby's binding to CRM1 in the nucleus and inhibits Cby's interaction with importin-α in the cytoplasm. 14-3-3 may accomplish repressed β-catenin mediated signaling if it promotes Cby's export from the nucleus and prevents its import while Cby is in a β-catenin bound state.

Cby itself is regulated by a small protein named thyroid cancer 1 (TC-1) [59]. TC-1 binds to Cby in competition with β-catenin, effectively abrogating Cby's antagonism. Downstream gene analysis by Jung *et al*. [59] showed that TC-1 up-regulates β-catenin target genes such as LAMC2, MMP-7, MMP-14, c-Met, c-Myc and cyclin D1.

Cby's function in the Wnt pathway suggests that it may be a tumour suppressor gene. However, very few studies have linked Cby to cancer. Some studies have shown that Cby is downregulated in colon carcinoma [60] and pediatric ependymomas [61] cell lines. Xu *et al*. [62] showed that Cby is highly downregulated in laryngeal squamous cell carcinoma (LSCC) tissues, however, no correlation between Cby expression and pathological features of LSCC were observed.

An overview of Cby's nucleo-cytoplasmic transport and its role in Wnt signaling is displayed in Figure 1.3 below. Cby plays a crucial role in the Wnt/β-catenin pathway, yet the understanding of the structural mechanisms it utilizes to interact with its binding targets is still in need of investigation. The following sections will explore the known structural information on Cby and its Wnt signaling binding partners β-catenin, 14-3-3 and TC-1.

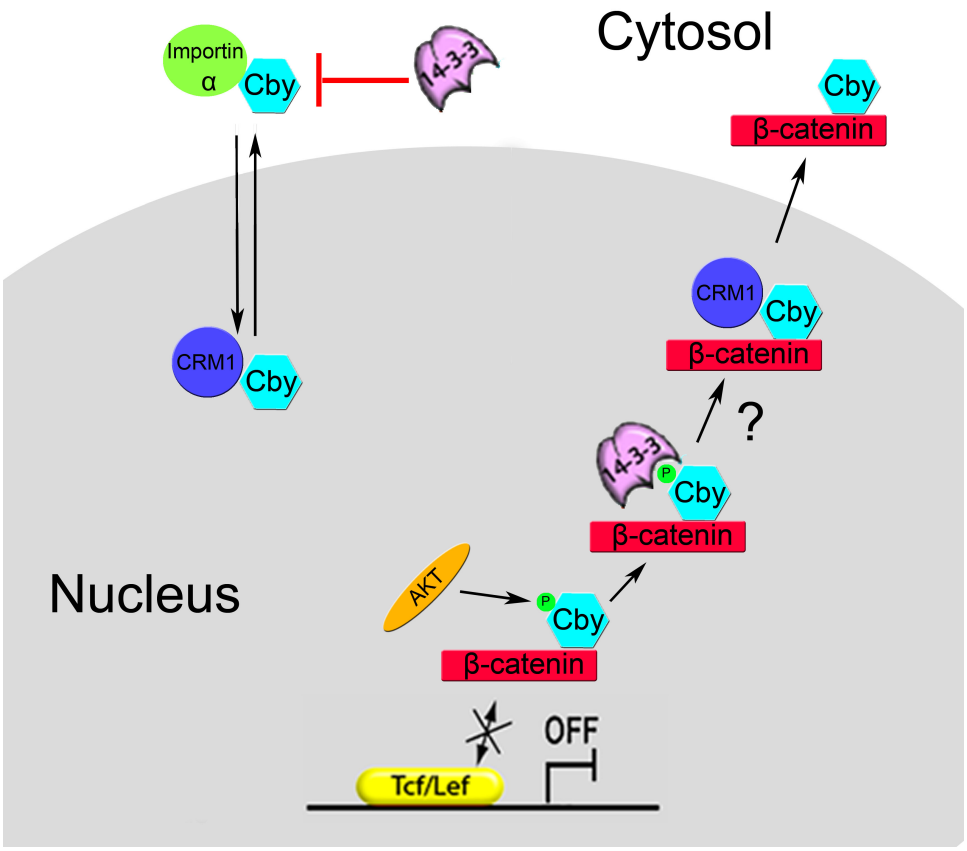

Figure 1.3 Cby in Wnt Signaling

Cby's nucleo-cytoplasmic shuttling is mediated by the transport proteins importin-α and CRM1. In Wnt signaling, Cby directly competes with the Tcf/Lef transcription factors for binding to β-catenin. The protein TC-1 alleviates this antagonism. Upon phosphorylation by Akt, Cby interacts with 14-3-3. CRM1 then translocates Cby and bound β-catenin out of the nucleus.

1.5 Structural features and characterization of Cby

Circular dichroism (CD) and NMR spectroscopies demonstrate that Cby's N-terminal half (residues 1-64) is intrinsically disordered [56]. Disordered regions within proteins exist as an ensemble of structures, allowing them to form specific, but commonly low-affinity interactions with their targets [63]. Their plasticity makes them well suited in signaling pathways, as the need for reversible binding and interaction with multiple partners is often necessary [64]. Cby's N-terminus comprises the protein's 14-3-3 and CRM1 binding motifs [54,55].

Analysis of Cby's sequence across species revealed the presence of a conserved coiled-coil motif along its C-terminal half [53]. Coiled-coils are common structural motifs, and typically consist of 2-5 α-helices wrapped around each other into a supercoil structure [65]. The simple structural design of coiled-coils makes them versatile folding motifs. They enable proteins to self-oligomerize, hetero-dimerize with compatible coiled-coil domains on other proteins, or mediate interactions with proteins and DNA [66]. Additionally, depending on their function, a coiled-coil may be highly thermostable, or may require volatility for dynamic folding or binding processes [66]. Coiled-coils are stabilized by the effective burial of hydrophobic side chains in the core of the supercoil. These motifs consist of a heptad repeat that follows a pattern of hydrophobic and charged/polar amino acids.

A classic example of a coiled-coil motif is the basic-region leucine zipper [67]. They are found in many transcription factors, including c-fos and c-jun [68,69]. The

zipper mediates dimerization of these transcription factors, which is necessary for them to bind to their DNA binding elements. Heptad repeats are commonly illustrated with helical wheel representations. The seven positions of each repeat are commonly labeled *a, b, c, d, e, f, g* with positions a and d being hydrophobic residues and e and g predominantly charged/polar [70]. The leucine zippers are so named as leucines are predominantly found at position *d* of their heptad repeats.

The first evidence of Cby's self-association came from a yeast-two-hybrid experiment that used Cby as bait and ultimately pulled itself out [71]. Gel filtration and cross-linking experiments by Mofunanya *et al*. [57] demonstrated that Cby exists predominantly as a homodimer. The coiled-coil domain of human Cby is displayed in helical wheel format with four consecutive heptad repeats (residues 73-100) in Figure 1.4. Within the heptad repeats of the coiled-coil, there are four conserved leucines (L77, L84, L91 and L98) at position *d* in the helical wheel. Additionally, the coiled-coil contains two conserved asparagines (N81 and N88), which are buried in the hydrophobic core (position *a*). For dimeric coiled-coils, asparagine is commonly found at this position to promote parallel assembly of the coiled-coil. The parallel assembly is the result of self-complementary hydrogen bonding of the two asparagines' side-chains [72].

The dimerization of Cby has been shown to have functional significance in the Wnt signaling pathway. Alanine mutations to the core leucine residues were previously shown to disrupt the coiled-coil and monomerize the protein [57]. While these monomeric mutants maintained the ability to bind to β-catenin and repress β-catenin mediated signaling, monomeric Cby was incapable of binding to importin-α, thus disrupting its nuclear import [57].

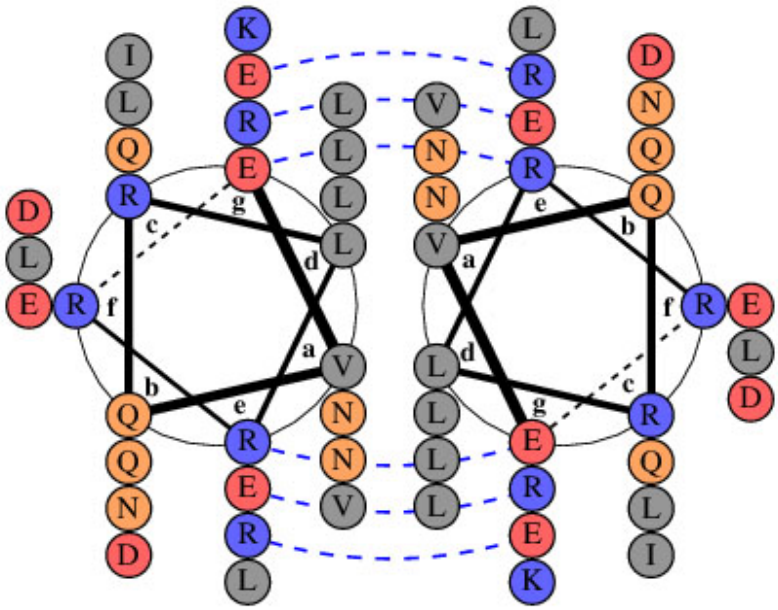

Figure 1.4 Cby's coiled-coil domain

Helical wheel diagrams for the predicted Cby coiled-coil domain (residues 73-100). Four heptad repeats, starting at position *g* (Glu 73), are displayed as parallel and homodimeric. Potential interfacial electrostatic bridges are drawn as broken blue lines. Model was generated using DrawCoil 1.0 (http://www.grigoryanlab.org/drawcoil/).

Biophysical studies of recombinantly expressed Cby are hindered by its insolubility [56]. Cby forms inclusion bodies upon expression in *E. coli* and must be purified using urea to denature the protein, followed by a refolding procedure. Cby, with a predicted pI of 9.1, must be refolded in a low pH (pH 5) and low ionic strength buffer. This restrictive buffer requirement hinders the ability to conduct binding studies between Cby and its binding targets. As the protein cannot be crystallized, due to its mostly disordered structure and insolubility, NMR spectroscopy is an attractive method for the structural characterization of this protein. However, the coiled-coil domain of Cby suffers from severe line-broadening; only peaks corresponding to Cby's N-terminus are observable in Cby's ^{1}H-^{15}N HSQC spectrum. Deuteration of the protein by expressing the protein in M9 salts with 100% D_2O does not render these peaks observable. The lack of observable resonances for residues within the coiled-coil domain may be the result of monomer-dimer exchange, tumbling time of the coiled-coil, or intramolecular conformational exchange [56].

1.6 Structure of β-catenin and modes of interaction with Wnt signaling components

Structurally, the 781-residue human β-catenin consists of a central scaffolding region (amino acids 141-664) made up of 12 armadillo repeats (R1-R12) which are flanked by intrinsically disordered N- and C-terminal domains (NTD and CTD) [73] (Figure 1.5 A). Between R12 and the CTD is a conserved helix, termed helix-C, comprised of residues 667-683 [74]. The armadillo repeats, named after the historical name for β-catenin in *Drosophila* [75], are comprised of ~ 42 residues which form three helices arranged in a triangular fashion [73]. The 12 armadillo repeats collectively form

an elongated superhelix that harbors a large, positively charged groove that functions as a binding site for many of β-catenin's binding partners including Tcf [76], Lef [77], Axin [78], APC [79], E-cadherin [40] and ICAT [80]. Figure 1.5 B and C illustrate crystal structures of β-catenin in complex with these Wnt signaling partners. Many of these β-catenin interacting partners share overlapping binding regions and cannot bind β-catenin simultaneously [81,82]. As such, spatial segregation of these signaling components could be critical to their function, or competition may be necessary for the regulation of Wnt signaling.

Tcf/Lef transcription factors all bind similarly to β-catenin [77], with their N-terminal region binding in an extended state along armadillo repeats R5-R10 and a C-terminal α-helix that interacts with repeats R2-R5. Axin binds to the third and fourth armadillo repeats of β-catenin as a continuous helix [78]. APC contains multiple β-catenin interaction motifs, which include three 15 amino acid (aa) repeats and seven 20-aa repeats. Crystal structures revealed that the 15-aa and 20-aa repeats bound to R5-R8 of β-catenin. Intriguingly, upon phosphorylation of the 20- aa repeats, a downstream region of APC adopts the ability to interact with R1-R5 of β-catenin, effectively enabling the phosphorylated protein to outcompete Axin for binding to β-catenin [83]. The antagonist ICAT is composed of an N-terminal 3-helix bundle and a disordered C-terminus. The 3-helix bundle is anchored within repeats R10-R12 of β-catenin while the disordered C-terminus binds along repeats R5-R9, where it can displace Tcf/Lef [80].

The majority of cellular β-catenin participates in adherens junctions, interacting with cadherins [84]. The cytoplasmic domain of E-cadherin interacts with armadillo

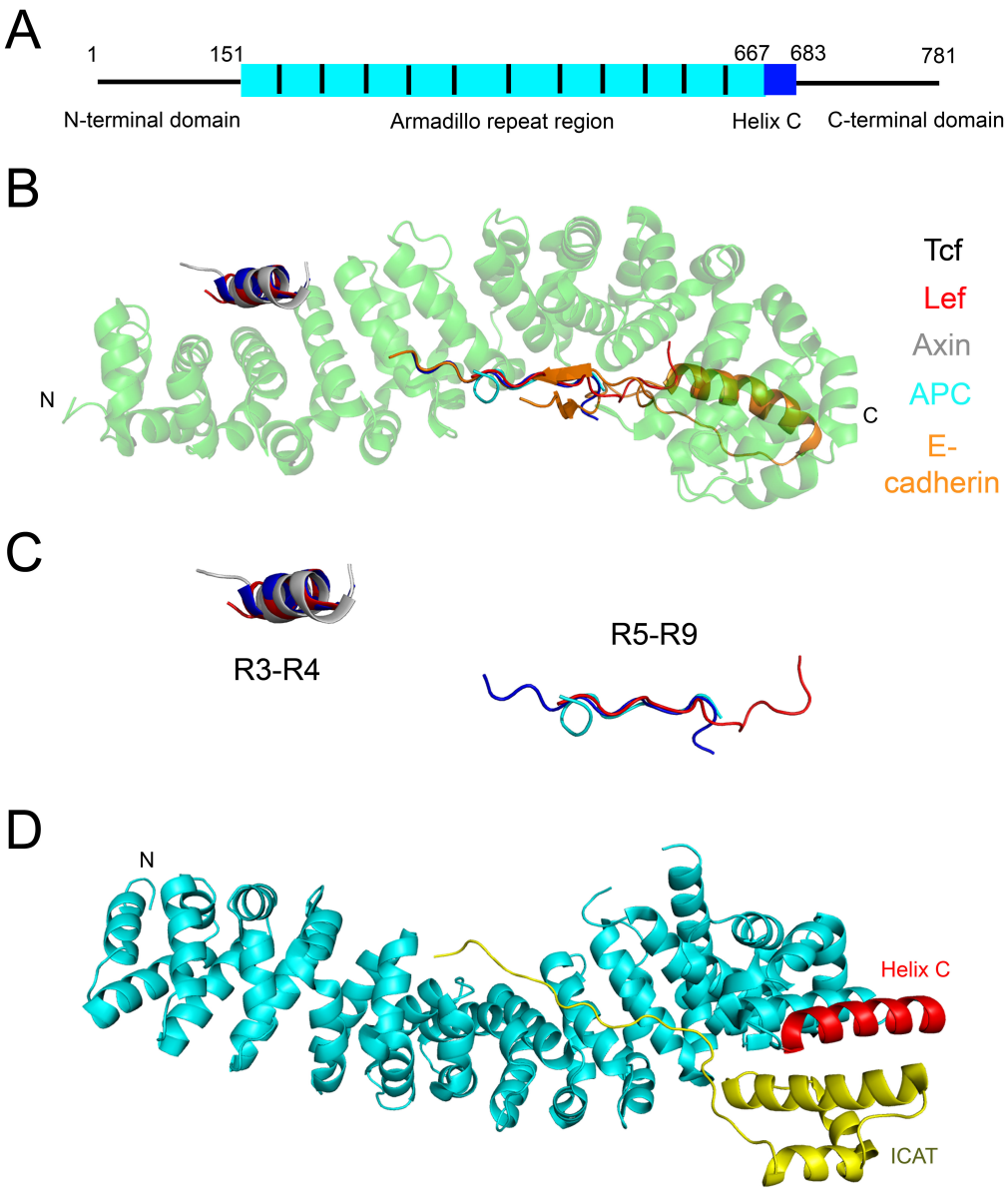

Figure 1.5 Structure of β-catenin and its binding partners

A. Schematic of the major structural domains β-catenin. **B.** Cartoon ribbon crystal structure of β-catenin (PDB: 3OUW, green) in complex with the structurally aligned proteins Lef-1 (3OUW, red), Tcf-4 (1JPW, blue), Axin (1QZ7, grey), APC (1JPP, cyan) and E-cadherin (1I7X, orange). **C.** Structural alignment of Lef-1, Tcf-4, Axin and APC protein without the visual hindrance of β-catenin and the armadillo repeats they bind to. **D.** ICAT in complex with β-catenin (1LUJ). β-catenin from 1LUJ was superimposed onto a β-catenin molecule from a solved structure where helix C is observed (2Z6H).

repeats R5-R9. Additionally, upon phosphorylation, a disordered region in E-cadherin interacts extensively with repeats R3-R4 [40]. A shared binding site between cadherins and Tcf/Lef makes targeting β-catenin therapeutically very challenging.

Pull-down experiments using truncated β-catenin constructs revealed that the helix C is critical to the protein's interaction with Cby, as Cby was observed to bind markedly weaker to a β-catenin construct comprising of only the armadillo repeat region [74]. However, detailed structural characterization of the Cby/β-catenin complex has been mired by the buffer incompatibility of the two proteins. Additionally, NMR spectroscopy represents a challenging avenue to study this complex due to the severe line broadening experienced in Cby's C-terminal half, as well as β-catenin's large size (~ 88 kDa) and elongated shape.

1.7 Structure, function and binding modes of 14-3-3 proteins

Members of the 14-3-3 family are abundant, ~ 30 kDa acidic proteins found across all eukaryotic organisms [85]. These proteins were first discovered in 1967, and are named after the nomenclature used by the researchers Moore and Perez [86] in their systematic classification of proteins found in bovine brain tissue. Using DEAE-cellulose chromatography and starch-gel electrophoresis, the 14-3-3 proteins eluted in their 14th fraction of bovine homogenate and migrated to position 3.3 on their starch gels. In mammals, there are seven heavily conserved isoforms of 14-3-3 (β, γ, ε, ζ, η, θ, σ) [87] (Figure 1.6 A). These family members are able to form homo- or hetero-dimers, with differing levels of preference [88]. For example, the σ isoform preferentially forms homo-dimers [89] while ε prefers forming hetero-dimers [90]. 14-3-3 dimers interact

with hundreds of protein targets, including tumour suppressors, kinases, transcription factors, apoptotic factors and cytoskeletal proteins [91]. With so many binding partners, 14-3-3 plays critical roles in cellular function such as signaling, cell cycle progression, intracellular trafficking, transcription and apoptosis [87]. Studies have demonstrated that 14-3-3 is directly involved in cellular processes that drive tumour development [92] and form protein complexes found in neurodegenerative diseases including Creutzfeldt-Jacob disease (CJD), Parkinson's and Huntington's disease [93].

The crystal structures of all 14-3-3 isoforms have been solved and share an identical fold [88]. The 14-3-3 proteins are nearly entirely α-helical, consisting of nine α-helices (numbered αA-αI) tightly arranged to form a horseshoe like structure (Figure 1.6 A). A positively charged, concave groove comprised of helices αC, αE, αG and αI, serves as the binding interface for 14-3-3 ligands. Since 14-3-3 proteins are dimeric, each monomer may scaffold two separate ligands. These ligands may be the same protein or two distinct ligands. Such a scenario could allow 14-3-3 to juxtapose two molecules against each other, allowing for molecular communication between the two ligands. Alternatively, proteins with multiple 14-3-3 binding sites, such as PKCε, may bind to both 14-3-3 monomers simultaneously, increasing the affinity of the interaction through avidity [94]. Sequence analysis of 14-3-3 binding partners reveals two major binding motifs named mode I (RXX[pS/pT]XP) and mode II (RXXX[pS/pT]XP), where pS and pT represents phosphorylated serine and threonine respectively [95,96]. In crystal structures of solved 14-3-3 complexes, the phosphorylated serine residue is anchored in 14-3-3's binding groove by predominantly positively charged residues (in the human ζ isoform, they are K49, R56, R127 and Y128). Notably, not all 14-3-3 phosphorylated

binding targets conform to these modes [97] and some do not require phosphorylation at all [98].

Bioinformatic analysis of 14-3-3 binding sites indicates that they are frequently found within disordered regions of proteins [99]. The plasticity of these disordered regions may facilitate the diffusive search for the 14-3-3 binding groove. While 14-3-3 binding motifs make up the core contacts in 14-3-3 complexes, secondary contacts by residues out of the 14-3-3 motif may also interact with regions outside of the 14-3-3 binding groove. For instance, the only full-length binding partner to have been successfully co-crystallized to 14-3-3, the 14-3-3/Serotonin N-acetyltransferase complex [100], displays such secondary contacts, while secondary contacts have also been demonstrated in 14-3-3 interactions with integrin tails [101]. As the 14-3-3 binding groove is heavily conserved amongst all isoforms, the presence of these secondary contacts may direct which isoforms bind to a particular target. Such is the case with the phosphatase Cdc25, which binds to all 14-3-3 isoforms except the σ isoform [102].

Cby's 14-3-3 binding motif (RKSApSLS), located within its disordered N-terminus, most closely resembles the mode II motif, with the main exception being a serine as opposed to a proline at the +2 position relative to the phosphoserine [54]. Co-immunoprecipitation experiments revealed that Cby binds to at least three 14-3-3 isoforms; ε, η and σ [54]. However, whether Cby can interact with the other isoforms of the 14-3-3 family, or if it preferentially binds particular isoforms is unknown. While the importance of the Cby/14-3-3 interaction in Wnt signaling has been demonstrated, the structural details of the complex are not clear.

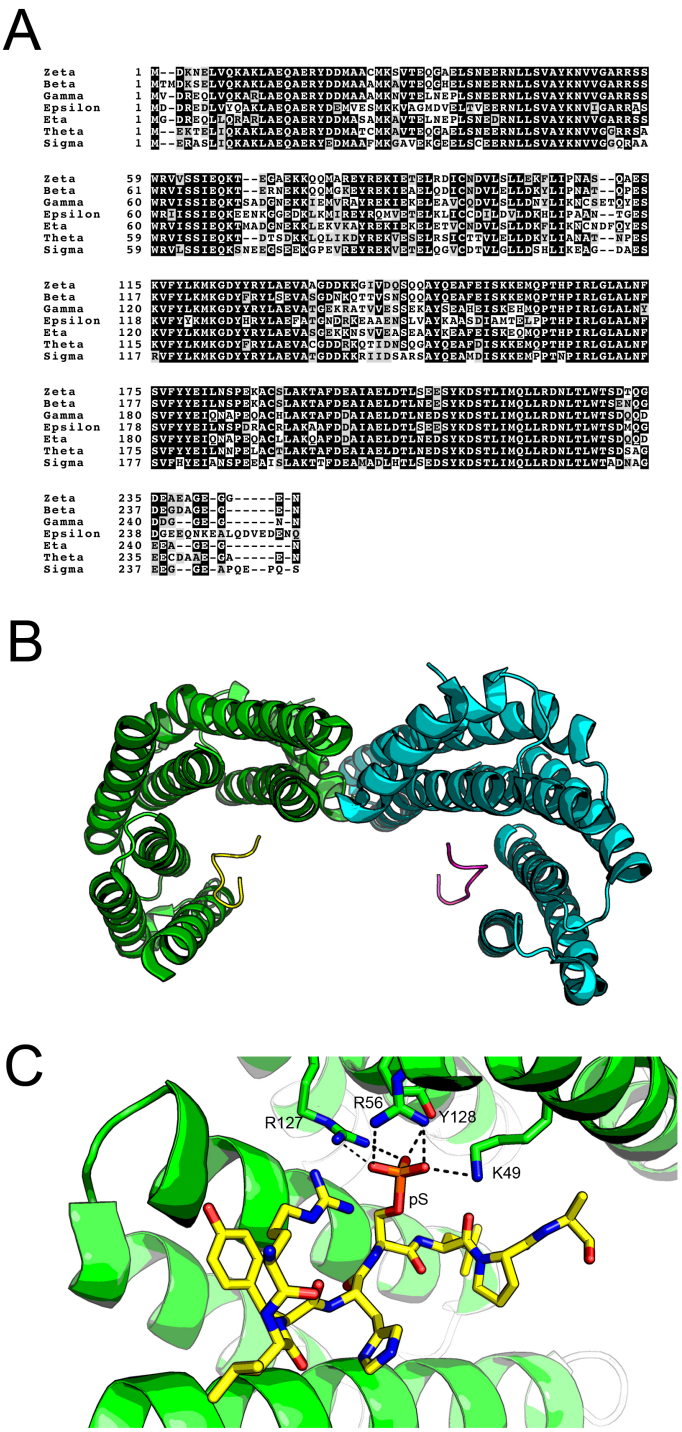

Figure 1.6 14-3-3 Sequence, Structure and its Canonical Binding Mode
A. Sequence alignment of the seven human 14-3-3 isoforms generated using T-Coffee and illustrated using BoxShade. **B.** Cartoon representation of dimeric structure of 14-3-3 (PDB: 1QJA) in complex with synthetic phosphorylated peptides. **C.** The phosphorylated serine residue of the synthetic peptide (pS) making polar contacts (black dotted lines) with 14-3-3 residues K49, R56, R127 and Y128.

1.8 The Cby antagonist TC-1

The Cby antagonist and binding partner TC-1 was identified as a gene overexpressed in papillary thyroid cancer [103]. It enhances β-catenin signaling by relieving the suppression induced by Cby [59]. Its expression has been correlated with aggressive behavior in lung and gastric cancers, potentially through activation of the Wnt pathway [104,105].

Structurally, the 106 residues of TC-1 contain no known functional domains. CD and NMR spectroscopy experiments demonstrate that the protein is intrinsically disordered [106,107]. However, secondary structure propensity (SSP) scores, calculated using the Cα and Cβ chemical shifts, and backbone relaxation experiments reveal three regions (D44-R53, K58-A64, and D73-T88) in the C-terminal half of the protein with α-helical propensity [106] (Figure 1.7).

Pull-down experiments by Jung *et al*. [59] showed that the C-terminal half of TC-1 (residues 51-106) maintained the ability to interact with Cby while the N-terminal half (residues 1-60) could not. This observation was confirmed by NMR binding experiments, in which TC-1's Cby binding site was mapped to the three regions with α-helical propensity [106].

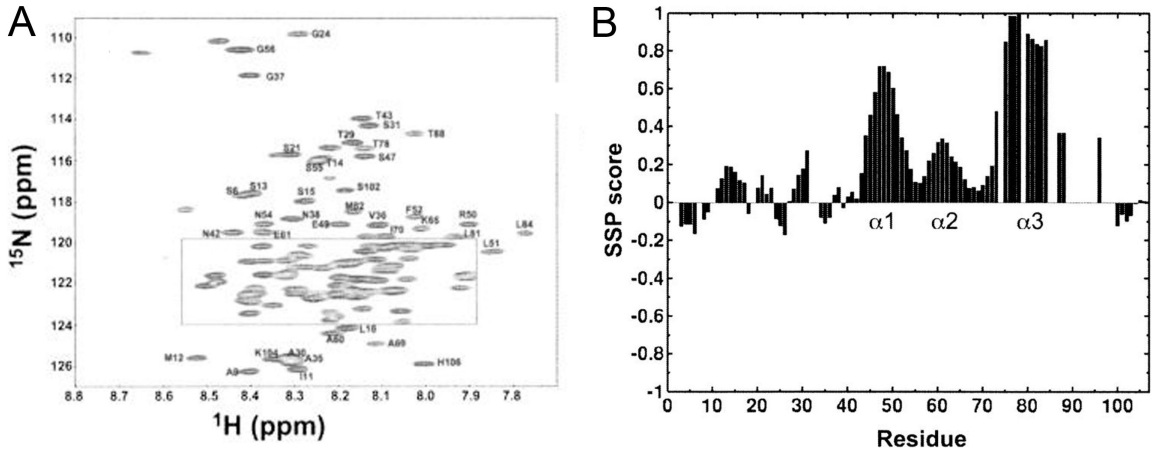

Figure 1.7 Previous TC-1 NMR Studies

NMR spectroscopy reveals TC-1 is intrinsically disordered and contains three regions with α-helical propensity. **A.** ^{1}H-^{15}N HSQC of 15-N labeled TC-1. **B.** SSP scores for TC-1 residues. Regions with α-helical propensity are labeled. This figure has been adapted from figures generated in [106].

1.9 Scope of thesis

The partially disordered protein Cby is an antagonist of the Wnt/β-catenin pathway. Cby's repression of β-catenin signaling is accomplished by two mechanisms: it competes with the Tcf/Lef transcription factors for binding to β-catenin, and facilitates β-catenin export from the nucleus. The Cby mediated nuclear export of β-catenin is dependent on Cby's interaction with the adaptor protein 14-3-3. 14-3-3 can form a tripartite complex with Cby and β-catenin (Figure 1.8), and the formation of this complex is thought to enable β-catenin's nuclear export. The protein TC-1 abates Cby's antagonism through competitive binding for Cby. In this thesis, the structural details of Cby's interactions with the Wnt signaling proteins 14-3-3, β-catenin and TC-1 were investigated.

In Chapter 2, the 14-3-3/Cby complex was structurally characterized. Using X-ray crystallography, the structure of the complex was solved. A canonical binding mode between the two proteins was revealed. NMR spectroscopy and isothermal titration calorimetry experiments reveal that residues flanking Cby's 14-3-3 binding motif contribute to the interaction.

NMR studies on Cby have been hindered due to severe line broadening from residues within its C-terminal half. To structurally analyze Cby's coiled-coil domain, hydrogen-deuterium exchange mass spectrometry (HDX-MS) was used. HDX-MS data revealed that Cby's C-terminal ~25 residues are disordered, providing evidence for an additional structural element along with its disordered N-terminus and coiled-coil domain (Chapter 3). Several Cby constructs that comprise various combinations of Cby's structural elements were generated and their interactions with the protein TC-1 were

studied. It was discovered that Cby's C-terminal half alone (disordered N-terminus removed) binds to TC-1 as a dimer and with significantly greater affinity than the full-length protein, demonstrating that Cby's disordered regions regulate its target recognition.

A major challenge in structurally characterizing the Cby/β-catenin complex is buffer incompatibility. Additionally, the severe line broadening experienced by Cby's C-terminal half, as well as the large elongated shape of β-catenin, represent significant obstacles for studying the complex using NMR spectroscopy. In Chapter 4, alanine substitutions within the core of Cby's coiled-coil proved effective in disrupting coiled-coil formation and in the process increased the solubility of Cby and lead to the appearance of C-terminal peaks in HSQC spectra of mutant Cby proteins. Importantly, the mutants retained the ability to interact with β-catenin in an NMR titration experiment, suggesting Cby may bind to β-catenin as a monomer. Conversely, these mutants failed to interact with TC-1, providing additional evidence that Cby binds to TC-1 as a dimer.

Using a variety of biophysical techniques, the work presented in this thesis provides valuable structural insights into how Cby employs its disordered regions and coiled-coil domain to interact with Wnt signaling binding partners.

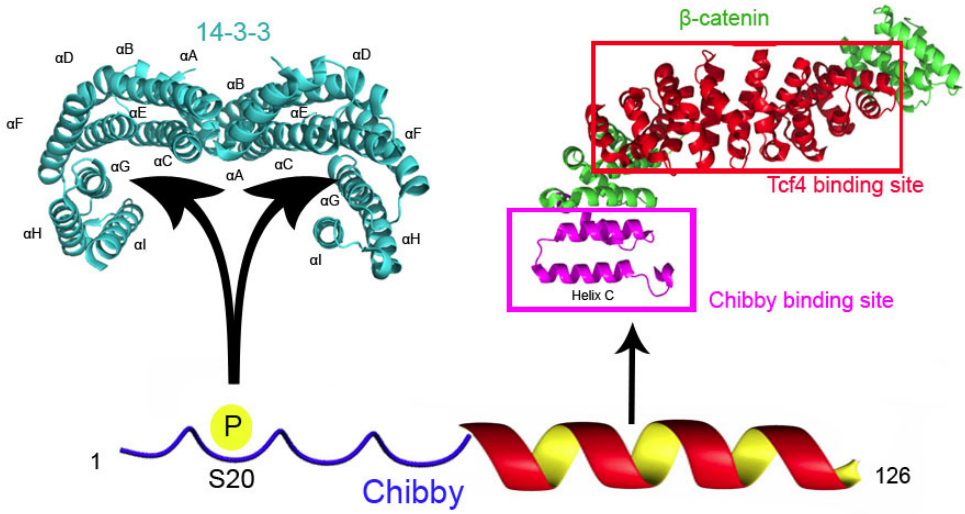

Figure 1.8 The Cby/14-3-3/β-catenin Tripartite Complex

Schematic of Cby binding to 14-3-3 (PDB: 1QJA) and β-catenin (PDB:2Z6H).Cby utilizes its C-terminus to bind to the helix C of β-catenin and its phosphorylated (S20) N-terminus binds to 14-3-3.

1.10 References

1. Cadigan KM, Nusse R (1997) Wnt signaling: a common theme in animal development. Genes Dev 11: 3286-3305.

2. Clevers H (2006) Wnt/beta-catenin signaling in development and disease. Cell 127: 469-480.

3. Clevers H, Nusse R (2012) Wnt/beta-catenin signaling and disease. Cell 149: 1192-1205.

4. De A (2011) Wnt/Ca2+ signaling pathway: a brief overview. Acta Biochim Biophys Sin (Shanghai) 43: 745-756.

5. Wang Y (2009) Wnt/Planar cell polarity signaling: a new paradigm for cancer therapy. Mol Cancer Ther 8: 2103-2109.

6. Rao TP, Kuhl M (2010) An updated overview on Wnt signaling pathways: a prelude for more. Circ Res 106: 1798-1806.

7. Gordon MD, Nusse R (2006) Wnt signaling: multiple pathways, multiple receptors, and multiple transcription factors. J Biol Chem 281: 22429-22433.

8. Moon RT, Bowerman B, Boutros M, Perrimon N (2002) The promise and perils of Wnt signaling through beta-catenin. Science 296: 1644-1646.

9. Kimelman D, Xu W (2006) beta-catenin destruction complex: insights and questions from a structural perspective. Oncogene 25: 7482-7491.

10. Liu C, Li Y, Semenov M, Han C, Baeg GH, et al. (2002) Control of beta-catenin phosphorylation/degradation by a dual-kinase mechanism. Cell 108: 837-847.

11. Aberle H, Bauer A, Stappert J, Kispert A, Kemler R (1997) beta-catenin is a target for the ubiquitin-proteasome pathway. EMBO J 16: 3797-3804.

12. Cavallo RA, Cox RT, Moline MM, Roose J, Polevoy GA, et al. (1998) Drosophila Tcf and Groucho interact to repress Wingless signalling activity. Nature 395: 604-608.

13. Roose J, Molenaar M, Peterson J, Hurenkamp J, Brantjes H, et al. (1998) The Xenopus Wnt effector XTcf-3 interacts with Groucho-related transcriptional repressors. Nature 395: 608-612.

14. van Amerongen R, Nusse R (2009) Towards an integrated view of Wnt signaling in development. Development 136: 3205-3214.

15. Behrens J, von Kries JP, Kuhl M, Bruhn L, Wedlich D, et al. (1996) Functional interaction of beta-catenin with the transcription factor LEF-1. Nature 382: 638-642.

16. Molenaar M, van de Wetering M, Oosterwegel M, Peterson-Maduro J, Godsave S, et al. (1996) XTcf-3 transcription factor mediates beta-catenin-induced axis formation in Xenopus embryos. Cell 86: 391-399.

17. Brunner E, Peter O, Schweizer L, Basler K (1997) pangolin encodes a Lef-1 homologue that acts downstream of Armadillo to transduce the Wingless signal in Drosophila. Nature 385: 829-833.

18. Bilic J, Huang YL, Davidson G, Zimmermann T, Cruciat CM, et al. (2007) Wnt induces LRP6 signalosomes and promotes dishevelled-dependent LRP6 phosphorylation. Science 316: 1619-1622.

19. Schwarz-Romond T, Metcalfe C, Bienz M (2007) Dynamic recruitment of axin by Dishevelled protein assemblies. J Cell Sci 120: 2402-2412.

20. Li VS, Ng SS, Boersema PJ, Low TY, Karthaus WR, et al. (2012) Wnt signaling through inhibition of beta-catenin degradation in an intact Axin1 complex. Cell 149: 1245-1256.

21. Kinzler KW, Nilbert MC, Su LK, Vogelstein B, Bryan TM, et al. (1991) Identification of FAP locus genes from chromosome 5q21. Science 253: 661-665.

22. Nishisho I, Nakamura Y, Miyoshi Y, Miki Y, Ando H, et al. (1991) Mutations of chromosome 5q21 genes in FAP and colorectal cancer patients. Science 253: 665-669.

23. Kinzler KW, Vogelstein B (1996) Lessons from hereditary colorectal cancer. Cell 87: 159-170.

24. Wood LD, Parsons DW, Jones S, Lin J, Sjoblom T, et al. (2007) The genomic landscapes of human breast and colorectal cancers. Science 318: 1108-1113.

25. Liu W, Dong X, Mai M, Seelan RS, Taniguchi K, et al. (2000) Mutations in AXIN2 cause colorectal cancer with defective mismatch repair by activating beta-catenin/TCF signalling. Nat Genet 26: 146-147.

26. Morin PJ, Sparks AB, Korinek V, Barker N, Clevers H, et al. (1997) Activation of beta-catenin-Tcf signaling in colon cancer by mutations in beta-catenin or APC. Science 275: 1787-1790.

27. Polakis P (2000) Wnt signaling and cancer. Genes Dev 14: 1837-1851.

28. Kanazawa A, Tsukada S, Sekine A, Tsunoda T, Takahashi A, et al. (2004) Association of the gene encoding wingless-type mammary tumor virus integration-site family member 5B (WNT5B) with type 2 diabetes. Am J Hum Genet 75: 832-843.

29. Christodoulides C, Scarda A, Granzotto M, Milan G, Dalla Nora E, et al. (2006) WNT10B mutations in human obesity. Diabetologia 49: 678-684.

30. Grant SF, Thorleifsson G, Reynisdottir I, Benediktsson R, Manolescu A, et al. (2006) Variant of transcription factor 7-like 2 (TCF7L2) gene confers risk of type 2 diabetes. Nat Genet 38: 320-323.

31. Kim JH, Liu X, Wang J, Chen X, Zhang H, et al. (2013) Wnt signaling in bone formation and its therapeutic potential for bone diseases. Ther Adv Musculoskelet Dis 5: 13-31.

32. Inestrosa NC, Varela-Nallar L (2014) Wnt signaling in the nervous system and in Alzheimer's disease. J Mol Cell Biol 6: 64-74.

33. Voronkov A, Krauss S (2013) Wnt/beta-catenin signaling and small molecule inhibitors. Curr Pharm Des 19: 634-664.

34. Huang SM, Mishina YM, Liu S, Cheung A, Stegmeier F, et al. (2009) Tankyrase inhibition stabilizes axin and antagonizes Wnt signalling. Nature 461: 614-620.

35. Lu J, Ma Z, Hsieh JC, Fan CW, Chen B, et al. (2009) Structure-activity relationship studies of small-molecule inhibitors of Wnt response. Bioorg Med Chem Lett 19: 3825-3827.

36. Nile AH, Hannoush RN (2016) Fatty acylation of Wnt proteins. Nat Chem Biol 12: 60-69.

37. ten Berge D, Kurek D, Blauwkamp T, Koole W, Maas A, et al. (2011) Embryonic stem cells require Wnt proteins to prevent differentiation to epiblast stem cells. Nat Cell Biol 13: 1070-1075.

38. McCrea PD, Turck CW, Gumbiner B (1991) A homolog of the armadillo protein in Drosophila (plakoglobin) associated with E-cadherin. Science 254: 1359-1361.

39. Kemler R (1993) From cadherins to catenins: cytoplasmic protein interactions and regulation of cell adhesion. Trends Genet 9: 317-321.

40. Huber AH, Weis WI (2001) The structure of the beta-catenin/E-cadherin complex and the molecular basis of diverse ligand recognition by beta-catenin. Cell 105: 391-402.

41. Graham TA, Weaver C, Mao F, Kimelman D, Xu W (2000) Crystal structure of a beta-catenin/Tcf complex. Cell 103: 885-896.

42. Chen Z, Venkatesan AM, Dehnhardt CM, Dos Santos O, Delos Santos E, et al. (2009) 2,4-Diamino-quinazolines as inhibitors of beta-catenin/Tcf-4 pathway: Potential treatment for colorectal cancer. Bioorg Med Chem Lett 19: 4980-4983.

43. Lepourcelet M, Chen YN, France DS, Wang H, Crews P, et al. (2004) Small-molecule antagonists of the oncogenic Tcf/beta-catenin protein complex. Cancer Cell 5: 91-102.

44. Zhang N, Wei P, Gong A, Chiu WT, Lee HT, et al. (2011) FoxM1 promotes beta-catenin nuclear localization and controls Wnt target-gene expression and glioma tumorigenesis. Cancer Cell 20: 427-442.

45. Wu X, Tu X, Joeng KS, Hilton MJ, Williams DA, et al. (2008) Rac1 activation controls nuclear localization of beta-catenin during canonical Wnt signaling. Cell 133: 340-353.

46. Cong F, Varmus H (2004) Nuclear-cytoplasmic shuttling of Axin regulates subcellular localization of beta-catenin. Proc Natl Acad Sci U S A 101: 2882-2887.

47. Wiechens N, Heinle K, Englmeier L, Schohl A, Fagotto F (2004) Nucleo-cytoplasmic shuttling of Axin, a negative regulator of the Wnt-beta-catenin Pathway. J Biol Chem 279: 5263-5267.

48. Henderson BR (2000) Nuclear-cytoplasmic shuttling of APC regulates beta-catenin subcellular localization and turnover. Nat Cell Biol 2: 653-660.

49. Tago K, Nakamura T, Nishita M, Hyodo J, Nagai S, et al. (2000) Inhibition of Wnt signaling by ICAT, a novel beta-catenin-interacting protein. Genes Dev 14: 1741-1749.

50. Ye F, Chen Y, Hoang T, Montgomery RL, Zhao XH, et al. (2009) HDAC1 and HDAC2 regulate oligodendrocyte differentiation by disrupting the beta-catenin-TCF interaction. Nat Neurosci 12: 829-838.

51. Park JI, Kim SW, Lyons JP, Ji H, Nguyen TT, et al. (2005) Kaiso/p120-catenin and TCF/beta-catenin complexes coordinately regulate canonical Wnt gene targets. Dev Cell 8: 843-854.

52. Wu Y, Zhang Y, Zhang H, Yang X, Wang Y, et al. (2010) p15RS attenuates Wnt/{beta}-catenin signaling by disrupting {beta}-catenin.TCF4 Interaction. J Biol Chem 285: 34621-34631.

53. Takemaru K, Yamaguchi S, Lee YS, Zhang Y, Carthew RW, et al. (2003) Chibby, a nuclear beta-catenin-associated antagonist of the Wnt/Wingless pathway. Nature 422: 905-909.

54. Li FQ, Mofunanya A, Harris K, Takemaru K (2008) Chibby cooperates with 14-3-3 to regulate beta-catenin subcellular distribution and signaling activity. J Cell Biol 181: 1141-1154.

55. Li FQ, Mofunanya A, Fischer V, Hall J, Takemaru K (2010) Nuclear-cytoplasmic shuttling of Chibby controls beta-catenin signaling. Mol Biol Cell 21: 311-322.

56. Mokhtarzada S, Yu C, Brickenden A, Choy WY (2011) Structural characterization of partially disordered human Chibby: insights into its function in the Wnt-signaling pathway. Biochemistry 50: 715-726.

57. Mofunanya A, Li FQ, Hsieh JC, Takemaru K (2009) Chibby forms a homodimer through a heptad repeat of leucine residues in its C-terminal coiled-coil motif. BMC Mol Biol 10: 41.

58. Di Tommaso P, Moretti S, Xenarios I, Orobitg M, Montanyola A, et al. (2011) T-Coffee: a web server for the multiple sequence alignment of protein and RNA sequences using structural information and homology extension. Nucleic Acids Res 39: W13-17.

59. Jung Y, Bang S, Choi K, Kim E, Kim Y, et al. (2006) TC1 (C8orf4) enhances the Wnt/beta-catenin pathway by relieving antagonistic activity of Chibby. Cancer Res 66: 723-728.

60. Schuierer MM, Graf E, Takemaru K, Dietmaier W, Bosserhoff AK (2006) Reduced expression of beta-catenin inhibitor Chibby in colon carcinoma cell lines. World J Gastroenterol 12: 1529-1535.

61. Karakoula K, Suarez-Merino B, Ward S, Phipps KP, Harkness W, et al. (2008) Real-time quantitative PCR analysis of pediatric ependymomas identifies novel candidate genes including TPR at 1q25 and CHIBBY at 22q12-q13. Genes Chromosomes Cancer 47: 1005-1022.

62. Xu J, Ren G, Zhao DA, Li BA, Cai CF, et al. (2014) Downregulated Chibby in laryngeal squamous cell carcinoma with increased expression in laryngeal carcinoma Hep-2 cells. Oncol Rep 32: 1947-1956.

63. Dunker AK, Silman I, Uversky VN, Sussman JL (2008) Function and structure of inherently disordered proteins. Curr Opin Struct Biol 18: 756-764.

64. Uversky VN, Oldfield CJ, Dunker AK (2008) Intrinsically disordered proteins in human diseases: introducing the D2 concept. Annu Rev Biophys 37: 215-246.

65. Mason JM, Arndt KM (2004) Coiled coil domains: stability, specificity, and biological implications. Chembiochem 5: 170-176.

66. Burkhard P, Stetefeld J, Strelkov SV (2001) Coiled coils: a highly versatile protein folding motif. Trends Cell Biol 11: 82-88.

67. Landschulz WH, Johnson PF, McKnight SL (1988) The leucine zipper: a hypothetical structure common to a new class of DNA binding proteins. Science 240: 1759-1764.

68. Kouzarides T, Ziff E (1988) The role of the leucine zipper in the fos-jun interaction. Nature 336: 646-651.

69. Sassone-Corsi P, Ransone LJ, Lamph WW, Verma IM (1988) Direct interaction between fos and jun nuclear oncoproteins: role of the 'leucine zipper' domain. Nature 336: 692-695.

70. Lupas A (1996) Coiled coils: new structures and new functions. Trends Biochem Sci 21: 375-382.

71. Hidaka S, Konecke V, Osten L, Witzgall R (2004) PIGEA-14, a novel coiled-coil protein affecting the intracellular distribution of polycystin-2. J Biol Chem 279: 35009-35016.

72. Woolfson DN (2005) The design of coiled-coil structures and assemblies. Adv Protein Chem 70: 79-112.

73. Huber AH, Nelson WJ, Weis WI (1997) Three-dimensional structure of the armadillo repeat region of beta-catenin. Cell 90: 871-882.

74. Xing Y, Takemaru K, Liu J, Berndt JD, Zheng JJ, et al. (2008) Crystal structure of a full-length beta-catenin. Structure 16: 478-487.

75. Riggleman B, Wieschaus E, Schedl P (1989) Molecular analysis of the armadillo locus: uniformly distributed transcripts and a protein with novel internal repeats are associated with a Drosophila segment polarity gene. Genes Dev 3: 96-113.

76. Poy F, Lepourcelet M, Shivdasani RA, Eck MJ (2001) Structure of a human Tcf4-beta-catenin complex. Nat Struct Biol 8: 1053-1057.

77. Sun J, Weis WI (2011) Biochemical and structural characterization of beta-catenin interactions with nonphosphorylated and CK2-phosphorylated Lef-1. J Mol Biol 405: 519-530.

78. Xing Y, Clements WK, Kimelman D, Xu W (2003) Crystal structure of a beta-catenin/axin complex suggests a mechanism for the beta-catenin destruction complex. Genes Dev 17: 2753-2764.

79. Eklof Spink K, Fridman SG, Weis WI (2001) Molecular mechanisms of beta-catenin recognition by adenomatous polyposis coli revealed by the structure of an APC-beta-catenin complex. EMBO J 20: 6203-6212.

80. Graham TA, Clements WK, Kimelman D, Xu W (2002) The crystal structure of the beta-catenin/ICAT complex reveals the inhibitory mechanism of ICAT. Mol Cell 10: 563-571.

81. Hulsken J, Birchmeier W, Behrens J (1994) E-cadherin and APC compete for the interaction with beta-catenin and the cytoskeleton. J Cell Biol 127: 2061-2069.

82. von Kries JP, Winbeck G, Asbrand C, Schwarz-Romond T, Sochnikova N, et al. (2000) Hot spots in beta-catenin for interactions with LEF-1, conductin and APC. Nat Struct Biol 7: 800-807.

83. Ha NC, Tonozuka T, Stamos JL, Choi HJ, Weis WI (2004) Mechanism of phosphorylation-dependent binding of APC to beta-catenin and its role in beta-catenin degradation. Mol Cell 15: 511-521.

84. Nagafuchi A (2001) Molecular architecture of adherens junctions. Curr Opin Cell Biol 13: 600-603.

85. Aitken A (1995) 14-3-3 proteins on the MAP. Trends Biochem Sci 20: 95-97.

86. Moore BW, Perez V.J (1967) Specific acidic proteins of the nervous system: Englewood Cliffs, NJ: Prentice-Hall.

87. Fu H, Subramanian RR, Masters SC (2000) 14-3-3 proteins: structure, function, and regulation. Annu Rev Pharmacol Toxicol 40: 617-647.

88. Yang X, Lee WH, Sobott F, Papagrigoriou E, Robinson CV, et al. (2006) Structural basis for protein-protein interactions in the 14-3-3 protein family. Proc Natl Acad Sci U S A 103: 17237-17242.

89. Jones DH, Ley S, Aitken A (1995) Isoforms of 14-3-3-Protein Can Form Homodimers and Heterodimers in-Vivo and in-Vitro - Implications for Function as Adapter Proteins. Febs Letters 368: 55-58.

90. Chaudhri M, Scarabel M, Aitken A (2003) Mammalian and yeast 14-3-3 isoforms form distinct patterns of dimers in vivo. Biochemical and Biophysical Research Communications 300: 679-685.

91. Mhawech P (2005) 14-3-3 proteins--an update. Cell Res 15: 228-236.

92. Wilker E, Yaffe MB (2004) 14-3-3 Proteins--a focus on cancer and human disease. J Mol Cell Cardiol 37: 633-642.

93. Steinacker P, Aitken A, Otto M (2011) 14-3-3 proteins in neurodegeneration. Semin Cell Dev Biol 22: 696-704.

94. Kostelecky B, Saurin AT, Purkiss A, Parker PJ, McDonald NQ (2009) Recognition of an intra-chain tandem 14-3-3 binding site within PKCepsilon. EMBO Rep 10: 983-989.

95. Yaffe MB, Rittinger K, Volinia S, Caron PR, Aitken A, et al. (1997) The structural basis for 14-3-3:phosphopeptide binding specificity. Cell 91: 961-971.

96. Muslin AJ, Tanner JW, Allen PM, Shaw AS (1996) Interaction of 14-3-3 with signaling proteins is mediated by the recognition of phosphoserine. Cell 84: 889-897.

97. Johnson C, Crowther S, Stafford MJ, Campbell DG, Toth R, et al. (2010) Bioinformatic and experimental survey of 14-3-3-binding sites. Biochem J 427: 69-78.

98. Zhai J, Lin H, Shamim M, Schlaepfer WW, Canete-Soler R (2001) Identification of a novel interaction of 14-3-3 with p190RhoGEF. J Biol Chem 276: 41318-41324.

99. Uhart M, Bustos DM (2014) Protein intrinsic disorder and network connectivity. The case of 14-3-3 proteins. Front Genet 5: 10.

100. Obsil T, Ghirlando R, Klein DC, Ganguly S, Dyda F (2001) Crystal structure of the 14-3-3zeta:serotonin N-acetyltransferase complex. a role for scaffolding in enzyme regulation. Cell 105: 257-267.

101. Bonet R, Vakonakis I, Campbell ID (2013) Characterization of 14-3-3-zeta Interactions with integrin tails. J Mol Biol 425: 3060-3072.

102. Wilker EW, Grant RA, Artim SC, Yaffe MB (2005) A structural basis for 14-3-3sigma functional specificity. J Biol Chem 280: 18891-18898.

103. Chua EL, Young L, Wu WM, Turtle JR, Dong Q (2000) Cloning of TC-1 (C8orf4), a novel gene found to be overexpressed in thyroid cancer. Genomics 69: 342-347.

104. Su K, Huang L, Li W, Yan X, Li X, et al. (2013) TC-1 (c8orf4) enhances aggressive biologic behavior in lung cancer through the Wnt/beta-catenin pathway. J Surg Res 185: 255-263.

105. Kim B, Koo H, Yang S, Bang S, Jung Y, et al. (2006) TC1(C8orf4) correlates with Wnt/beta-catenin target genes and aggressive biological behavior in gastric cancer. Clin Cancer Res 12: 3541-3548.

106. Gall C, Xu H, Brickenden A, Ai X, Choy WY (2007) The intrinsically disordered TC-1 interacts with Chibby via regions with high helical propensity. Protein Sci 16: 2510-2518.

107. Sunde M, McGrath KC, Young L, Matthews JM, Chua EL, et al. (2004) TC-1 is a novel tumorigenic and natively disordered protein associated with thyroid cancer. Cancer Res 64: 2766-2773.

Chapter 2

2 Structural Analysis of the 14-3-3ζ/Chibby Interaction Involved in Wnt/β-catenin Signaling

2.1 Introduction

Chibby (Cby) is a small (14.5 kDa), highly conserved protein that functions as a Wnt/β-catenin signaling antagonist [1]. While the Wnt pathway plays crucial roles in cell proliferation and differentiation, embryonic development and tissue homeostasis, its dysregulation contributes to the pathogenesis of an array of human disorders, including cancer [2,3]. Because of this, pharmacological modulation of the pathway has great therapeutic potential for disease treatments [4,5,6,7].

Activation of the Wnt pathway promotes the stabilization of the transcriptional co-activator β-catenin within the cytoplasm, allowing it to translocate to the nucleus and bind to Tcf/Lef (T cell factor/lymphoid enhancer factor) transcription factors to activate Wnt target genes [8,9,10,11]. Multiple regulatory strategies employed by the cell focus on various stages of the Wnt pathway [12], with β-catenin being a focal point. Cby is one such regulatory protein, suppressing β-catenin-mediated signaling via two distinct molecular mechanisms. First, in the nucleus, it competes with the Tcf/Lef transcription factors for binding to β-catenin [1]. Secondly, Cby facilitates β-catenin export from the nucleus in conjunction with the proteins 14-3-3 and the nuclear export receptor chromosomal region maintenance 1 (CRM1) [13,14]. In this mode of regulation, Cby forms a stable trimolecular complex with 14-3-3 and β-catenin [13]. Interestingly,

binding of 14-3-3 to Cby also leads to an enhanced interaction between Cby and CRM1, promoting nuclear exclusion of Cby-bound β-catenin [14].

The ability of the 126-residue human Cby to function as a scaffold protein likely arises from its partially disordered nature. It is well documented that intrinsically disordered proteins bind to multiple targets by adopting different conformations or via linear motifs located at different regions in the proteins [15,16,17]. Previous work has shown that Cby consists of an unstructured N-terminus and contains a coiled-coil motif within its C-terminus (residues 73-100) that enables dimerization [18,19]. Cby uses its C-terminus to bind to β-catenin [1], although residues critical for this interaction have yet to be elucidated. 14-3-3 recognizes the motif ^{16}RKSA(pS)LS^{22} located in the disordered N-terminus of Cby, when the serine 20 residue is phosphorylated by the kinase Akt [13]. In this manner, N- and C-terminal binding modules on Cby work together to facilitate the nuclear export of β-catenin; however, how Cby forms such complexes from a structural standpoint remains unknown. Our work here focuses on elucidating the binding mode between Cby and 14-3-3.

The 14-3-3 proteins, which consist of seven isoforms in mammals (β, ε, η, γ, θ, ζ and σ), function as adaptor molecules and are involved in a large range of cellular processes, including apoptosis, DNA damage response and transcriptional regulation [20]. Structurally, the ~30 kDa 14-3-3 proteins assemble into homo- or heterodimers, with each monomer composed of nine anti-parallel alpha-helices (αA-αI) [21]. An amphipathic groove composed of helices αC, αE, αG, and αI comprise the ligand-binding interface. Generally, 14-3-3 isoforms recognize three consensus binding motifs:

RXX(pS/pT)XP (mode I), RXXX(pS/pT)XP (mode II) and (pS/pT)X1-2-COOH (mode III) where pS/pT represents phosphorylated serine/threonine [22,23]. However, there are several 14-3-3 binding partners that deviate significantly from these canonical motifs, including examples of non-phosphorylated partners [24,25].

With hundreds of binding partners discovered to date [26], the 14-3-3 proteins are classified as signaling hub proteins. Interestingly, many well-structured hub proteins are found to preferentially bind to unstructured proteins [15]. In fact, the vast majority of 14-3-3 binding motifs are either found or predicted to be within disordered regions [27,28]. While this is due in large part to the phospho-dependence of 14-3-3 interactions, as kinases predominantly target unstructured regions for phosphorylation [29], the structural plasticity of 14-3-3 binding motifs and their neighbouring residues allows 14-3-3 proteins to target many different proteins with high specificity.

14-3-3 targets are hypothesized to bind to 14-3-3 via primary and secondary interactions (discussed by Yang *et al.* [21]). The primary interactions are made between the 14-3-3 binding motif (including the pS/pT residue) of the target and a conserved binding groove in the 14-3-3 protein. Secondary interactions occur when residues flanking the target's 14-3-3 binding-motif contact regions outside of the conserved 14-3-3 binding groove. While various crystal structures of 14-3-3 complexes have been solved, the majority of them have been co-crystallized with short peptides. Observable electron density is typically only present for 4-10 residues flanking the phosphorylated residue of the target peptide. While this provides a structural basis for the primary contacts of the interaction, information regarding the secondary contacts is limited. To

date, only one (nearly) full-length, globular partner has been co-crystallized with 14-3-3 [30].

The disordered Cby is able to interact with at least three of the seven 14-3-3 isoforms (ε, η and ζ) [13], however, whether it can bind to the β, θ, γ, or η isoforms is unknown. Its 14-3-3 binding motif (^{16}RKSA(pS)LS^{22}) closely resembles the mode II motif (RXXX(pS/pT)XP), the difference being that Cby contains a serine instead of proline at the +2 position from the phosphoserine. It is noteworthy that even though proline is found to be the +2 residue in ~ 50% of known 14-3-3 binding motifs, serine is in fact the second most commonly found amino acid at that position [25]. To our knowledge, no 14-3-3/phosphopeptide structure with serine as the +2 residue has been determined to date.

In this work, the crystal structure of 14-3-3ζ in complex with an 18-residue phosphorylated Cby-derived peptide was solved to reveal the primary binding interactions. Secondary interactions between 14-3-3 and the Cby peptide were further investigated by using nuclear magnetic resonance (NMR) spectroscopy and isothermal titration calorimetry (ITC). By combining the X-ray and NMR techniques, we were able to obtain additional molecular details of the binding interface of Cby on 14-3-3. Additionally, Cby was shown to interact with all seven human isoforms of 14-3-3. Notably, the backbone assignment of 14-3-3ζ completed in this work will also facilitate mapping of regions on the 14-3-3ζ surface that are involved in binding other targets.

2.2 Materials and Methods

2.2.1 Expression and Purification of 14-3-3ζ

The human 14-3-3ζ and 14-3-3σ ORFs were purchased from GeneCopoeia and were each transferred into a Gateway® pDEST17 vector (Invitrogen). The 14-3-3ζΔC12, where the 12 C-terminal residues were deleted, was then generated from the full-length construct using the QuikChange II Site-Directed Mutagenesis Kit (Strategene). The constructs for human 14-3-3 β, ε, γ, η, and θ were kindly gifted by the Structural Genomics Consortium. All 14-3-3 proteins used in this work had their DNA constructs sequenced. 14-3-3 proteins were expressed as His-tagged protein in *Escherichia coli* (*E. coli*) BL21 (DE3) (14-3-3 β, ε, γ, η, and θ) or *E. coli* BL21 pLysS (14-3-3ζ, 14-3-3ζΔC12 and 14-3-3σ) in M9 medium. For unlabeled protein, protein expression was induced at an $O.D._{600}$ of 0.9 by adding 0.75 mM IPTG at 18 ºC for 24 h. The ^{15}N, ^{13}C, ^{2}H labeled 14-3-3ζΔC12 was produced by growing *E. coli* in deuterated M9 medium. Cells adapted to 70% D_2O were used to inoculate a 1 L culture of M9 prepared in 100% D_2O. Cells were grown at 37 °C and overexpression was induced at an $O.D._{600}$ of 0.6 with 0.75 mM IPTG. After a 60-h induction at 18 °C, the cells were harvested. All 14-3-3 constructs used in this study were purified from the crude lysate by affinity chromatography using Ni Sepharose™ Fast Flow beads (Amersham Biosciences). The tag was then cleaved by overnight incubation with His-tagged tobacco etch virus (TEV) protease at 25ºC. The cleaved 14-3-3 was purified from TEV by passing the mixture through Ni Sepharose™ Fast Flow beads. The final yields for the 14-3-3ζ proteins were ~50 mg per L of M9 media (including deuterated media). All 14-3-3 proteins were analyzed on SDS-PAGE for purity and analyzed for correct mass using electrospray ionization mass spectrometry.

2.2.2 Peptide Synthesis

The Cby peptides used in this study were purchased from GenScript USA Inc. and the Tufts University Core Facility. From GenScript USA Inc.: Cby 13-mer (NH_2-^{12}KTPPRKSASLSNL^{24}-COOH), Cby S20D 13-mer (NH_2-^{12}KTPPRKSADLSNL^{24}-COOH), Cby S20E 13-mer (NH_2-^{12}KTPPRKSAELSNL^{24}-COOH), pCby 13-mer (NH_2-^{12}KTPPRKSApSLSNL^{24}-COOH) and pCby 18-mer (NH_2-^{12}KTPPRKSApSLSNLHSLDR^{29}-COOH). From Tufts: pCby 7-mer (Ac-^{16}RKSApSLS^{22}-NH_2), pCby 11-mer (NH_2-^{12}KTPPRKSApSLS^{22}-NH_2), pCby S22P 7-mer (Ac-^{16}RKSApSLP^{22}-NH_2), pCby S22P 13-mer (NH_2-^{12}KTPPRKSApSLPNL^{24}-COOH) and pCby S22P 18-mer (NH_2-^{12}KTPPRKSApSLSNLHSLDR^{29}-COOH). Peptides were dissolved and dialyzed in 50 mM sodium phosphate, 100 mM NaCl at pH 6.8 for ITC and NMR experiments.

2.2.3 Crystallization and Structure Determination

Crystals grew within 2 months at 4ºC in sitting drops containing 1 μL of complexed 14-3-3ζ (10 mg/mL) and phosphorylated Cby 18-mer peptide (protein:peptide molar ratio 1:4) in 20 mM Tris, pH 7.5, and 100 mM NaCl and 1 μL of reservoir solution containing 200 mM NH_4HCO_2 and 16-20% PEG 3350. The mother liquor with 15% glycerol served as the cryoprotectant for flash-cooling in liquid nitrogen. Data were collected at the Macromolecular Crystallographic Facility (University of Western Ontario). The structure was solved via rigid body molecular replacement, using Protein Data Bank entry 1QJA (14-3-3ζ in complex with mode II peptide) [31] as the starting model. The Cby peptide was built manually using *Coot* [32] and refinement was carried out using PHENIX [33].

2.2.4 NMR Experiments

All NMR experiments were performed using ^{15}N, ^{13}C, ^{2}H-labeled protein samples in 50 mM sodium phosphate, 100 mM NaCl at pH 6.8. Samples contained 10% D_2O and 1 mM 2,2-dimethyl-2-sila-pentane-5-sulfonic acid (DSS) as ^{1}H chemical shift reference. NMR experiments for the backbone resonance assignment of 14-3-3ζΔC12 were conducted at 25 °C on a Bruker Avance 800 MHz (National University of Singapore) spectrometer equipped with cryogenic probe. Sequential assignments were obtained from ^{1}H-^{15}N TROSY HSQC, HNCACB, HN(CO)CACB and ^{15}N-NOESY-HSQC spectra. Data were processed using NMRPipe [34] and analyzed using CARA [35].

For the NMR titrations, either phosphorylated Cby 7-mer or 18-mer peptides were titrated into 600 μL of ~ 200 μM ^{15}N, ^{13}C, ^{2}H labeled 14-3-3ζΔC12 until a 3:1 (peptide: 14-3-3ζΔC12) molar ratio was reached. A ^{1}H-^{15}N HSQC spectrum was collected for each titration point for a total of 12 points for the pCby WT 7-mer and 18-mer and 6 points for the pCby S22P 18-mer. All spectra were analyzed using NMRView [36].

2.2.5 Isothermal Titration Calorimetry (ITC) Experiments

ITC experiments were performed on a VP-ITC instrument (MicroCal) at 25 °C. The protein and peptide samples were dialyzed into a buffer containing 50 mM sodium phosphate, 100 mM NaCl, 1 mM DTT at pH 6.8 and degassed before the experiments. For ITC experiments testing the binding of the Cby 18-mer to all 14-3-3 isoforms, as well as the 14-3-3ζ S184E and 14-3-3σ S186E mutants, the buffer used comprised 20 mM MES, 100 mM NaCl, pH 6.5. In a typical experiment, 5 μL aliquots of ~1-2 mM peptide were titrated stepwise into the 1.4 mL sample cell containing ~100-200 μM 14-3-3. The

association constant (K_a), molar binding stoichiometry (n) and the binding enthalpy (ΔH), entropy (ΔS) and Gibbs free energy (ΔG) were determined by fitting the binding isotherm to a one-site model with MicroCal Origin7 software. All ITC experiments were performed in duplicate. Peptide and protein concentrations were determined from amino acid analysis (Amino Acid Analysis Facility, SickKids, Toronto, ON).

2.2.6 Accession Numbers

The atomic coordinates for the 14-3-3ζ/Cby complex have been deposited in the Protein Data Bank under accession number 4WRQ. The ^{1}H, ^{15}N and $^{13}C\alpha/\beta$ chemical shifts of the backbone resonances have been deposited in the BioMagResBank (http://www.bmrb.wisc.edu), under BMRB accession number 25231.

2.3 Results

2.3.1 Phosphorylation of serine 20 on Cby is critical for its binding to 14-3-3ζ

A previous study by Li *et al.* [13] showed that S20 of Cby is essential for its interaction with 14-3-3, with the binding being regulated by the phosphorylation of this serine residue. To quantitatively assess the importance of the phosphorylation of S20 to the complex formation with 14-3-3ζ, we have used ITC to measure the affinities of a Cby peptide (^{12}KTPPRKSASLSNL^{24}) encompassing the 14-3-3 binding motif, in both its non-phosphorylated and phosphorylated forms, to 14-3-3ζ. The same peptides containing the phospho-mimetic mutants S20D and S20E were also included in this study. Our data show that only the phosphorylated Cby peptide was able to interact with 14-3-3ζ (K_D ~ 15 μM, Table 2.1 and 2.2), while the other three peptides display no observable binding (Figure 2.1). Importantly, the phospho-mimetic mutations were unable to rescue the binding, indicating that the Cby/14-3-3ζ association is driven by the phosphate group on S20.

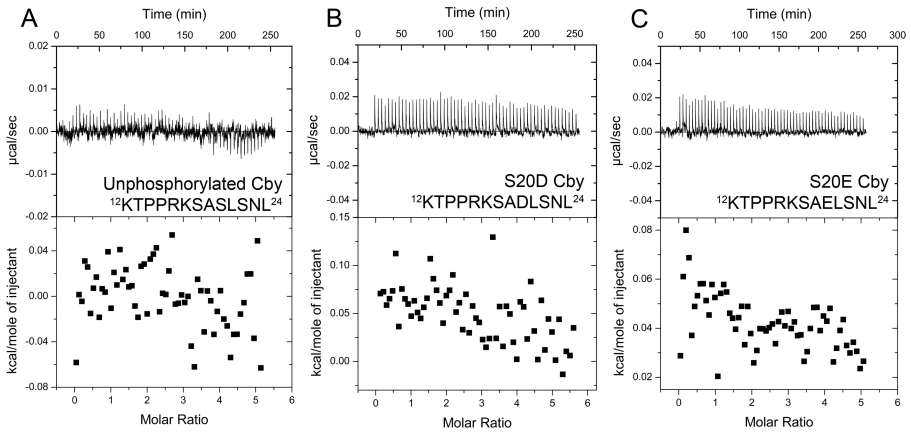

Figure 2.1 ITC thermograms with unphosphorylated Cby peptides

ITC thermograms for titrations of unphosphorylated or phospho-mimetic Cby peptides to 14-3-3ζ. **A.** Cby WT 13-mer. **B.** Cby S20D 13-mer. **C.** Cby S20E 13-mer.

2.3.2 Flanking residues of the consensus 14-3-3 binding motif play important roles in the Cby/14-3-3ζ association

Next, we assessed the contributions of residues flanking the consensus 14-3-3 binding motif of Cby to the interaction with 14-3-3ζ. The results of our ITC measurements show that a 7-mer Cby peptide (^{16}RKSA(pS)LS^{22}) comprising the minimal 14-3-3 binding motif bound to 14-3-3ζ with a K_D of ~44 μM (Table 2.1 and 2.2, Figure 2.2). Interestingly, phosphopeptides of increasing length exhibit a systematic increase in binding affinity to 14-3-3ζ (the results are summarized in Tables 2.1 and 2.2 and the thermograms are shown in Figure 2.2). First, a Cby 11-mer peptide which contains 4 additional residues (^{12}KTPP^{15}) than the Cby 7-mer peptide (^{16}RKSA(pS)LS^{22}) bound with more than two-fold greater affinity than the Cby 7-mer, with a K_D of ~18 μM. A Cby 13-mer, with a 2 residue C-terminal extension to the 11-mer (^{23}NL^{24}), bound with only slightly higher affinity, with a K_D of ~15 μM. Lastly, an 18-mer, which contains a five-residue C-terminal extension to the 13-mer (^{25}HSLDR^{29}), bound with nine-fold greater affinity compared to the 7-mer, with a K_D of ~5 μM. The results clearly indicate that residues flanking the binding-motif on Cby play significant roles in mediating the interaction with 14-3-3ζ.

Table 2.1 Thermodynamic parameters of binding of phosphorylated Cby peptides to 14-3-3

Thermodynamic parameters for the binding of phosphorylated Cby peptides to 14-3-3. A duplicate set of experimental values for all ITC experiments is reported in Table 2.2.

Peptide	n[a]	K_d[b] (10^{-6} M)	ΔH[b] (kcal/mol)	$T\Delta S$[b] (kcal/mol)	ΔG[b] (kcal/mol)
In ITC Cell: 14-3-3 ζ					
WT Cby					
Cby 7-mer ^{16}RKSA(pS)LS^{22}	1.01	43.5 ± 1.9	-3.35 ± 0.06	2.60	-5.95 ± 0.03
Cby 11-mer ^{12}KTPPRKSA(pS)LS^{22}	0.95	17.5 ± 0.6	-3.26 ± 0.02	3.23	-6.49 ± 0.02
Cby 13-mer ^{12}KTPPRKSA(pS)LSNL^{24}	1.00	14.5 ± 0.6	-2.63 ± 0.02	3.97	-6.60 ± 0.02
Cby 18-mer ^{12}KTPPRKSA(pS)LSNLHSLDR^{29}	0.96	4.6 ± 0.2	-4.35 ± 0.05	2.93	-7.28 ± 0.03
Cby Mutants					
Cby 7-mer S22P ^{16}RKSA(pS)LP^{22}	1.03	2.9 ± 0.05	-6.16 ± 0.01	1.39	-7.55 ± 0.01
Cby 13-mer S22P ^{12}KTPPRKSA(pS)LPNL^{24}	1.06	1.1 ± 0.03	-4.64 ± 0.01	3.49	-8.13 ± 0.02
Cby 18-mer S22P ^{12}KTPPRKSA(pS)LPNLHSLDR^{29}	1.05	0.36 ± 0.01	-8.03 ± 0.02	0.76	-8.79 ± 0.02
Cby 18-mer L24A ^{12}KTPPRKSA(pS)LSNAHSLDR^{29}	0.99	21.3 ± 1.7	-1.56 ± 0.05	4.81	-6.37 ± 0.05
***In ITC Cell: 14-3-3 ζ* K49A**					
Cby 18-mer WT ^{12}KTPPRKSA(pS)LSNLHSLDR^{29}	1.01	3.8 ± 0.3	-4.16 ± 0.05	3.23	-7.39 ± 0.05
Cby 18-mer S22P ^{12}KTPPRKSA(pS)LPNLHSLDR^{29}	1.07	1.9 ± 0.2	-7.13 ± 0.03	0.67	-7.80 ± 0.06
In ITC Cell: 14-3-3 ζ ΔC12					
Cby 13-mer ^{12}KTPPRKSA(pS)LSNL^{24}	0.99	14.9 ± 0.9	-2.08 ± 0.03	4.50	-6.58 ± 0.04
Cby 18-mer ^{12}KTPPRKSA(pS)LSNLHSLDR^{29}	1.04	6.8 ± 0.4	-3.35 ± 0.06	3.70	-7.05 ± 0.03

[a] Binding stoichiometry of monomeric 14-3-3 and Cby peptide.

[b] K_d is the dissociation constant ΔH, ΔS and ΔG are the change in enthalpy, entropy and Gibbs free energy upon binding at T=298.15 K, respectively.

Table 2.2 Duplicate set of thermodynamic parameters for the binding of phosphorylated Cby peptides to 14-3-3ζ

Peptide	n[a]	K_d[b] (10^{-6} M)	ΔH[b] (kcal/mol)	TΔS[b] (kcal/mol)	ΔG[b] (kcal/mol)
In ITC Cell: 14-3-3 ζ					
WT Cby					
Cby 7-mer ^{16}RKSA(pS)LS^{22}	0.94	47.6 ± 1.6	-3.70 ± 0.04	2.20	-5.90 ± 0.02
Cby 11-mer ^{12}KTPPRKSA(pS)LS^{22}	0.96	17.5 ± 0.6	-3.27 ± 0.02	3.22	-6.49 ± 0.02
Cby 13-mer ^{12}KTPPRKSA(pS)LSNL^{24}	1.07	12.8 ± 0.5	-2.60 ± 0.03	4.07	-6.67 ± 0.02
Cby 18-mer ^{12}KTPPRKSA(pS)LSNLHSLDR^{29}	0.94	4.9 ± 0.3	-4.33 ± 0.06	2.91	-7.24 ± 0.04
Cby Mutants					
Cby 7-mer S22P ^{16}RKSA(pS)LP^{22}	1.02	3.2 ± 0.1	-6.21 ± 0.02	1.29	-7.50 ± 0.02
Cby 13-mer S22P ^{12}KTPPRKSA(pS)LPNL^{24}	1.02	1.3 ± 0.04	-4.70 ± 0.01	3.33	-8.03 ± 0.02
Cby 18-mer S22P ^{12}KTPPRKSA(pS)LPHSLDR^{29}	1.08	0.38 ± 0.01	-7.97 ± 0.01	0.79	-8.76 ± 0.02
Cby 18-mer L24A ^{12}KTPPRKSA(pS)LSNAHSLDR^{29}	1.05	25.0 ± 2.5	-1.37 ± 0.05	4.91	-6.28 ± 0.06
***In ITC Cell: 14-3-3 ζ* K49A**					
Cby 18-mer WT ^{12}KTPPRKSA(pS)LSNLHSLDR^{29}	1.07	5.5 ± 0.6	-3.76 ± 0.07	3.41	-7.17 ± 0.06
Cby 18-mer S22P ^{12}KTPPRKSA(pS)LPHSLDR^{29}	0.97	1.8 ± 0.1	-6.67 ± 0.04	1.17	-7.84 ± 0.03
In ITC Cell: 14-3-3 ζ ΔC12					
Cby 13-mer ^{12}KTPPRKSA(pS)LSNL^{24}	1.06	14.5 ± 0.6	-2.08 ± 0.03	4.52	-6.60 ± 0.02
Cby 18-mer ^{12}KTPPRKSA(pS)LSNLHSLDR^{29}	1.02	8.5 ± 0.5	-3.15 ± 0.04	3.77	-6.92 ± 0.03

[a] Binding stoichiometry of monomeric 14-3-3 and Cby peptide.

[b] K_d is the dissociation constant. ΔH, ΔS and ΔG are the change in enthalpy, entropy and Gibbs free energy upon binding at T=298.15 K, respectively.

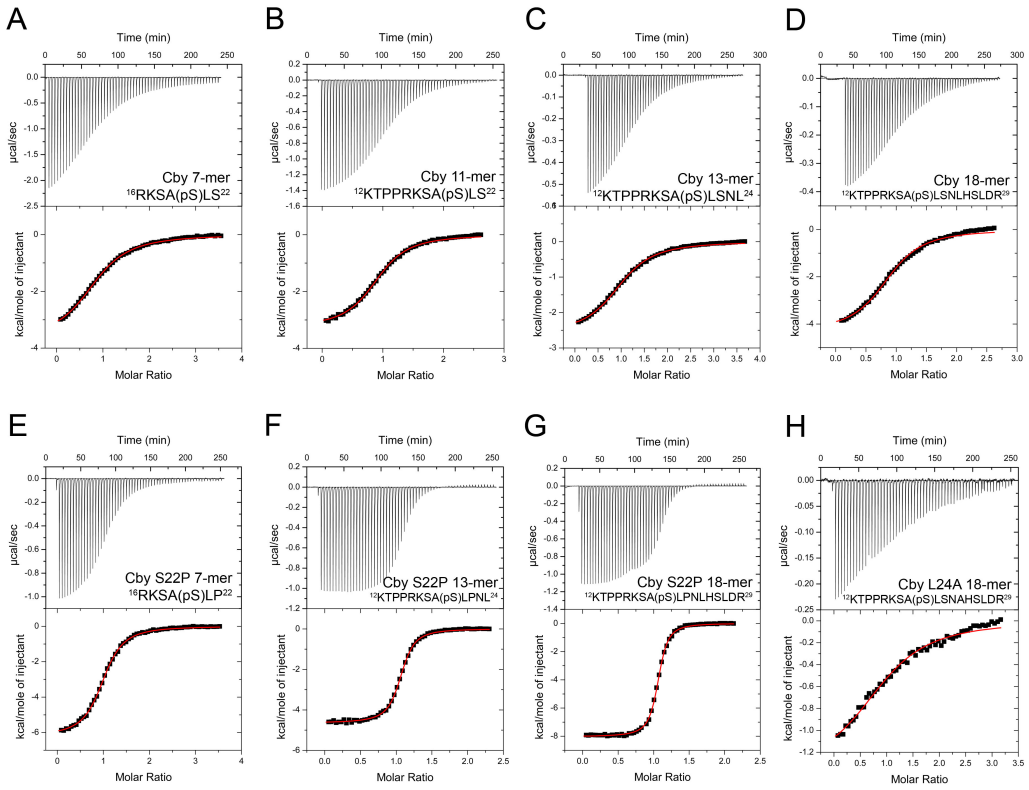

Figure 2.2 ITC thermograms for various phosphorylated WT and mutant Cby peptides titrated into 14-3-3ζ

A. Cby 7-mer. **B.** Cby 11-mer. **C.** Cby 13-mer. **D.** Cby 18-mer. **E.** Cby S22P 7-mer **F.** Cby S22P 13-mer. **G.** Cby S22P 18-mer. **H.** Cby L24A 18-mer.

2.3.3 Molecular basis of the interaction between 14-3-3ζ and the non-canonical mode II binding-motif of Cby

We used X-ray crystallography to elucidate the molecular basis of the 14-3-3ζ/Cby interaction. Purified 14-3-3ζ protein was co-crystallized with the phosphorylated Cby 18-mer (^{12}KTPPRKSA(pS)LSNLHSLDR^{29}) and diffraction data were collected to a resolution of 2.41 Å (Table 2.3). The 14-3-3ζ protein, which crystallized as the typical cup-shaped dimer [20], has the Cby peptide bound in an extended conformation to each 14-3-3 monomer (Figure 2.3 A). The dimer comprises the asymmetric unit of the crystal, and the visible electron density was slightly more extensive for the peptide bound to the B-chain of the dimer. Thus, of the 18 residues in the Cby peptide, eight residues, ^{18}SA(pS)LSNLH^{25}, were resolved in the peptide bound to the 14-3-3 B-chain (Figure 2.3 B) and seven residues, ^{18}SA(pS)LSNL^{24}, for that bound to the 14-3-3 A-chain (not shown). Both bound peptides adopted similar conformations and made the same interactions with the 14-3-3 protein. The lack of observable electron density for the remaining residues suggests that they remain flexible within the complex.

The overall structural features of the 14-3-3ζ/Cby complex are similar to that of other 14-3-3ζ/phosphopeptide complexes. The Cby peptide occupies the conserved binding groove of 14-3-3 with the same orientation as other phosphopeptides previously characterized. The hydrogen bonding potential of the phosphate group on pS20 is fully realized, with two hydrogen bonds made to each of R56 and R127, and another hydrogen bond to the side-chain hydroxyl of Y128 (Figure 2.3 C); 3 water molecules and the side chain of Cby-S22 mediate four additional hydrogen bonds to the phosphate oxygens. Thus, each of the phosphate oxygens has 3 hydrogen bonding partners positioned in an

Table 2.3 Crystallographic data collection and refinement statistics
Values in parentheses refer to the highest resolution shell.

Data Collection	
Wavelength (Å)	1.54179
Cell Parameters	
a, b, c (Å)	70.83, 71.96, 130.99
Space group	$P2_12_12_1$
Resolution (Å)	65.49 – 2.41 (2.53-2.41)
Total reflections	139,670 (16,075)
Unique reflections	26,474 (3445)
R_{merge}	0.072 (0.516)
Completeness (%)	98.4 (89.5)
Multiplicity	5.3 (4.7)
I/σ(I)	13.9 (3.2)
Refinement	
R_{work}/R_{free} (%)	0.203/0.256
RMSD from ideal values	
Bonds (Å)	0.008
Angles (°)	1.12
Overall mean B values (Å^2)	
Protein	21.71
Peptide	26.69
Solvent	19.22
Number of amino acid residues per asymmetric unit	464
Number of water molecules	147
Ramachandran plot	
Favoured regions (%)	98
Allowed regions (%)	1.8
Disallowed regions (%)	0.2
Cβ deviations greater than 0.25 Å	0

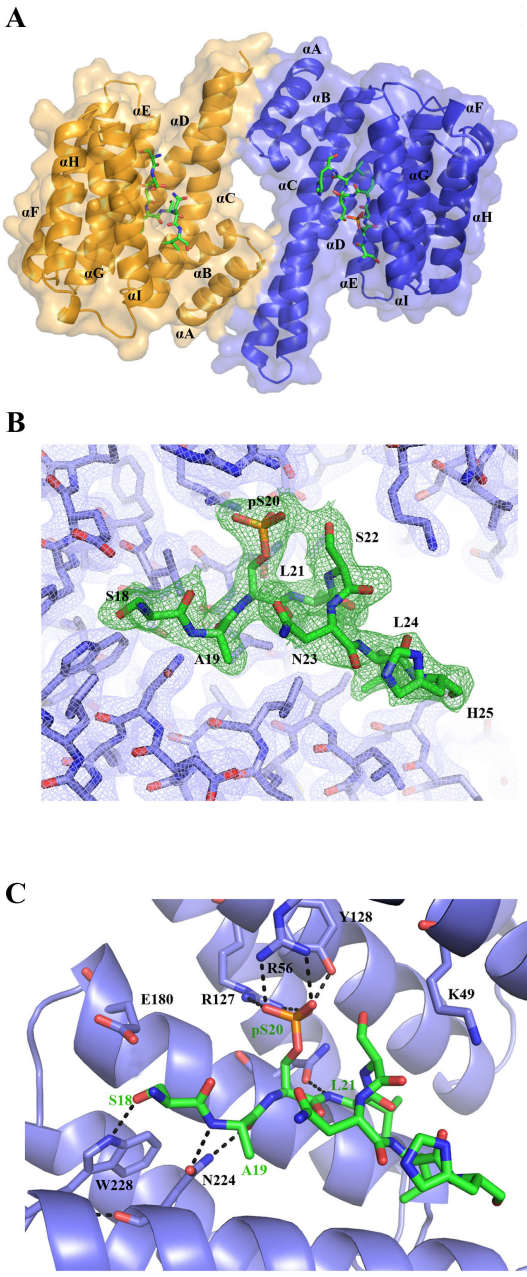

Figure 2.3 Crystal structure of the 14-3-3ζ/Cby 18-mer complex

A. Crystal structure of the 14-3-3ζ /Cby 18-mer complex. Each 14-3-3ζ monomer (coloured orange and blue) is bound to one Cby phosphopeptide. **B.** Final $2F_o - F_c$ electron density of 14-3-3ζ (blue mesh) and Cby 18-mer (green mesh) contoured to 1σ. **C.** Polar contacts (black hashed lines) between 14-3-3ζ residues (light blue sticks) and the Cby 18-mer (green sticks).

ideal tetrahedral arrangement, explaining why mutation of S20 to D or E fails to promote high affinity binding of Cby to 14-3-3ζ. The peptide is further coordinated by hydrogen bonds between the carboxamide of 14-3-3ζ-N224 with the backbone nitrogen and carbonyl of Cby-A19, the carboxamide of 14-3-3ζ-N173 to the backbone nitrogen of Cby-L21, and the side-chain of either E180 (chain-C) or W228 (chain-D) of 14-3-3ζ to the hydroxyl group on the side-chain of Cby-S18. Intra-chain contacts exist within the Cby peptide as well. On chain-D of the model, consisting of residues ^{18}SA(pS)LSNLH^{25}, the pS20 amide is hydrogen bonded to the N23 side-chain, the phosphate group itself on S20 hydrogen bonds with the hydroxyl group on the S22 side-chain, the pS20 carboxyl contacts both the amide and the side-chain of N23 and the carboxyl of L21 contacts the amide of L24.

2.3.4 An S22P mutation to Cby enhances its interaction to 14-3-3ζ

As mentioned, Cby comprises a serine (S22) in the +2 position to the phosphoserine, as opposed to the canonical proline. A comparison between the 14-3-3ζ/Cby structure with other 14-3-3ζ/phosphopeptide complexes with different +2 residues [including the canonical proline (Raf1), aspartate (PKCε [37]), glycine (Histone H3 [38]), threonine (β2 integrin [39]) and leucine (α4 integrin [40])], reveals that the S22 side chain is oriented uniquely, projecting between 14-3-3ζ residues R56 and K49 (Figure 2.4). Also, superimposition of these peptides onto Cby demonstrates that the backbones of residues -2 to +1 typically align well but diverge quickly C-terminally from the +2 residue.

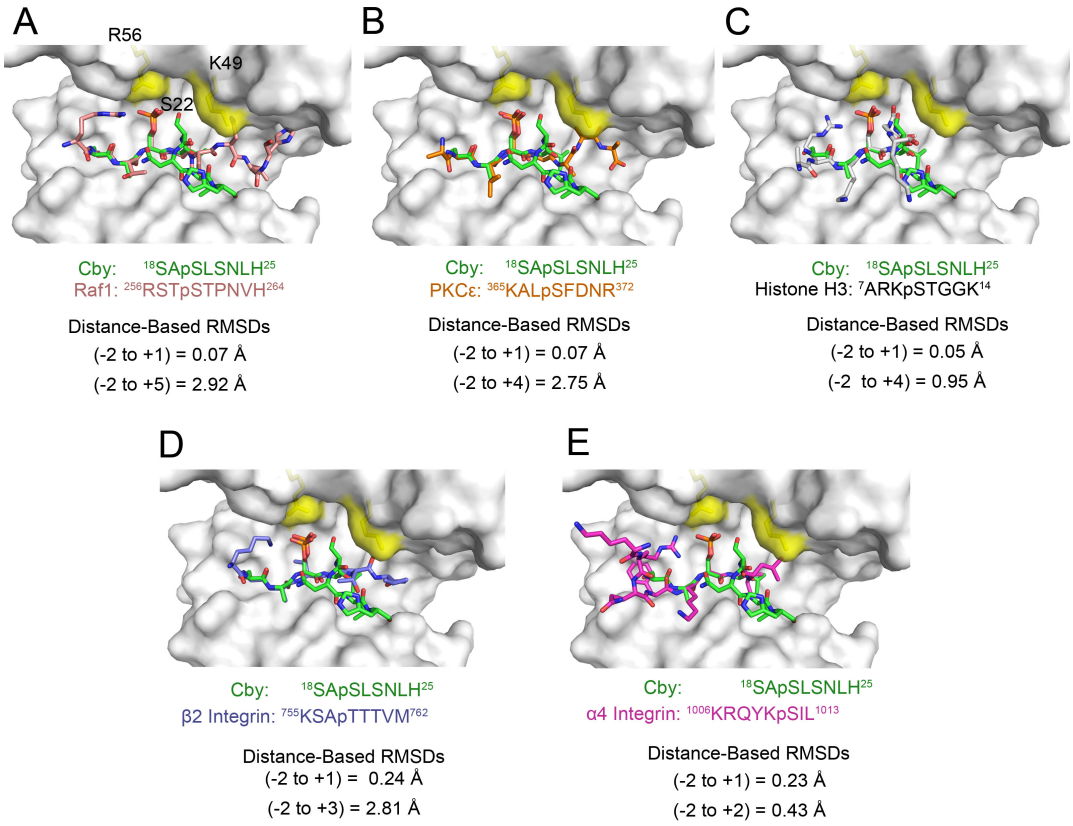

Figure 2.4 Structural comparison of 14-3-3ζ-bound Cby with other 14-3-3 binding motifs comprising various +2 residues

Residues K49 and R56 are coloured yellow on the white surface representation of 14-3-3ζ. Structural and sequence alignment of Cby (green sticks) with the binding-motifs of **A.** Raf1 (pink sticks, PDB: 3CU8), **B.** PKCε (orange sticks, PDB: 2WH0), **C.** Histone H3 (white sticks, PDB: 2C1N), **D.** β2 integrin (blue sticks, PDB: 2V7D) and **E.** α4 integrin (purple sticks. PDB: 4HKC). The Cα RMSD values were computed by subtracting a Cα distance matrix between the -2 and +1 residues of Cby and each peptide as well as the -2 and most C-terminal residue in the respective alignments.

With the side chain on Cby-S22 distinctively positioned relative to other +2 residues in 14-3-3/phosphopeptide structures, we sought to determine if mutating this serine to the canonical proline would have a significant effect on Cby's interaction with 14-3-3ζ. The same 7-mer, 13-mer and 18-mer Cby phosphopeptides used previously, but now containing the S22P mutation, were used in ITC experiments to determine the binding affinity to 14-3-3ζ (Table 2.1, Figure 2.2). Interestingly, for all S22P Cby peptides, the binding affinity was approximately 15-fold tighter for each peptide respective to its wild-type counterpart (for 7-mer, K_D ~3 versus ~44 μM; for 13-mer, K_D ~1 versus ~15 μM; for 18-mer, K_D ~360 nM versus ~5 μM). The increases in binding affinity for the three S22P mutant peptides were all due to more negative ΔH of binding. Moreover, the flanking residues within the S22P Cby peptides, like the WT, appear to play a role in the interaction as well. The Cby S22P 18-mer bound ~9 fold tighter than the S22P 7-mer, similar to the difference observed between the WT Cby 18-mer and 7-mer peptides.

In numerous crystal structures of 14-3-3 proteins in complex with phosphorylated S/T peptides, the conserved K49 (numbering refers to the ζ isoform) side-chain is observed forming a hydrogen bond with the phosphate group on pS/pT (illustrated in Figure 2.5 with an elucidated 14-3-3ζ/Raf1 structure). With Cby's S22 side-chain juxtaposed between 14-3-3ζ residues K49 and R56, the K49 side-chain is sterically hindered from contacting pS20. As such, we speculated that the increases in binding affinity to 14-3-3ζ observed for the S22P mutant peptides might be the result of the favorable contacts between K49 and pS20 facilitated by the proline-induced conformational changes. To test this, a K49A mutation was introduced into 14-3-3ζ and

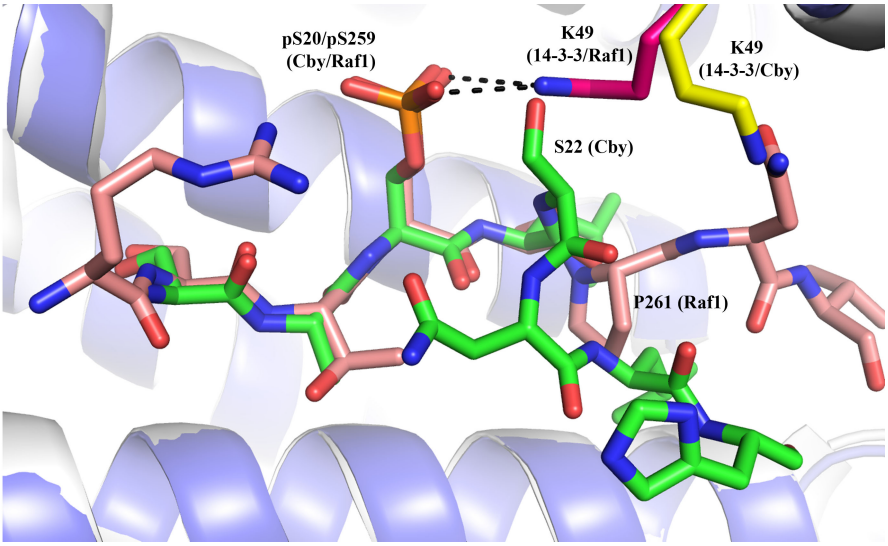

Figure 2.5 A comparison of the orientation of 14-3-3ζ's K49 side-chain in the 14-3-3ζ/Cby and 14-3-3ζ/Raf1 (PDB: 3CU8) complexes
Cby is represented by the green sticks and Raf1 by the light pink sticks. K49 in the 14-3-3ζ/Cby and 14-3-3ζ/Raf1 complexes is shown in yellow and dark pink, respectively.

ITC titrations were performed with 18-mer WT and S22P Cby peptides. Interestingly, the data show that the K49A mutation only had a minor effect (WT – 4.9 μM, K49A – 5.5 μM, ΔΔG ~ 0.1 kcal/mol) on the binding to the WT Cby peptide, however, the mutant bound with lower affinity to the S22P Cby peptide compared to the WT 14-3-3ζ (WT – 0.38 μM, K49A – 1.8 μM, ΔΔG ~ 1.0 kcal/mol) (Table 2.1 and 2.2, Figure 2.6). Therefore, K49 appears to at least partially responsible for the enhanced binding affinity observed between WT 14-3-3ζ and the S22P Cby peptide.

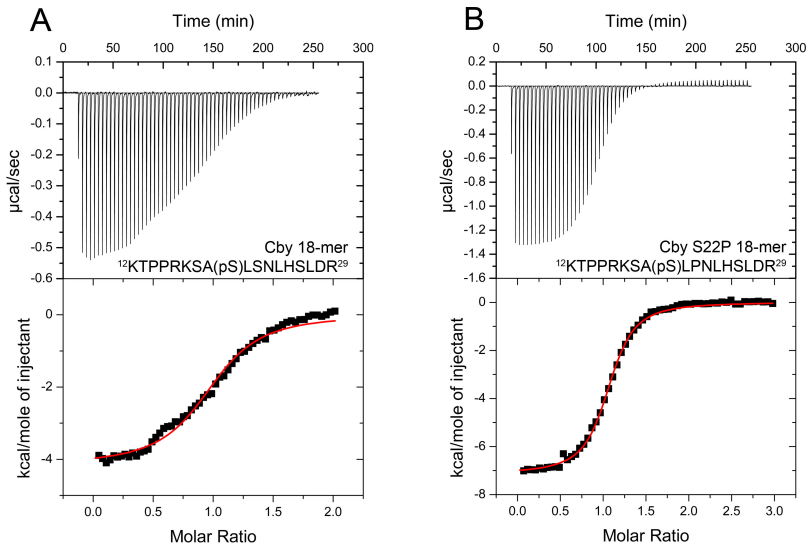

Figure 2.6 14-3-3ζ K49A ITC thermograms

ITC thermograms for the **A.** WT Cby 18-mer and **B.** Cby S22P 18-mer titrated to 14-3-3ζ K49A.

2.3.5 Probe for secondary interactions between 14-3-3ζ and Cby using NMR spectroscopy

The crystal structure of 14-3-3ζ/Cby complex clearly reveals the molecular basis of primary interactions between 14-3-3ζ and the non-canonical mode II binding motif within Cby. However, like most of the 14-3-3/phosphopeptide structures available to date, the

lack of electron density for residues outside the phosphorylated binding motif of Cby hinders our understanding of the secondary interactions in complex formation. Notably, our ITC results showed that the Cby 18-mer (^{12}KTPPRKSA(pS)LSNLHSLDR^{29}) used in the crystallographic study has a significantly higher affinity compared to the 7-mer (^{16}RKSA(pS)LS^{22}; the minimal 14-3-3 binding motif) for 14-3-3ζ. However, only residues ^{23}NLH^{25} outside the minimal binding motif were observable in the crystal structure. Of the three, only the L24 side-chain is buried within the interface, projecting toward a hydrophobic patch consisting of 14-3-3ζ residues L216 and I217. Intriguingly, immunoprecipitation experiments performed by Li *et al.*[14] demonstrated that an alanine substitution at L24 on Cby abolished binding to 14-3-3ζ. Our ITC titrations with the Cby 18-mer comprising the L24A mutation revealed that its interaction with 14-3-3ζ was indeed impaired but not abolished, binding approximately 4-fold weaker than the wild-type peptide with a K_D ~21 μM (Table 2.1 and 2.2, Figure 2.2). To gain a more thorough understanding of the secondary interactions between 14-3-3ζ and Cby, we sought to determine if there are additional regions in 14-3-3ζ that interact with the Cby 18-mer compared to the 7-mer using NMR chemical shift mapping, a powerful technique for identifying binding interfaces in solution.

Due to the relatively high molecular weight of the 14-3-3ζ dimer (~56 kDa), deuterated protein samples were used in our NMR studies. An initial ^{1}H-^{15}N TROSY-HSQC spectrum of 14-3-3ζ displayed many well-dispersed resonance signals along with a small number of extremely intense peaks (Figure 2.7). These strong peaks do not display any chemical shift changes upon titration of the unlabeled 18-mer Cby peptide, indicating that their corresponding residues are not involved in the interaction (Figure

2.7). However, their presence in the ^{1}H-^{15}N TROSY-HSQC spectrum unavoidably complicates the spectral analysis by masking many underlying resonances. We speculated that these high intensity resonances originate from 14-3-3ζ's C-terminal tail, which has been shown to be disordered [41]. With this in mind, we have generated the 14-3-3ζΔC12 construct, which is full-length 14-3-3ζ with the C-terminal 12 residues being removed. The ^{1}H-^{15}N TROSY-HSQC of 14-3-3ζΔC12 overlays almost perfectly with that of 14-3-3ζ, except that the highly intense peaks are no longer observable, confirming that these resonances originate from the C-terminal tail. Importantly, ITC experiments show that 14-3-3ζΔC12 binds to Cby peptides with almost the same affinity as full-length 14-3-3ζ (Table 2.1 and 2.2, Figure 2.8).

Backbone resonance assignments for $^{1}H^{N}$, ^{15}N, $^{13}C\alpha$ and $^{13}C\beta$ were obtained for 14-3-3ζΔC12 (Figure 2.9 A). We were able to assign 82 % of the $^{1}H^{N}$ and ^{15}N resonances of non-proline residues, 81 % of all $^{13}C\alpha$ and 81 % of all $^{13}C\beta$ resonances. The presence of weak peaks prevented a higher percentage of resonance assignments. The residue-specific secondary structure propensity (SSP) scores using $^{13}C\alpha/\beta$ chemical shifts [42] indicate that the protein is, as expected, largely α-helical (Figure 2.9 B).

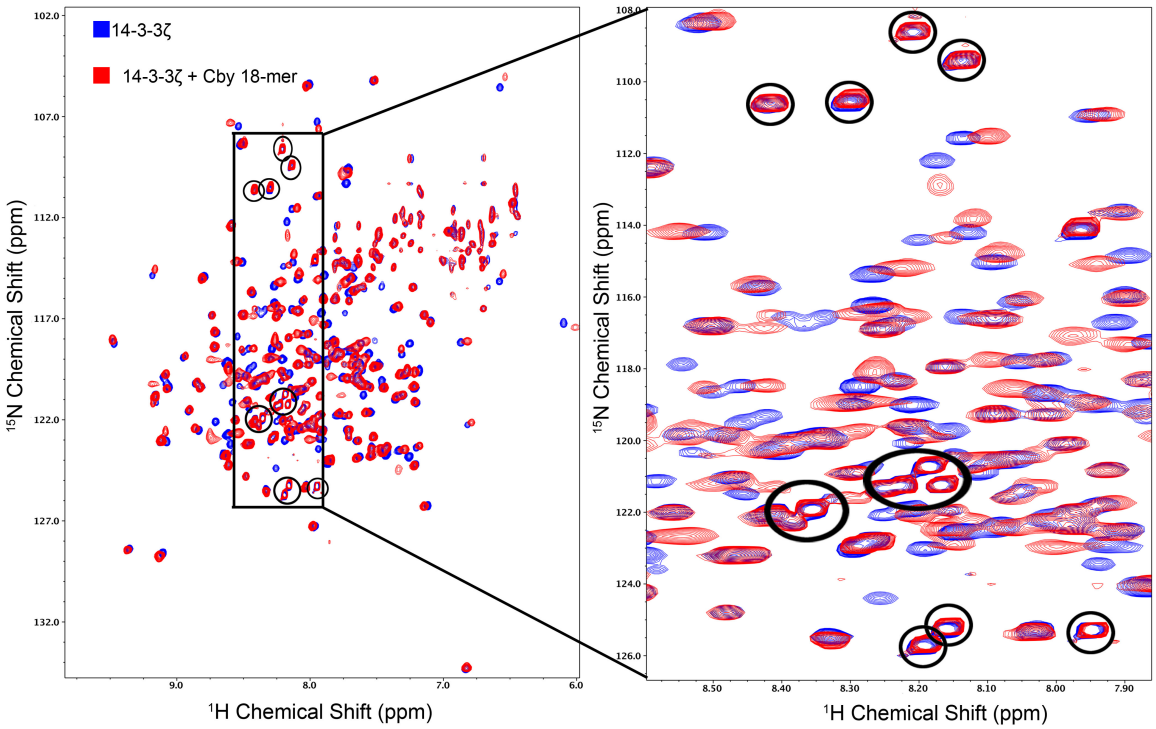

Figure 2.7 ^{1}H-^{15}N TROSY-HSQC of ^{2}H/^{13}C/^{15}N 14-3-3ζ in the absence (blue) and presence of a 1:1 molar ratio of the Cby 18-mer (red).
Circled resonances represent the intense signals arising from 14-3-3ζ's disordered C-terminal tail. A zoomed-in view displays the intense signals derived from 14-3-3ζ's disordered C-terminal tail.

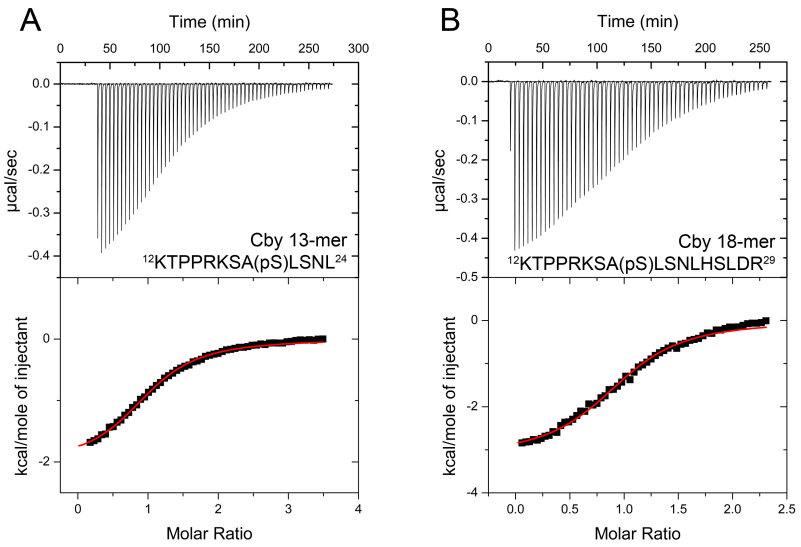

Figure 2.8 ITC thermograms for 14-3-3ζΔC12
ITC thermograms for the **A.** Cby 13-mer and **B.** Cby 18-mer titrated to 14-3-3ζΔC12.

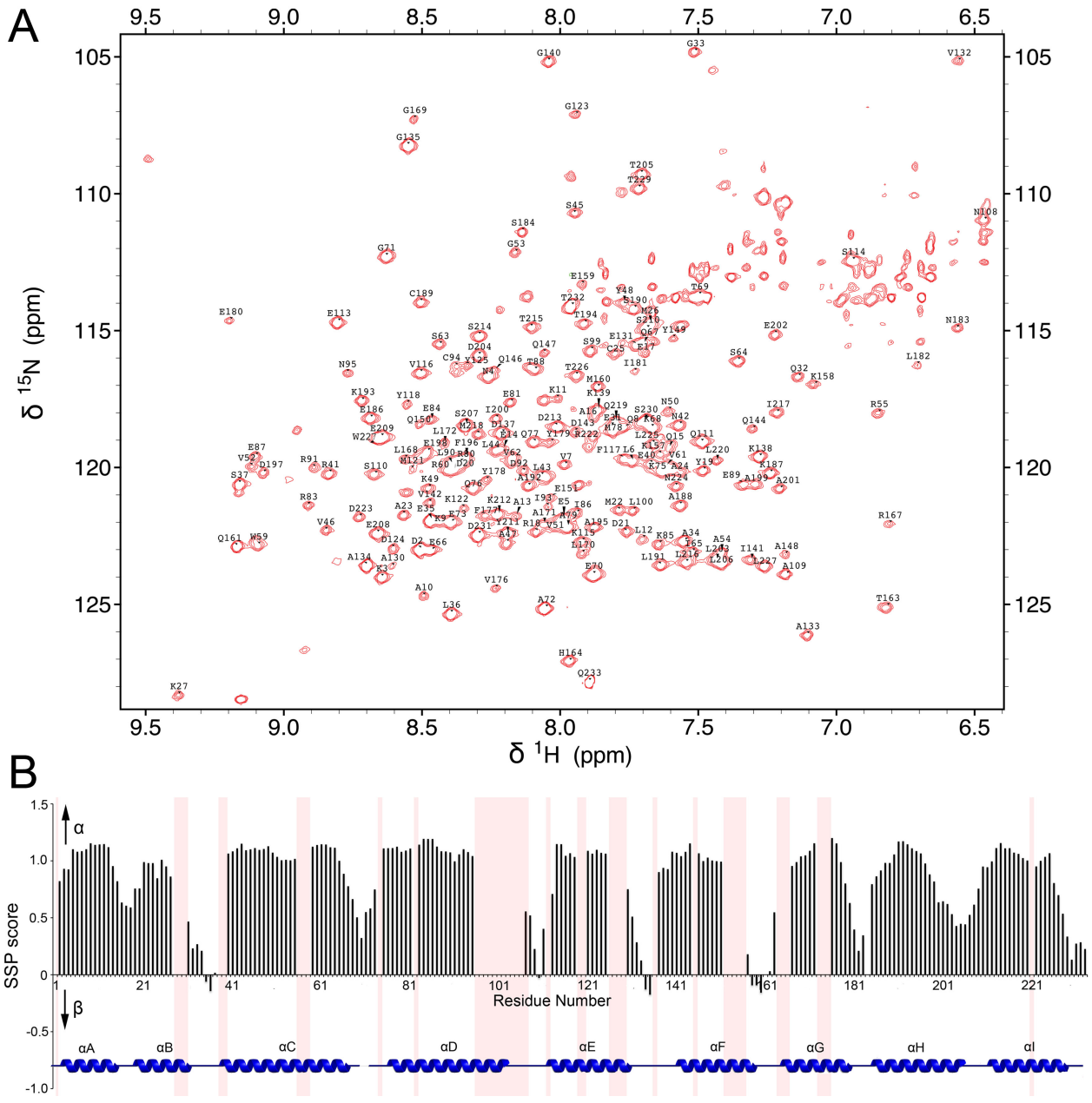

Figure 2.9 Backbone resonance assignment of 14-3-3ζΔC12
A. ^{1}H-^{15}N TROSY-HSQC spectrum and backbone resonance assignment of ^{2}H/^{13}C/^{15}N labeled 14-3-3ζΔC12. **B.** Secondary structure propensity (SSP) scores for 14-3-3ζΔC12. SSP scores were calculated based upon the ^{13}Cα/β chemical shifts.

2.3.6 Mapping the Cby peptides binding regions on 14-3-3ζΔC12

The nearly complete backbone assignment of 14-3-3ζΔC12 affords an opportunity to map the binding regions of different Cby peptides on 14-3-3ζ in a highly efficient manner. The 7-mer and 18-mer Cby peptides were titrated to 14-3-3ζΔC12 in a series of NMR experiments to a final molar ratio of 3:1 (peptide:protein) for chemical shift mapping (Figure 2.10 A). When comparing the ^{1}H-^{15}N TROSY-HSQC spectra of 14-3-3ζΔC12 in the apo and the 7-mer/18-mer Cby bound forms, a large number of chemical shift changes as well as peak broadenings are observed. The chemical shift perturbations were calculated for both titration sets and were mapped onto the 14-3-3ζ/Cby structure (Figure 2.11 B & C, Figure 2.12 A). From the generated maps, the residues exhibiting the largest chemical shift changes for both peptides are found within helices αC, αE and αI, matching well with the binding interface observed in the crystal structure (Figure 2.11 A). Additional peaks within the binding cleft were broadened out over the course of the titrations. For the Cby 18-mer titration, these peaks include M121, D124, Y125 and A130 within αE, L170, L172, V176 and Y178 within αG, and I217, L220 and R222 within αI. Broadened resonances within the binding cleft are similar for the Cby 7-mer titration, including F117, M121, D124 and A130 within αE, L170, L172, V176, F177 and Y178 within αG, and Y211 within αI. Even though residues that bond with the phosphate group of S20 on Cby, R56, R127 and Y128, could not be assigned, residues surrounding this basic patch either broaden out (M121, D124, Y125, V176) or exhibit large chemical shift changes (V52, G53) as expected. Large chemical shift perturbations or broadened resonances were not observed along the 14-3-3ζ dimer interface for either peptide.

Notably, the Cby 18-mer binding interface appears to be larger than that of the pCby 7-mer. Many 14-3-3ζ residues within the loop between αH and αI (204-208), along with N-terminal residues of αI (209-215) exhibit larger chemical shift perturbations when titrated with the Cby 18-mer compared to the Cby 7-mer (Figure 2.13). Based on the orientation of the peptide, we speculate that this region of 14-3-3 interacts with the C-terminal (^{26}SLDR^{29}) residues on the Cby 18-mer peptide.

Additional NMR titration experiments were performed with the Cby S22P 18-mer to compare its binding interface with the WT. The chemical shift analysis (Figure 2.10 B and 2.12 B) and subsequent mapping onto the 14-3-3ζ/Cby structure (Figure 2.11 D) revealed a similar interface to that observed for the Cby WT 18-mer. Interestingly, while the resonance signals of some residues in the αH - αI loop and residues within the 209-215 range in αI shift similarly when titrated with the WT or S22P peptides, the T205, L206, E209 and S210 peaks have much smaller shifts when titrated with the Cby S22P 18-mer. Having a proline at the +2 position may affect how the downstream C-terminal residues interact with this loop region.

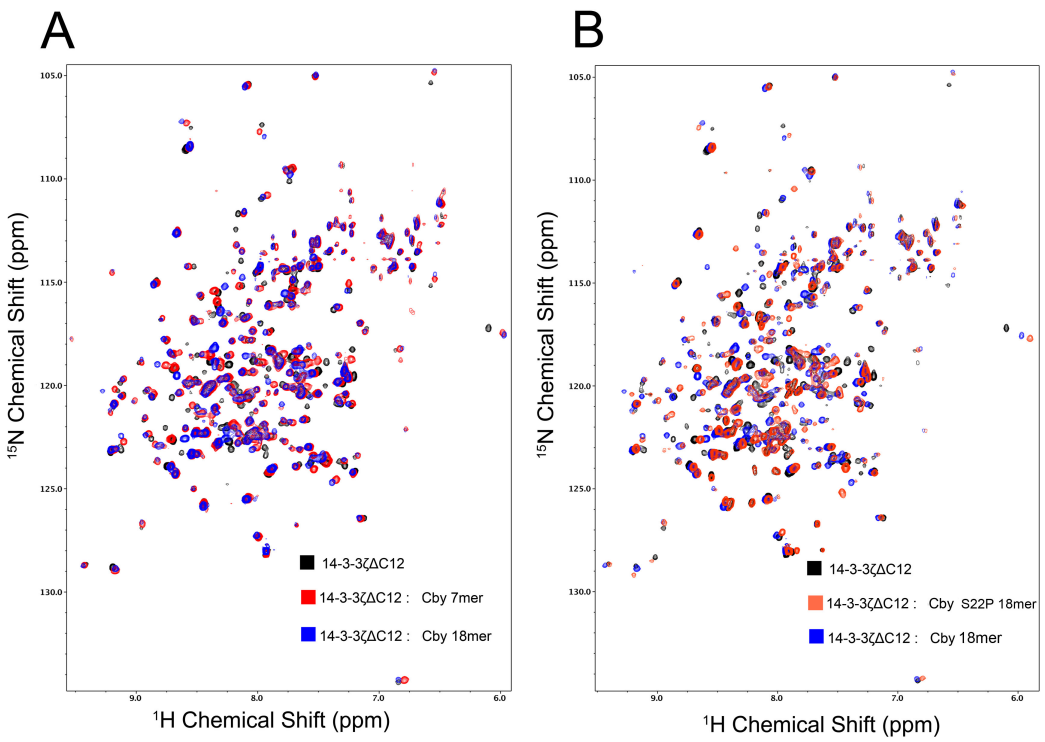

Figure 2.10 NMR titration experiments of 14-3-3ζΔC12 with Cby peptides
A. ^{1}H-^{15}N TROSY-HSQC spectra of 14-3-3ζΔC12 alone (black) and with 3 molar equivalents of the Cby 7-mer (red) and Cby 18-mer (blue). **B.** ^{1}H-^{15}N TROSY-HSQC spectra of 14-3-3ζΔC12 alone (black) and with 3 molar equivalents of the WT Cby 18-mer (blue) and Cby S22P 18-mer (blue).

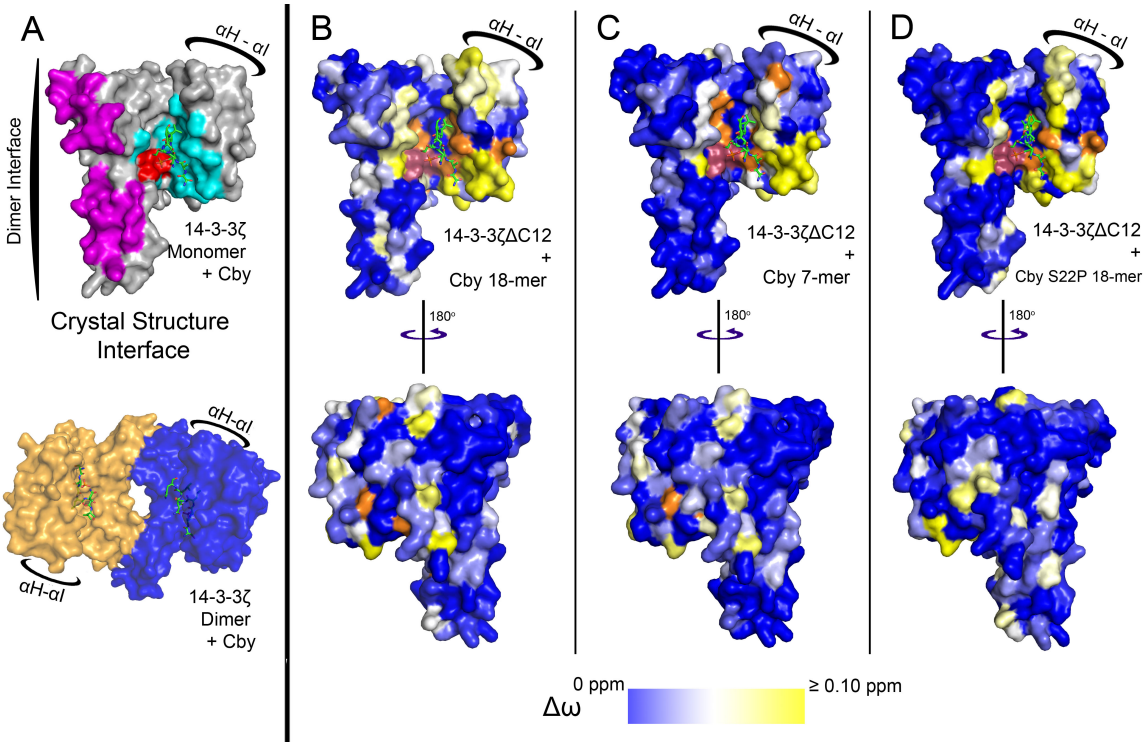

Figure 2.11 The mapping of chemical shifts on the crystal structure of the 14-3-3ζ/Cby complex

Due to the crowding of some peaks, the chemical shifts of some residues could not be confidently traced and were excluded from the analysis. **A**. (Above) A monomer of the 14-3-3ζ/Cby crystal structure interface based on Cby residues (^{18}SApSLSNLH^{25}). Residues R56, R127 and Y128 which contact the Cby phosphate group are coloured red, residues interfacing the peptide are coloured cyan, and 14-3-3ζ residues coloured magenta are found along the 14-3-3 dimer interface. (Below) The 14-3-3ζ dimer bound to Cby. **B.** (Cby 7-mer), **C.** (Cby 18-mer) and **D.** (Cby S22P 18-mer). Residues with traceable assigned resonances are coloured on a blue – white –yellow gradient (0 ppm to 0.1 ppm) based on their combined chemical shift [$\Delta\omega = ((\Delta\delta^{1}H)^{2} + (0.2*\Delta\delta^{15}N)^{2})^{1/2}$] at a 3:1 peptide:protein ratio. Residues coloured in orange represent peaks that broadened out to disappearance upon addition of peptide. Residues R56, R127 and Y128 are coloured pink.

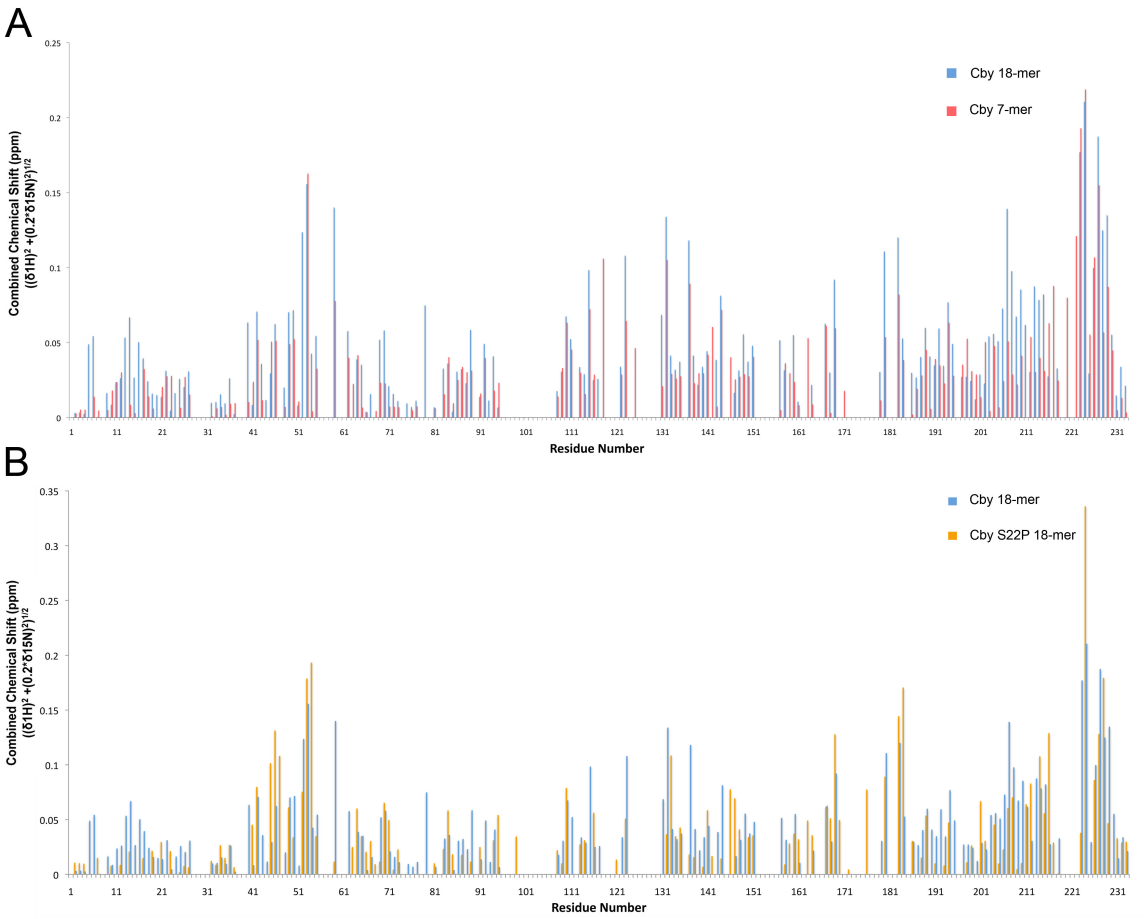

Figure 2.12 Composite $^{1}H_{N}$ and ^{15}N chemical shift perturbation analysis
Composite $^{1}H_{N}$ and ^{15}N chemical shift perturbation [$\Delta\omega = ((\Delta\delta^{1}H)^{2} + (0.2*\Delta\delta^{15}N)^{2})^{1/2}$] analysis of 14-3-3ζΔC12 in the presence of three molar equivalents of the **A.** Cby 7-mer, **A. + B.** Cby 18-mer and **B.** Cby S22P 18-mer. Due to the crowding of some peaks, the chemical shifts of some residues could not be confidently traced and were excluded from the analysis.

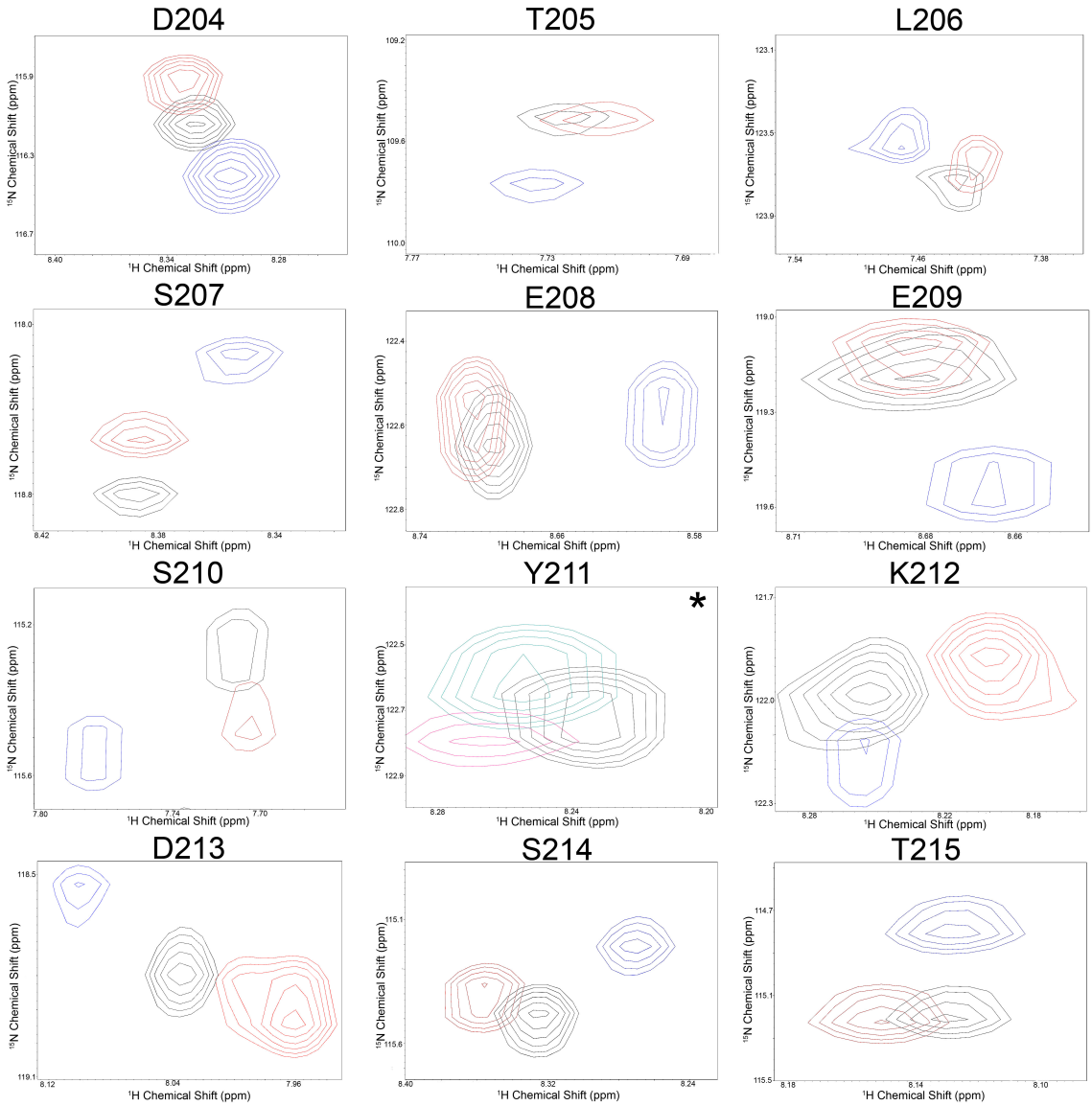

Figure 2.13 Observed chemical shifts for 14-3-3ζΔC12 residues 204-215
Resonances shown for each residue include the apo state (black), Cby 18-mer bound-state (blue) and the pCby 7-mer bound-state (red), at a 3:1 (pCby: 14-3-3ζΔC12) ratio. *Residue Y211 is displayed at a 1.25:1 (Cby: 14-3-3ζΔC12) ratio as it broadens out to disappearance at a 3:1 ratio with the Cby 7-mer. The Cby-18-mer bound-state is shown in cyan with the 7-mer bound-state in magenta.

2.3.7 Cby binds to all human 14-3-3 isoforms

From pull-down and coimmunoprecipitation experiments, Li *et al.* [13] found that in addition to the 14-3-3ζ isoform, Cby interacts with the ε and η isoforms. ITC experiments were designed to test whether Cby can bind to all human 14-3-3 isoforms and to determine whether there are any large differences in affinity across the isoforms. The ITC profiles for the Cby 18-mer/14-3-3 isoforms are shown in Figure 2.14 and the fitted data are tabulated in Table 2.4 and 2.5. The Cby 18-mer peptide bound to all seven isoforms with a spectrum of high nanomolar to low micromolar affinity, ranging from ~ 500 nM for the η isoform to ~ 11 μM for the ε isoform.

2.3.8 14-3-3 phosphomimetic mutations fail to abrogate the 14-3-3/Cby 18-mer interaction

Further to the importance of 14-3-3 linker regions in target recognition, Mancini *et al.* [49] suggested that phosphorylation at serine 186 on 14-3-3σ by the c-Jun N-terminal kinase (JNK) promotes the dissociation of Cby. Serine 186, located in the αG-αH linker on 14-3-3σ, along with the corresponding residue on the ζ isoform, S184, were each mutated to glutamate as a phospho-mimetic. Their binding to the Cby 18-mer was measured by ITC (Figure 2.15, Table 2.4 and 2.5) and no significant difference in binding affinity was observed for either mutant. Phosphomimicry may not be enough to promote dissociation of the complex.

Table 2.4 Thermodynamic parameters of Cby 18-mer binding to all 14-3-3 isoforms

Thermodynamic parameters for the binding of ^{12}KTPPRKSA(pS)LSNLHSLDR^{29} Cby 18-mer peptide to human 14-3-3 isoforms and mutants at 25°C.

Isoform	n[a]	K_d[b] (10^{-6} M)	ΔH[b] (kcal/mol)	$T\Delta S$[b] (kcal/mol)	ΔG[b] (kcal/mol)
14-3-3η	0.97 ± 0.00(2)	0.57 ± 0.02	-10.31 ± 0.05	-1.79	-8.53 ± 0.02
14-3-3γ	0.98 ± 0.00(4)	0.88 ± 0.04	-9.43 ± 0.06	-1.17	-8.27 ± 0.03
14-3-3β	0.95 ± 0.00(4)	1.45 ± 0.06	-11.56 ± 0.07	-3.61	-7.97 ± 0.02
14-3-3ζ	0.88 ± 0.00(4)	2.50 ± 0.10	-9.70 ± 0.07	-2.05	-7.65 ± 0.02
14-3-3ζ S184E	0.98 ± 0.00(4)	1.21 ± 0.05	-7.47 ± 0.04	0.61	-8.08 ± 0.04
14-3-3θ	0.93 ± 0.01	4.35 ± 0.14	-7.73 ± 0.06	-0.41	-7.32 ± 0.02
14-3-3σ	0.93 ± 0.01	5.02 ± 0.18	-7.88 ± 0.09	-0.65	-7.23 ± 0.02
14-3-3σ S186E	0.94 ± 0.00(5)	3.80 ± 0.04	-6.70 ± 0.05	0.69	-7.39 ± 0.06
14-3-3ε	0.85 ± 0.04	12.92 ± 0.81	-9.14 ± 0.50	-2.47	-6.67 ± 0.04

[a] Binding stoichiometry of monomeric 14-3-3 and Cby peptide.
[b] K_d is the dissociation constant. ΔH, ΔS and ΔG are the change in enthalpy, entropy and Gibbs free energy upon binding at T=298.15 K, respectively.

Table 2.5 Duplicate thermodynamic parameters for the binding of Cby 18-mer to 14-3-3 isoforms

Thermodynamic parameters for the binding of ^{12}KTPPRKSA(pS)LSNLHSLDR^{29} Cby peptide to human 14-3-3 isoforms and mutants at 25°C obtained using ITC.

Isoform	n[a]	K_d[b] (10^{-6} M)	ΔH[b] (kcal/mol)	$T\Delta S$[b] (kcal/mol)	ΔG[b] (kcal/mol)
14-3-3η	0.88 ± 0.00(2)	0.46 ± 0.03	-10.73 ± 0.04	-2.08	-8.65 ± 0.03
14-3-3γ	1.02 ± 0.03	0.63 ± 0.03	-9.67 ± 0.06	-1.21	-8.47 ± 0.03
14-3-3β	0.90 ± 0.01	2.08 ± 0.11	-11.57 ± 0.11	-3.81	-7.76 ± 0.03
14-3-3ζ	0.87 ± 0.01	2.85 ± 0.14	-10.06 ± 0.09	-2.49	-7.57 ± 0.03
14-3-3ζ S184E	1.02 ± 0.00(3)	1.29 ± 0.04	-7.23 ± 0.03	0.80	-8.03 ± 0.03
14-3-3θ	0.94 ± 0.00(5)	4.44 ± 0.17	-7.64 ± 0.06	-0.34	-7.31 ± 0.02
14-3-3σ	0.88 ± 0.01	4.29 ± 0.21	-8.34 ± 0.11	-1.02	-7.33 ± 0.03
14-3-3σ S186E	0.92 ± 0.00(5)	3.63 ± 0.04	-6.67 ± 0.05	0.75	-7.42 ± 0.06
14-3-3ε	0.80 ± 0.03	10.59 ± 1.05	-9.87 ± 0.54	-3.07	-6.79 ± 0.06

[a] Binding stoichiometry of monomeric 14-3-3 and Cby peptide.
[b] K_d is the dissociation constant. ΔH, ΔS and ΔG are the change in enthalpy, entropy and Gibbs free energy upon binding at T=298.15 K, respectively.

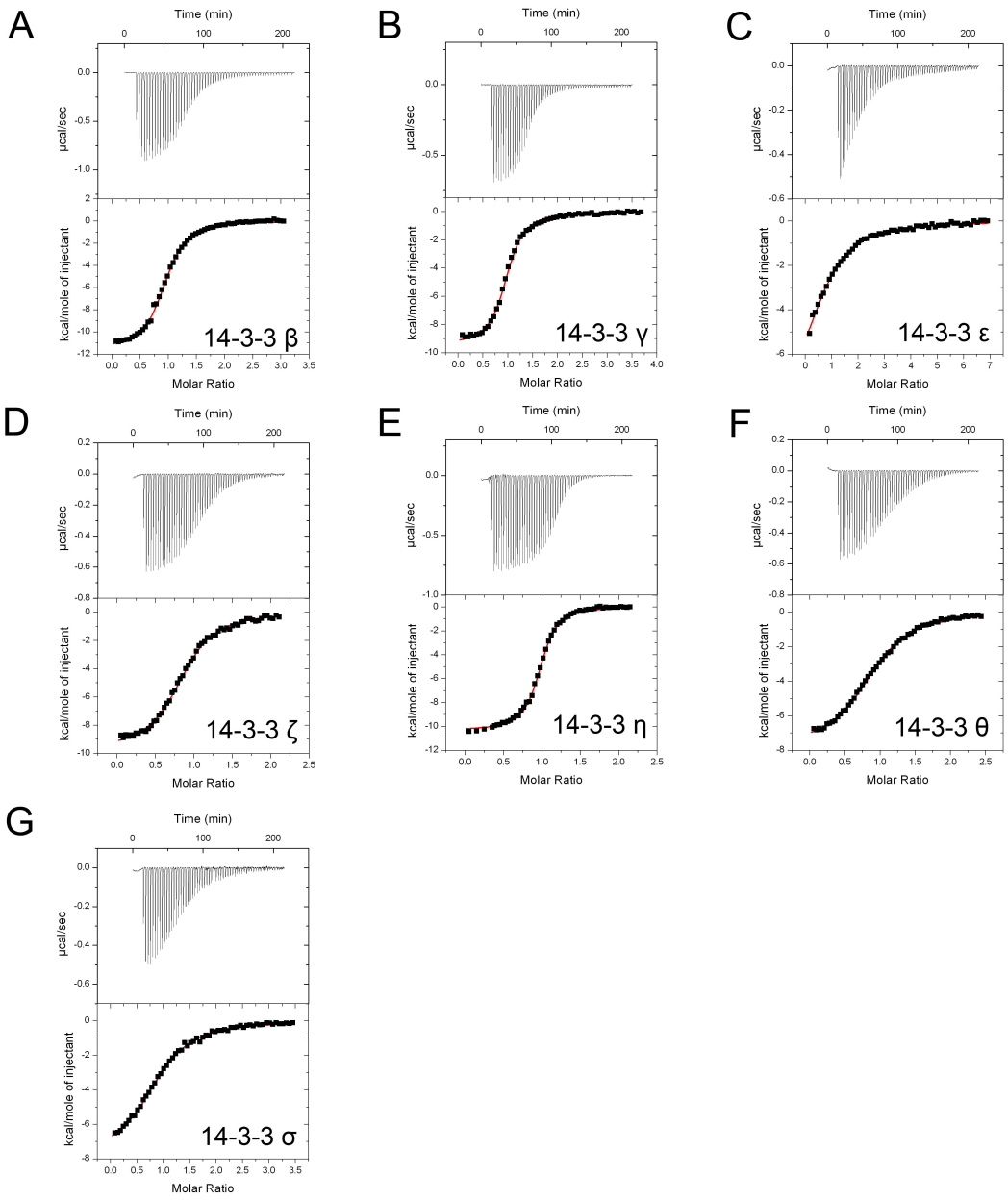

Figure 2.14 ITC thermograms for Cby 18-mer binding to all 14-3-3 isoforms
ITC thermograms for phosphorylated Cby 18-mer titrated into the seven human isoforms of 14-3-3. **A.** 14-3-3β **B.** 14-3-3γ **C.** 14-3-3ε **D.** 14-3-3ζ **E.** 14-3-3η **F.** 14-3-3θ **G.** 14-3-3σ

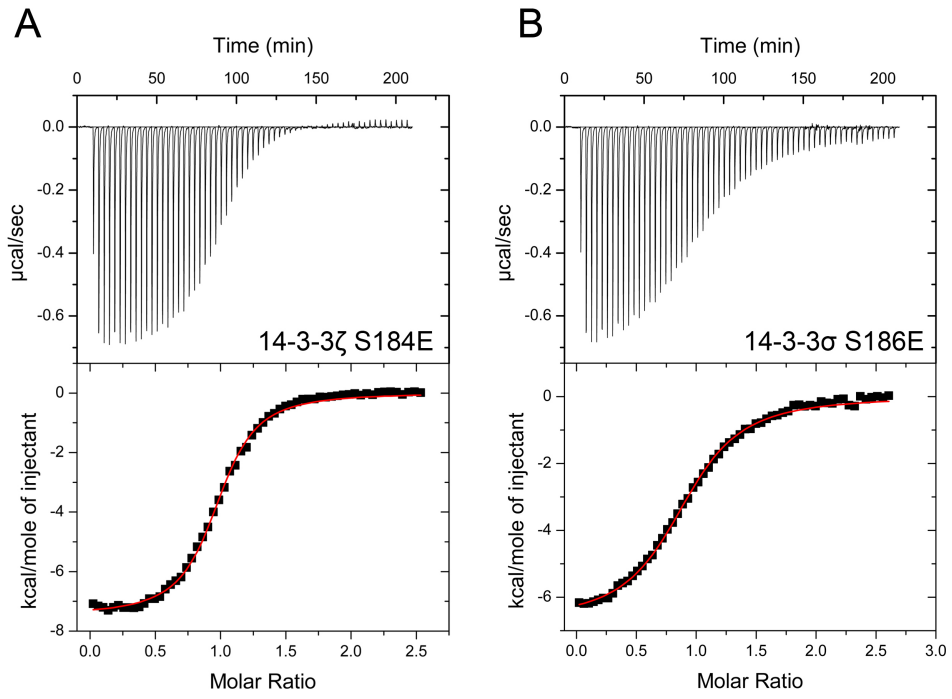

Figure 2.15 ITC thermograms for Cby 18-mer binding to 14-3-3 phosphomimetics
ITC thermograms for phosphorylated Cby 18-mer titrated into **A.** 14-3-3ζ S184E and **B.** 14-3-3σ S186E.

2.4 Discussion

The molecular basis of the interaction between 14-3-3ζ and Cby was extensively investigated by using a combination of X-ray crystallography, NMR spectroscopy, and ITC. Our ITC results show that even though phosphorylation of Cby-S20 is critical for the complex formation (as Cby peptides comprising S20D and S20E phospho-mimetics failed to bind to 14-3-3ζ), residues outside the 14-3-3 binding-motif also play an important role in the interaction. This is supported by the finding that a short, 7-residue phosphopeptide of Cby comprising the minimal 14-3-3 binding-motif bound 10-fold weaker compared to a longer, 18-residue phosphopeptide. A similar observation was made in a recent study of 14-3-3/α-integrin tail complexes, demonstrating that a 30-residue α4-integrin peptide comprising its 14-3-3-binding motif bound up to 15 times tighter to 14-3-3ζ than an 11-residue peptide [40]. Interestingly, in the same study, short and long phosphopeptides comprising the 14-3-3 binding motif for the β2-integrin bound with nearly the same high affinity, suggesting that secondary interactions from flanking residues are likely sequence specific.

Another interesting finding from our ITC experiments is that the phosphorylated Cby peptides comprising a mutation at the pS + 2 position to the canonical proline (S22P) bind ~15 fold tighter than the WT peptides. Our crystal structure provides molecular insight into the target binding specificity of 14-3-3. Based on available crystal structures of various 14-3-3 isoforms in complex with phosphorylated peptides comprising type I or type II binding motifs (for example, PDB: 1QJA [31], 1QJB [31], 3MHR [43]), the K49 (ζ sequence) side chain commonly forms a hydrogen bond with the phosphate group on pSer. However, in the 14-3-3ζ/Cby crystal structure, the side chain of S22 positions

between K49 and R56 of 14-3-3ζ and sterically hinders the interaction between K49 and pS20. Interestingly, introducing K49A mutation to 14-3-3ζ does not affect its affinity for the WT Cby peptide, but the binding affinity to the S22P peptide was reduced by ~5 fold. From these results, we speculate the S22P mutation of Cby promotes a conformational change in the bound state, allowing K49 on 14-3-3ζ to form hydrogen bond with the phosphate group on S20. However, it should be noted that there are examples of peptides containing a +2 proline co-crystallized with 14-3-3 proteins where K49 is either not making any direct contacts with the ligand (PDB: 4FL5) or it interacts with other residues within the phosphopeptides (PDB: 3UAL [44], 4IEA [45]) instead of the phosphorylation site. Additionally, a proline at the +2 position is not absolutely essential for a K49 – phosphate group interaction. This contact is observed in the 14-3-3γ/tyrosine hydroxylase structure (PDB: 4J6S [46]) and in the 14-3-3ζ/alpha-4 integrin, which both have a leucine at the +2 position.

With only 8 of the 18 residues in the Cby 18-mer peptide resolved in the crystal structure, it is likely that any secondary contacts made by flanking residues are very dynamic. This is a common issue in the co-crystallization of 14-3-3 proteins and peptides. Typically, only short regions (4-10 residues comprising residues nearby the pS/pT) within longer phosphopeptides are resolved. Because significant secondary interactions may be critical to 14-3-3ζ's interaction with Cby, we elected to pursue NMR spectroscopy as a means of further characterizing the complex.

Chemical shift analysis of ^{1}H-^{15}N TROSY-HSQC titration experiments, performed by titrating the 7-mer and 18-mer Cby peptides into isotopically labeled 14-3-3ζΔC12, allowed for chemical shift mapping to reveal any differences in the binding interface

between both peptides. We found that 14-3-3ζ residues 204-215 are involved in the interaction with the Cby 18-mer but not the 7-mer. Based on the orientation of the peptide in the crystal structure, this would correspond to the residues C-terminal to the pS20, ^{23}NLHSLDR^{29}, making transient contacts with this region of 14-3-3ζ. Chemical shift analysis of the Cby S22P 18-mer bound to 14-3-3ζΔC12 revealed a similar binding site to that of the WT 18-mer, however some variability in shifts for residues within the 204-215 range were observed. This suggests that the +2 residue can affect how downstream C-terminal residues interact with 14-3-3ζ. A +2 proline is of particular interest because while it is most commonly observed bound in a *trans* conformation (e.g. 1QJA [31]) it has been observed bound in the *cis* conformation (e.g. 1QJB [31]).

Residues 203-210, corresponding to 14-3-3ζ's αH-αI linker, have been shown to be part of a secondary binding site with another 14-3-3 target [30]. The crystal structure of the 14-3-3ζ/phosphorylated-AANAT complex, the only full-length protein to be solved in complex with 14-3-3, demonstrates that this linker is used by 14-3-3ζ to bind AANAT, highlighted by the 14-3-3ζ residue E208 making a salt bridge with R53 of phosphorylated AANAT, located in the globular region of the protein. Additionally, this linker region has been implicated in ligand discrimination between 14-3-3 isoforms [47,48]. For instance, the phosphatase Cdc25C can bind to all 14-3-3 isoforms except for σ; however, the mutation of divergent residues within 14-3-3σ's αH-αI linker to those conserved across all other isoforms enables the engineered σ to bind Cdc25C [48]. When we tested the binding of the Cby 18-mer to all 14-3-3 isoforms, a high nanonmolar to low micromolar spectrum of affinities was observed. The differences in affinity among the 14-3-3s may be attributed to sequence variations along the αH-αI or αG-αH linkers of

the isoforms. There are potentially greater differences in affinity across isoforms in the context of full-length Cby.

Building on this work, future studies may elucidate how the complex forms in the context of full-length Cby. It is conceivable that two Cby molecules could retain a coiled-coil structure while each is bound to 14-3-3ζ (Figure 2.16). Because of the orientation each 14-3-3ζ monomer adopts upon dimerization, the Cby residues lying on the C-terminal end of serine 20 will exit the binding interface at opposing ends of the 14-3-3ζ dimer. Since the N-terminal residues (1-64) of full-length Cby are disordered [19] it is feasible that each bound Cby molecule retains the flexibility necessary to orient itself to form a coiled-coil from residues 73-100, as well as to bind to the 88-kDa β-catenin. The model (Figure 2.16) is consistent with the results of Li *et al.*[13], which demonstrated that binding of Cby to β-catenin is not interfered by the increased level of 14-3-3. We are aware that a Cby dimer binding to the 14-3-3 dimer could presumably lead to a stronger interaction between the two molecules than what was reported in this study due to avidity. How the complex ultimately forms, i.e. its stoichiometry and conformation, will aid in providing the mechanistic basis by which the two proteins recruit β-catenin to form a trimolecular complex and promote β-catenin's nuclear exclusion.

Also of interest is the interplay of Cby's interactions with 14-3-3 and CRM1. Cby's 14-3-3 binding motif is juxtaposed with its nuclear export signal (NES) (^{21}LSNLHSLDR^{29}). Immunoprecipitation experiments by Li *et al.* [14] revealed that 14-3-3 enhanced the Cby-CRM1 interaction in a dose-dependent manner. It was postulated that 14-3-3 might induce a conformational change in Cby to expose its NES for CRM1

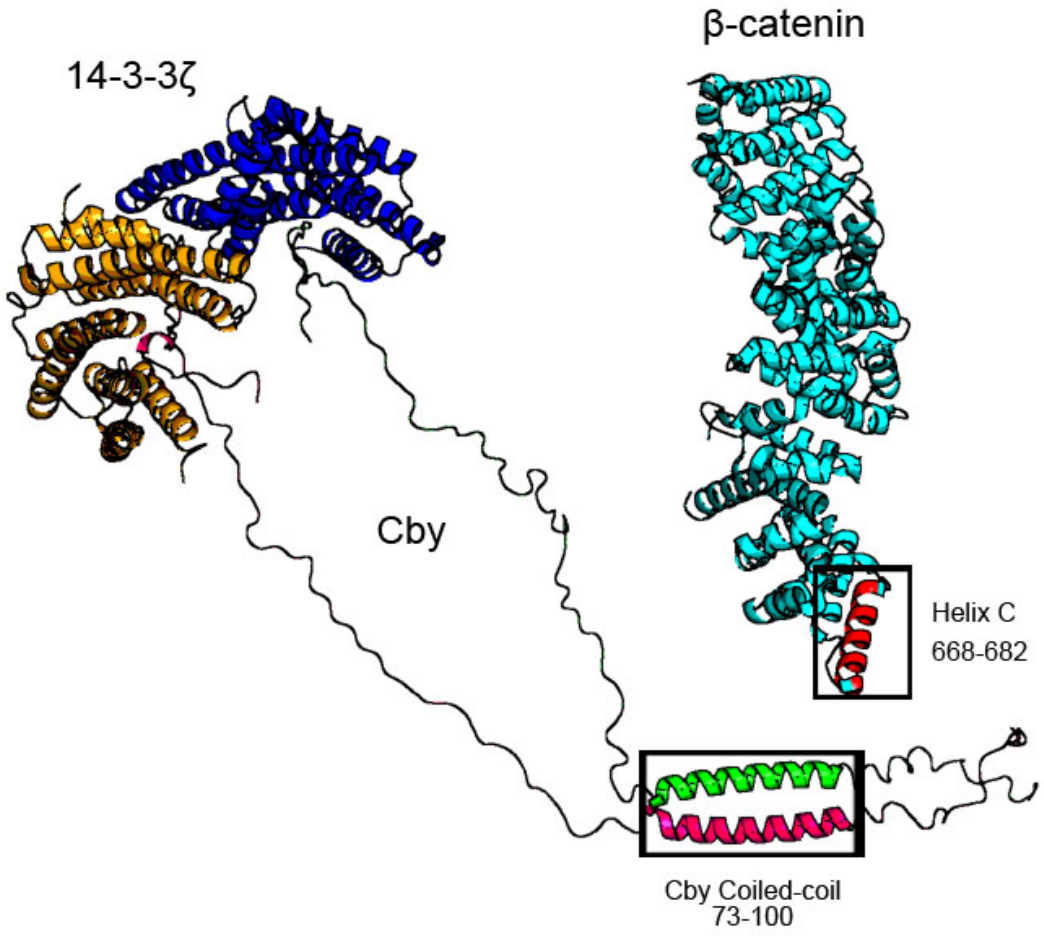

Figure 2.16 The 14-3-3ζ, Cby, β-catenin tripartite complex.
Model of dimeric 14-3-3ζ bound to two molecules of full-length Cby. The models of two full-length Cby proteins have disordered residues 30–73 of the N-terminus and 100–126 of the C-terminus presented in a highly extended fashion, and are shown forming a coiled-coil from residues 73–100. β-catenin (PDB: 2Z6H) is shown with its Cby binding-site (helix C) in red which then binds along the C-terminus (64–126) of Cby.

recruitment. In doing so, CRM1 could then mediate the nuclear exclusion of Cby. Our crystal structure demonstrates that this mechanism may not be the case. The consensus NES sequence is $\Phi^1(X_{2-3})\Phi^2(X_{2-3})\Phi^3X\Phi^4$, where Φ represents critical hydrophobic residues L, I, V, F or M and X is any amino acid [50,51]. In determined crystal structures of CRM1/target complexes, the critical hydrophobic residues are buried in a hydrophobic cleft formed by HEAT repeats 11 and 12 of CRM1 [52,53]. The hydrophobic residues on Cby's NES correspond to L21, L24 and L27. From our 14-3-3/Cby crystal structure, the L21 and L24 sidechains are projected toward 14-3-3's binding cleft, making them inaccessible for CRM1. Residues (^{26}SLDR^{29}) are unobservable in our structure and thus their accessibility remains unknown. However, Li *et al.* [14] demonstrated that a L27A mutation to Cby did not affect the Cby/CRM1 interaction, and showed normal, WT subcellular distribution. Meanwhile, L21A and L24A mutations abolished the interaction with CRM1 and led to the nuclear sequestration of Cby. As such, 14-3-3 may need to be dissociated from Cby to allow for the CRM1 interaction. Further cell experiments and structural studies of the Cby/CRM1 complex are needed to comprehend how 14-3-3 and CRM1 work in concert to promote the cytoplasmic sequestration of Cby.

Finally, NMR studies are critical to the characterization of 14-3-3 interactions as their interactome is predicted to predominantly consist of disordered targets [27]. The backbone resonance assignment of 14-3-3ζ completed in this work therefore will not just facilitate the studies of 14-3-3ζ with Cby, it will be invaluable for probing interactions between 14-3-3ζ and a continually growing list of protein targets by NMR. Such studies may allow the identification of ligand-binding interfaces on 14-3-3 in an efficient manner as illustrated in this work. Moreover, with 14-3-3ζ over-expression associated with

tumour progression and chemoresistance (reviewed in Matta *et al.* [54]), the protein is an attractive therapeutic target in cancer. With the availability of the backbone resonance assignment of 14-3-3ζ, NMR titration can be a quick way to test the binding/determine the binding site of small molecule or peptide 14-3-3 inhibitors [55,56]. Similarly, this may also be done for a number of recently discovered 14-3-3 protein-protein small-molecule stabilizers [55,56], which offer an alternative approach to modulating 14-3-3 activity.

2.5 Acknowledgements

This work was supported by the Canadian Institutes of Health Research (CIHR; MOP 74679) and Natural Sciences and Engineering Research (NSERC; RGPIN 06372-2014). We thank Kevin Leung for useful discussions on our X-ray crystallography experiments. We thank the Biomolecular NMR Facility, Macromolecular Crystallography Facility and the Biomolecular Interaction and Conformation Facility at the University of Western Ontario for their assistance and use of the facilities. We also acknowledge and thank the support from the NMR facility at the National University of Singapore.

2.6 References

1. Takemaru K, Yamaguchi S, Lee YS, Zhang Y, Carthew RW, et al. (2003) Chibby, a nuclear beta-catenin-associated antagonist of the Wnt/Wingless pathway. Nature 422: 905-909.

2. Clevers H (2006) Wnt/beta-catenin signaling in development and disease. Cell 127: 469-480.

3. Logan CY, Nusse R (2004) The Wnt signaling pathway in development and disease. Annu Rev Cell Dev Biol 20: 781-810.

4. Kahn M (2014) Can we safely target the WNT pathway? Nat Rev Drug Discov 13: 513-532.

5. Thakur R, Mishra DP (2013) Pharmacological modulation of beta-catenin and its applications in cancer therapy. J Cell Mol Med 17: 449-456.

6. Guo Y, Xiao L, Sun L, Liu F (2012) Wnt/beta-catenin signaling: a promising new target for fibrosis diseases. Physiol Res 61: 337-346.

7. Yao H, Ashihara E, Maekawa T (2011) Targeting the Wnt/beta-catenin signaling pathway in human cancers. Expert Opin Ther Targets 15: 873-887.

8. MacDonald BT, Tamai K, He X (2009) Wnt/beta-catenin signaling: components, mechanisms, and diseases. Dev Cell 17: 9-26.

9. Angers S, Moon RT (2009) Proximal events in Wnt signal transduction. Nat Rev Mol Cell Biol 10: 468-477.

10. Kimelman D, Xu W (2006) beta-catenin destruction complex: insights and questions from a structural perspective. Oncogene 25: 7482-7491.

11. Aberle H, Bauer A, Stappert J, Kispert A, Kemler R (1997) beta-catenin is a target for the ubiquitin-proteasome pathway. EMBO J 16: 3797-3804.

12. Kim W, Kim M, Jho EH (2013) Wnt/beta-catenin signalling: from plasma membrane to nucleus. Biochem J 450: 9-21.

13. Li FQ, Mofunanya A, Harris K, Takemaru K (2008) Chibby cooperates with 14-3-3 to regulate beta-catenin subcellular distribution and signaling activity. J Cell Biol 181: 1141-1154.

14. Li FQ, Mofunanya A, Fischer V, Hall J, Takemaru K (2010) Nuclear-cytoplasmic shuttling of Chibby controls beta-catenin signaling. Mol Biol Cell 21: 311-322.

15. Dunker AK, Cortese MS, Romero P, Iakoucheva LM, Uversky VN (2005) Flexible nets. The roles of intrinsic disorder in protein interaction networks. FEBS J 272: 5129-5148.

16. Das RK, Mao AH, Pappu RV (2012) Unmasking functional motifs within disordered regions of proteins. Sci Signal 5: pe17.

17. Davey NE, Van Roey K, Weatheritt RJ, Toedt G, Uyar B, et al. (2012) Attributes of short linear motifs. Mol Biosyst 8: 268-281.

18. Mofunanya A, Li FQ, Hsieh JC, Takemaru K (2009) Chibby forms a homodimer through a heptad repeat of leucine residues in its C-terminal coiled-coil motif. BMC Mol Biol 10: 41.

19. Mokhtarzada S, Yu C, Brickenden A, Choy WY (2011) Structural characterization of partially disordered human Chibby: insights into its function in the Wnt-signaling pathway. Biochemistry 50: 715-726.

20. Fu H, Subramanian RR, Masters SC (2000) 14-3-3 proteins: structure, function, and regulation. Annu Rev Pharmacol Toxicol 40: 617-647.

21. Yang X, Lee WH, Sobott F, Papagrigoriou E, Robinson CV, et al. (2006) Structural basis for protein-protein interactions in the 14-3-3 protein family. Proc Natl Acad Sci U S A 103: 17237-17242.

22. Yaffe MB, Rittinger K, Volinia S, Caron PR, Aitken A, et al. (1997) The structural basis for 14-3-3:phosphopeptide binding specificity. Cell 91: 961-971.

23. Coblitz B, Wu M, Shikano S, Li M (2006) C-terminal binding: an expanded repertoire and function of 14-3-3 proteins. FEBS Lett 580: 1531-1535.

24. Zhai J, Lin H, Shamim M, Schlaepfer WW, Canete-Soler R (2001) Identification of a novel interaction of 14-3-3 with p190RhoGEF. J Biol Chem 276: 41318-41324.

25. Johnson C, Crowther S, Stafford MJ, Campbell DG, Toth R, et al. (2010) Bioinformatic and experimental survey of 14-3-3-binding sites. Biochem J 427: 69-78.

26. Pozuelo Rubio M, Geraghty KM, Wong BH, Wood NT, Campbell DG, et al. (2004) 14-3-3-affinity purification of over 200 human phosphoproteins reveals new links to regulation of cellular metabolism, proliferation and trafficking. Biochem J 379: 395-408.

27. Bustos DM, Iglesias AA (2006) Intrinsic disorder is a key characteristic in partners that bind 14-3-3 proteins. Proteins 63: 35-42.

28. Uhart M, Bustos DM (2014) Protein intrinsic disorder and network connectivity. The case of 14-3-3 proteins. Front Genet 5: 10.

29. Iakoucheva LM, Radivojac P, Brown CJ, O'Connor TR, Sikes JG, et al. (2004) The importance of intrinsic disorder for protein phosphorylation. Nucleic Acids Res 32: 1037-1049.

30. Obsil T, Ghirlando R, Klein DC, Ganguly S, Dyda F (2001) Crystal structure of the 14-3-3zeta:serotonin N-acetyltransferase complex. a role for scaffolding in enzyme regulation. Cell 105: 257-267.

31. Rittinger K, Budman J, Xu J, Volinia S, Cantley LC, et al. (1999) Structural analysis of 14-3-3 phosphopeptide complexes identifies a dual role for the nuclear export signal of 14-3-3 in ligand binding. Mol Cell 4: 153-166.

32. Emsley P, Cowtan K (2004) Coot: model-building tools for molecular graphics. Acta Crystallogr D Biol Crystallogr 60: 2126-2132.

33. Adams PD, Afonine PV, Bunkoczi G, Chen VB, Davis IW, et al. (2010) PHENIX: a comprehensive Python-based system for macromolecular structure solution. Acta Crystallogr D Biol Crystallogr 66: 213-221.

34. Delaglio F, Grzesiek S, Vuister GW, Zhu G, Pfeifer J, et al. (1995) NMRPipe: a multidimensional spectral processing system based on UNIX pipes. J Biomol NMR 6: 277-293.

35. Keller R (2004) The computer aided resonance assignment tutorial.

36. Johnson BA (2004) Using NMRView to visualize and analyze the NMR spectra of macromolecules. Methods Mol Biol 278: 313-352.

37. Kostelecky B, Saurin AT, Purkiss A, Parker PJ, McDonald NQ (2009) Recognition of an intra-chain tandem 14-3-3 binding site within PKCepsilon. EMBO Rep 10: 983-989.

38. Macdonald N, Welburn JP, Noble ME, Nguyen A, Yaffe MB, et al. (2005) Molecular basis for the recognition of phosphorylated and phosphoacetylated histone h3 by 14-3-3. Mol Cell 20: 199-211.

39. Takala H, Nurminen E, Nurmi SM, Aatonen M, Strandin T, et al. (2008) Beta2 integrin phosphorylation on Thr758 acts as a molecular switch to regulate 14-3-3 and filamin binding. Blood 112: 1853-1862.

40. Bonet R, Vakonakis I, Campbell ID (2013) Characterization of 14-3-3-zeta Interactions with integrin tails. J Mol Biol 425: 3060-3072.

41. Williams DM, Ecroyd H, Goodwin KL, Dai H, Fu H, et al. (2011) NMR spectroscopy of 14-3-3zeta reveals a flexible C-terminal extension: differentiation of the chaperone and phosphoserine-binding activities of 14-3-3zeta. Biochem J 437: 493-503.

42. Marsh JA, Singh VK, Jia Z, Forman-Kay JD (2006) Sensitivity of secondary structure propensities to sequence differences between alpha- and gamma-synuclein: implications for fibrillation. Protein Sci 15: 2795-2804.

43. Schumacher B, Skwarczynska M, Rose R, Ottmann C (2010) Structure of a 14-3-3sigma-YAP phosphopeptide complex at 1.15 A resolution. Acta Crystallogr Sect F Struct Biol Cryst Commun 66: 978-984.

44. Molzan M, Weyand M, Rose R, Ottmann C (2012) Structural insights of the MLF1/14-3-3 interaction. FEBS J 279: 563-571.

45. Molzan M, Kasper S, Roglin L, Skwarczynska M, Sassa T, et al. (2013) Stabilization of physical RAF/14-3-3 interaction by cotylenin A as treatment strategy for RAS mutant cancers. ACS Chem Biol 8: 1869-1875.

46. Skjevik AA, Mileni M, Baumann A, Halskau O, Teigen K, et al. (2014) The N-terminal sequence of tyrosine hydroxylase is a conformationally versatile motif that binds 14-3-3 proteins and membranes. J Mol Biol 426: 150-168.

47. Benzinger A, Popowicz GM, Joy JK, Majumdar S, Holak TA, et al. (2005) The crystal structure of the non-liganded 14-3-3sigma protein: insights into determinants of isoform specific ligand binding and dimerization. Cell Res 15: 219-227.

48. Wilker EW, Grant RA, Artim SC, Yaffe MB (2005) A structural basis for 14-3-3sigma functional specificity. J Biol Chem 280: 18891-18898.

49. Mancini M, Leo E, Takemaru K, Campi V, Castagnetti F, et al. (2015) 14-3-3 Binding and Sumoylation Concur to the Down-Modulation of beta-catenin Antagonist chibby 1 in Chronic Myeloid Leukemia. PLoS One 10: e0131074.

50. Kutay U, Guttinger S (2005) Leucine-rich nuclear-export signals: born to be weak. Trends Cell Biol 15: 121-124.

51. la Cour T, Kiemer L, Molgaard A, Gupta R, Skriver K, et al. (2004) Analysis and prediction of leucine-rich nuclear export signals. Protein Eng Des Sel 17: 527-536.

52. Monecke T, Guttler T, Neumann P, Dickmanns A, Gorlich D, et al. (2009) Crystal structure of the nuclear export receptor CRM1 in complex with Snurportin1 and RanGTP. Science 324: 1087-1091.

53. Guttler T, Madl T, Neumann P, Deichsel D, Corsini L, et al. (2010) NES consensus redefined by structures of PKI-type and Rev-type nuclear export signals bound to CRM1. Nat Struct Mol Biol 17: 1367-1376.

54. Matta A, Siu KW, Ralhan R (2012) 14-3-3 zeta as novel molecular target for cancer therapy. Expert Opin Ther Targets 16: 515-523.

55. Mori M, Vignaroli G, Botta M (2013) Small molecules modulation of 14-3-3 protein-protein interactions. Drug Discov Today Technol 10: e541-547.

56. Ottmann C (2013) Small-molecule modulators of 14-3-3 protein-protein interactions. Bioorg Med Chem 21: 4058-4062.

Chapter 3

3 Conformational characterization of the intrinsically disordered protein Chibby: Interplay between structural elements in target recognition

3.1 Introduction

The Wnt/β-catenin pathway, a signaling cascade whose roles include embryonic development and stem-cell self-renewal, has been linked to a number of human diseases upon its dysregulation, including cancer [1,2,3]. Human Chibby (Cby), an evolutionarily conserved protein, plays a critical role in this pathway by functioning as an antagonist of the transcriptional co-activator β-catenin, the key mediator of Wnt signaling [4]. Cby achieves its antagonistic activity via two mechanisms. First, Cby interacts with β-catenin, forming a complex that prevents β-catenin from binding to and activating Tcf/Lef transcription factors [4]. Secondly, Cby/β-catenin forms a tripartite complex with 14-3-3 proteins to promote β-catenin's export from the nucleus, further suppressing Wnt signaling [5,6].

Besides binding to β-catenin and 14-3-3, Cby participates in the Wnt signaling pathway by interacting with several other partners including nuclear export receptor CRM1 [5], importin-α [5,7], and Thyroid Cancer 1 (TC-1, also known as C8orf4) [8,9]. In particular, TC-1, which was originally identified as a gene highly expressed in thyroid cancer, positively regulates Wnt signaling through its interaction with Cby [10]. By competing with β-catenin for binding to Cby, TC-1 enables free β-catenin to up-regulate Wnt target genes [9]. Recent studies show that TC-1 is also associated with ovarian

carcinoma [11], tongue squamous cell carcinomas [12], and lung cancer [13], all likely through the Wnt/β-catenin pathway.

In addition to these binding partners, Cby interacts with several proteins outside of Wnt signaling such as CEP164 [14], NBPF1, clusterin [15], polycystin-2 and GM130 [16]. Even though numerous Cby interactors have been identified, the molecular details of most of these interactions remain largely unknown. It has been suggested that the ability of Cby to bind multiple targets is facilitated by its partially disordered nature [17]. In our previous work and that of others [7,17], biophysical and biochemical techniques, which include circular dichroism (CD) spectropolarimetry, nuclear magnetic resonance (NMR) spectroscopy, cross-linking and gel filtration experiments, were used to characterize the structure of Cby. The results demonstrated that the N-terminal half of Cby is largely unstructured, whereas its C-terminal half is α-helical and harbors a predicted coiled-coil domain [7,17]. The coiled-coil domain allows for the self-association of Cby in solution, where it exists predominantly as a homodimer [7]. These distinct structural elements of Cby are important for mediating its interactions with various targets. For example, in Wnt/β-catenin signaling, the disordered N-terminus of Cby binds to the 14-3-3 proteins (upon phosphorylation at residue 20 by the kinase Akt) [5,18] and the nuclear export receptor CRM1 [5], whereas its C-terminal half is responsible for binding to β-catenin [4], TC-1 [9], and importin-α [5,7].

Proteins containing both unstructured regions and coiled-coil motifs are widespread. As in the case of Cby, utilization of both types of structural elements may be critical to their biological function [19,20,21,22]. For instance, disordered regions can

tune the affinity for protein interaction partners [23]. Increasing or decreasing these affinities may be accomplished by different mechanisms [23,24]. Examples include providing enhanced stability to the protein or its complex [25], as well as disorder-to-order transitions upon interaction [26] or autoinhibition [27]. In this work, we sought to determine how the disordered regions of Cby affect the stability and target recognition of its coiled-coil domain.

NMR spectroscopy is a valuable tool to dissect the structural details and dynamics of partially disordered proteins [28,29,30]. However, in the case of Cby, its characterization by NMR spectroscopy has proven to be a challenge. Previous work in our lab showed that most of the NMR resonances for Cby's C-terminal half are too broad to be observed under non-denaturing conditions, likely due to the monomer/dimer conformational exchange or formation of higher oligomeric forms [17]. This behavior is not unique to Cby, as severe NMR broadening has been seen in other proteins that are comprised of long disordered regions and coiled-coil motifs [31,32,33].

Hydrogen/deuterium exchange-mass spectrometry (HDX-MS) is another widely used technique to analyze protein folding, structure, dynamics, and interactions [34,35,36,37,38]. Backbone amide hydrogens within disordered regions will exchange rapidly upon D_2O exposure, in comparison to residues in well-folded, rigid regions, where slow D_2O uptake is mediated by conformational fluctuations that lead to transient opening of hydrogen bonds. In this work, we combined HDX-MS, NMR spectroscopy, CD, and isothermal titration calorimetry (ITC) to investigate the interplay of different Cby structural elements during target (TC-1) recognition.

3.2 Materials and Methods

3.2.1 Protein Expression and Purification

The expression and purification protocols for full-length Cby, CbyΔC20 (deletion of the last 20 residues of Cby), N-Cby (residues 1-63) and TC-1 were carried out as described previously [8,10,17]. The pET-15b plasmid containing human TC-1 with an N-terminal His_6-tag was a gift from Dr. E. Chua (University of Sydney, Australia) [10]. The His-tags remained uncleaved from the recombinant Cby constructs to increase their solubility.

C-Cby (residues 67-126) and Coil-Cby (residues 67-104) were cloned into the Gateway destination vector pDEST-HisMBP. The His-MBP fusion constructs were expressed in *Esherichia Coli* (*E. coli*) BL21(DE3) pLysS in M9 minimal media and induced with 0.75 mM isopropyl-β-D-thiogalactopyranoside (IPTG; Bioshop). For pull-down assays the His-tagged proteins were purified from crude lysate by affinity chromatography using Ni-Sepharose 6 Fast Flow beads (Amersham Biosciences). To purify C-Cby and Coil-Cby, the His-MBP tag were cleaved by overnight incubation with tobacco etch virus (TEV) protease at room temperature in 20 mM Tris-HCl, 50 mM NaCl, pH 7.5. The tag-less Cby constructs precipitated out of solution during the cleavage and were subsequently re-solubilized in 20 mM Tris-HCl, 100 mM NaCl, 6 M Guanidine, pH 7.5. The protein was passed through a Superdex 200 column (GE Healthcare) in the same guanidine-containing buffer. For refolding, C-Cby was dialyzed immediately into 10 mM ammonium acetate, pH 5.0 while Coil-Cby was first dialyzed into 10 mM sodium acetate, 8 M urea, pH 5.0 and later into 10 mM ammonium acetate, pH 5.0. All experiments of this work were performed at pH 5.0 as both Cby and TC-1 are

soluble at low pH. All DNA constructs used in this work were sequenced. Purified proteins were analyzed on SDS-PAGE for purity and mass spectrometry analysis ensured they were the correct mass.

3.2.2 Peptide Synthesis

The Cby peptide comprising its C-terminal 25 residues (CbyC25) was purchased from the Tufts University Core facility. The peptide was dissolved and dialyzed in 10 mM ammonium acetate, pH 5.0 for NMR experiments.

3.2.3 Hydrogen/Deuterium Exchange – Mass Spectrometry

HDX-MS of Cby was performed by mixing protein stock solution in a 1:9 ratio with D_2O-based labelling buffer at pH-meter reading of 5.0. The final protein concentration was 2 μM. Aliquots were removed at selected time points ranging between 1 min and 2 h. These aliquots were quenched at pH 2.4 by addition of HCl on ice, followed by flash freezing in liquid nitrogen. Prior to analysis the aliquots were rapidly thawed to ~0 °C and injected into a nanoACQUITY HDX/UPLC (Waters, Milford, MA)[39] for peptic digestion, trapping, and peptide separation. A peptic cleavage map of Cby is provided in Figure 3.1. Deuteration percentages were calculated as $100\% \times (m - m_0)/ (m_{100} - m_0)$ where m is the centroid m/z for the partially deuterated peptide of interest, and where m_0 and m_{100} correspond to minimally and fully deuterated controls, respectively [39].

3.2.4 Circular Dichroism Spectropolarimetry

CD spectra and thermal melting curves were collected on a Jasco J-810 spectropolarimeter (Easton, MD). Spectra of the various Cby constructs (0.15 mg/mL to

0.30 mg/mL) were collected at 25 °C in 10 mM ammonium acetate, pH 5.0, with 5 accumulated scans for each construct. For the melting curves, the temperature was scanned from 15 °C to 95 °C, with the ellipticity monitored at 222 nm. The analysis program CDSSTR included in the DichroWeb online analysis software was used to deconvolute the CD spectra [40]. Deconvolution was performed using the SMP180 (optimized for 190-240 nm) reference set [41].

3.2.5 NMR Spectroscopy

NMR experiments were carried out on a Varian Inova 600-MHz spectrometer equipped with xyz-gradient triple resonance probe at 25 °C in 10 mM ammonium acetate buffer, pH 5.0. Samples contained 10% D_2O and 1 mM 2,2-dimethyl-2-sila-pentane-5-sulfonic acid (DSS) as an internal standard for chemical shift referencing. Data were processed using NMRPipe [42] and analyzed using NMRView [43]. The backbone assignment of TC-1 was previously completed by our lab (BMRB accession code: 15141) [8].

3.2.6 Isothermal Titration Calorimetry (ITC)

ITC experiments were performed on a VP-ITC instrument (MicroCal) at 25 °C in 10 mM ammonium acetate, pH 5.0. 8 μL aliquots of 230 μM TC-1 were titrated stepwise into the 1.4 mL sample cell containing 20 μM C-Cby. Titrations of TC-1 to buffer and buffer to C-Cby revealed negligible heat changes. The dissociation constant (K_d), molar binding stoichiometry (n) and the binding enthalpy (ΔH), entropy (ΔS) and Gibbs free energy (ΔG) were determined by fitting the binding isotherm to a one-site model with MicroCal Origin7 software. Protein concentrations were determined from amino acid analysis (Amino Acid Analysis Facility, SickKids, Toronto, ON).

3.3 Results

3.3.1 Identifying the coiled-coil region of Cby using HDX-MS

Owing to previous difficulties encountered during NMR-based characterization attempts of full-length Cby [17], we resorted to HDX-MS. The primary goal of these measurements was to delineate the coiled-coil dimerization domain of Cby. Figure 3.1 displays the Cby peptic peptides used in the HDX-data analysis while Figure 3.2 shows the deuterium uptake curves for these peptides. Deuteration was quasi-instantaneous for the N-terminal half of Cby, i.e., deuterium levels of > 90% were observed already for the first experimental time point of 1 min. Similarly, residues 102-126, which make up the very C-terminal end of Cby, exhibited extremely rapid deuterium uptake. Strong HDX protection is observed in peptides that are near (residues 53-59) and within (residues 60-90) the predicted boundaries of Cby's coiled-coil domain (residues 68-102) [7,44], with nearly no exchange in the range of residues 91-98.

For visualization of these data, the deuteration percentages were mapped onto a structural model of dimeric Cby for t = 60 min (Figure 3.3). In this model, the coiled-coil is presented as residues 73-100, corresponding to four turns of heptad repeats. However, we should point out that the N-terminal boundary of the coiled-coil domain is not clearly defined in our HDX data since only relatively large peptic fragments (60-84 and 60-90) were obtained for this region. In contrast, it is clear that the coiled-coil ends around residues 98, as the significant protection observed is immediately succeeded by rapid deuterium uptake in the 102-111 peptic fragment. For the rest of the model, Cby's N-termini and very C-termini (which will be denoted as its C-terminal extension from now on) are displayed in a largely extended state.

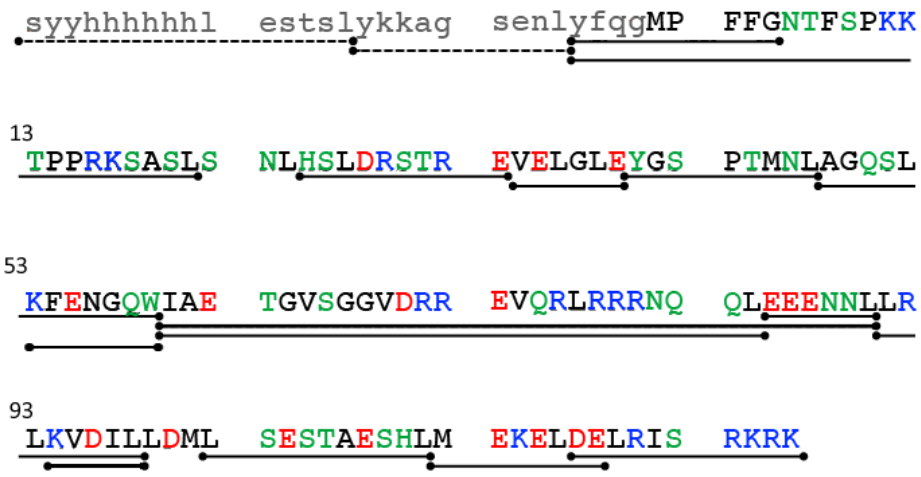

Figure 3.1 Sequence of human Cby and peptides used in HDX-MS data analysis
Sequence of *human Cby and its His tag (lower case, grey colour)*. Black lines below the sequence are the peptic peptides used in the HDX-MS data analysis, and the broken lines are peptides originating from solely the His-tag. Colour scheme: negatively charged residues in red, positively charged residues in blue, polar residues in green and non-polar residues in black.

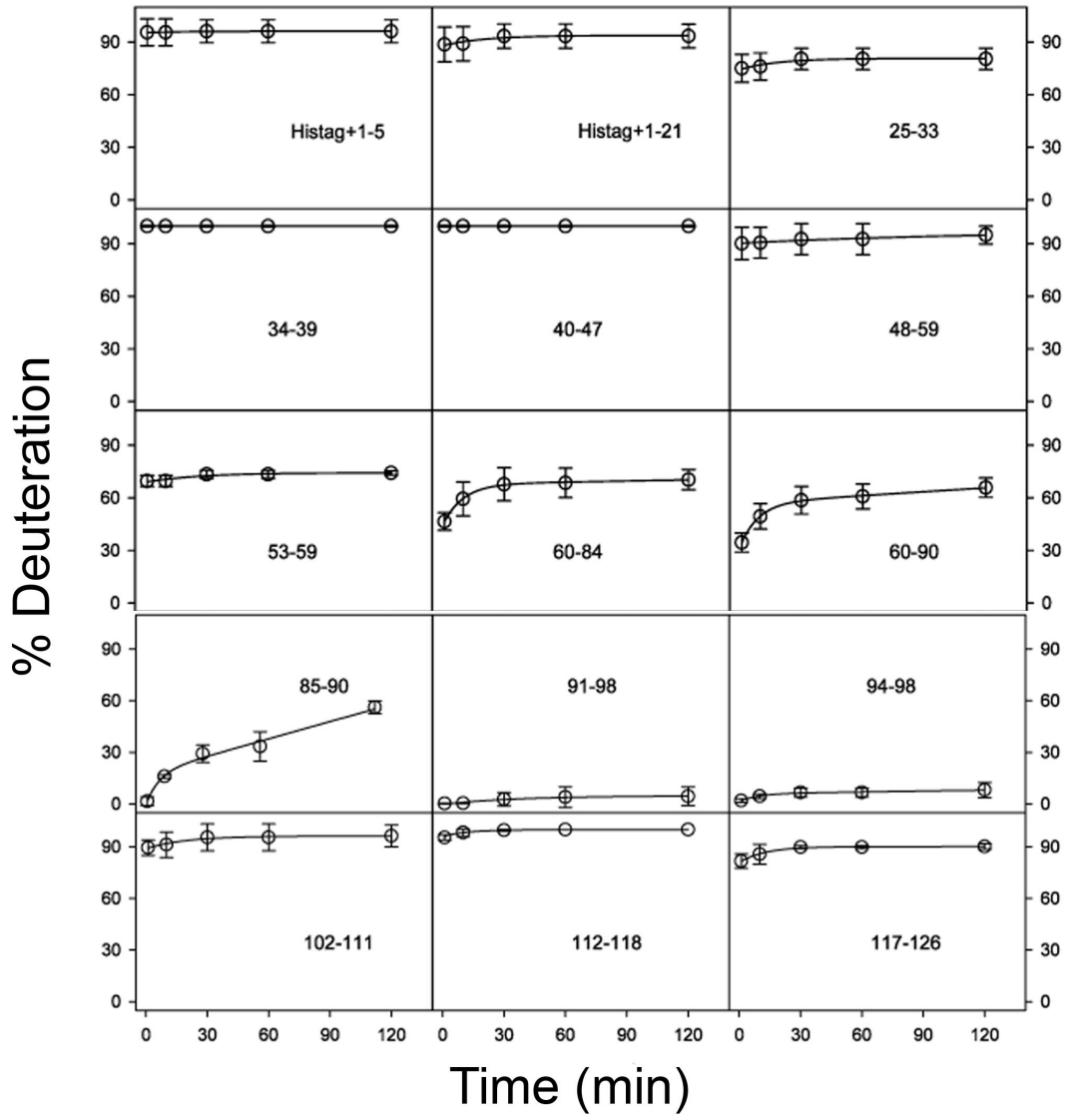

Figure 3.2 HDX kinetics of peptides in Cby
The 28-residue His-tag and Cby residue numbers are indicated in each panel. Lines are bi-exponential fits. Standard deviations of triplicate measurements are shown as error bars.

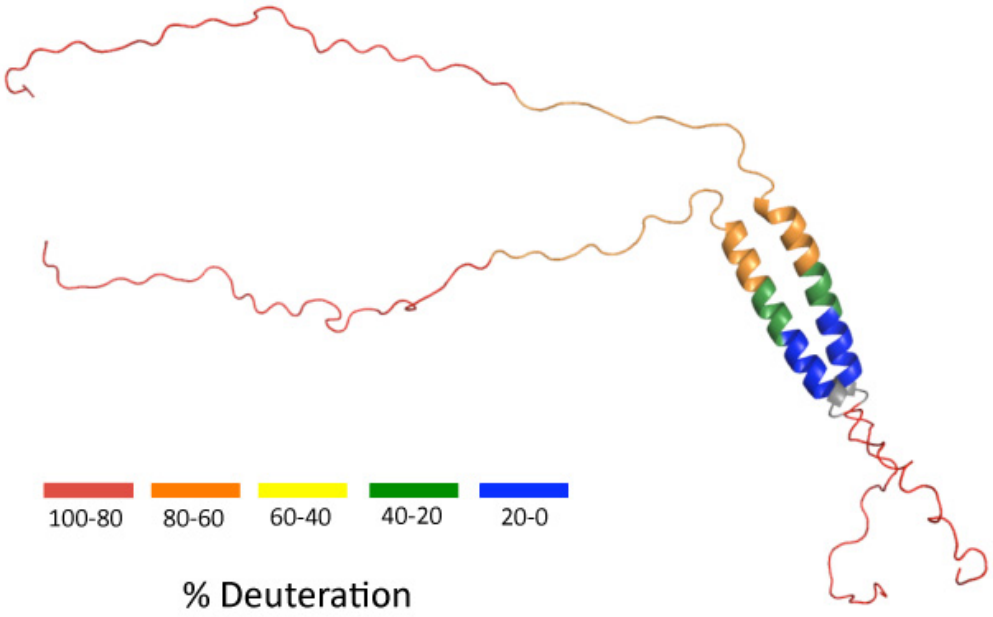

Figure 3.3 HDX-MS data of Figure 3.2 mapped onto a structural model of Cby for t=60 min

The 126-residue Cby is shown as a dimer. Residues 1-72 are shown in a highly extended state, the coiled-coil is comprised of residues 73-100 and residues 101-126 are displayed in a disordered form. The colouring represents a range of deuteration percentages. Peptide mapping did not cover the grey regions.

3.3.2 The disordered N-terminal half and C-terminal extension of Cby

As identified by HDX-MS, Cby contains two disordered regions of different length flanking the coiled-coil motif. We sought to determine whether these two unstructured segments have differing effects on the stability of the coiled-coil structure. A number of truncated Cby constructs were generated for this purpose (Figure 3.4). First, we tested if Cby's C-terminal extension plays a role in the formation of the coiled-coil by truncating the last 20 residues of Cby (CbyΔC20). A CD spectrum of CbyΔC20 in 10 mM ammonium acetate, pH 5.0 is highly similar to that of full-length Cby (Figure 3.5 A). Deconvolution of the spectra using the DichroWeb software [40] gives 30% helical, 21% strand and 49% disordered/turn structure for the full-length Cby and 41% helical, 17% strand and 42% disordered/turn for CbyΔC20. The data indicate that the C-terminal 20 residues are not structured and that the helical content of Cby is maintained upon deletion of this disordered extension. Notably, the CD spectrum of a synthetic construct comprising the C-terminal 25 residues of Cby (CbyC25), shows that the C-terminal extension is largely disordered but does have α-helical propensity (deconvolution: 42% helical, 12% strand and 46% turns/disordered) (Figure 3.5 C).

Next, we investigated the effect of C-terminal truncation on the thermal stability of the coiled-coil motif. Figure 3.5 B shows the CD thermal denaturation profiles of wild-type Cby and CbyΔC20. For the full-length Cby, the ellipiticity at 222 nm gradually becomes less negative as the temperature increases from 20 to 50 ^{o}C, while the signal remains steady for the truncated CbyΔC20 over this temperature range. Once the temperature reaches ~60 ^{o}C, both constructs display a significant increase (becoming less

negative) in ellipiticity, signifying the melting of the coiled-coil. A thermal melt of the CbyC25 peptide shows a gradual loss of signal at 222 nm in the 20-50 ^{o}C range, which likely explains the differences between the thermal denaturation profiles of wild-type Cby and CbyΔC20 in that temperature range (Figure 3.5 B).

While the thermal denaturation of the full-length Cby is reversible, as the CD spectrum of the protein at 25 ^{o}C is identical before and after the melt, CbyΔC20 precipitates upon denaturation. Also, during optimization of the CbyΔC20 purification strategy, we observed that the truncated version tends to aggregate in the presence of NaCl at low concentrations (50 mM) while full-length Cby remains soluble in 100 mM NaCl up to a protein concentration of 200 μM. Taken together, these observations suggest that the C-terminal extension is important for Cby's solubility, consistent with the prevalence of charged side chains in this region (Figure 3.1).

An overlay of the ^{1}H-^{15}N HSQC NMR spectra of full-length Cby and CbyΔC20 is shown in Figure 3.6. Similar to the full-length protein, only peaks from the N-terminal half of CbyΔC20 can be observed in the HSQC spectrum. Consistent with the CD data, the NMR spectrum suggests that Cby's coiled-coil structure remains intact upon deletion of the C-terminal extension, rendering the peaks from this region unobservable by NMR. Notably, truncation of the C-terminal extension of Cby does not induce significant chemical shift changes or intensity attenuation to the signals originating from the N-terminal half, indicating that there are no long-range interactions between the N- and C-terminal disordered regions of Cby.

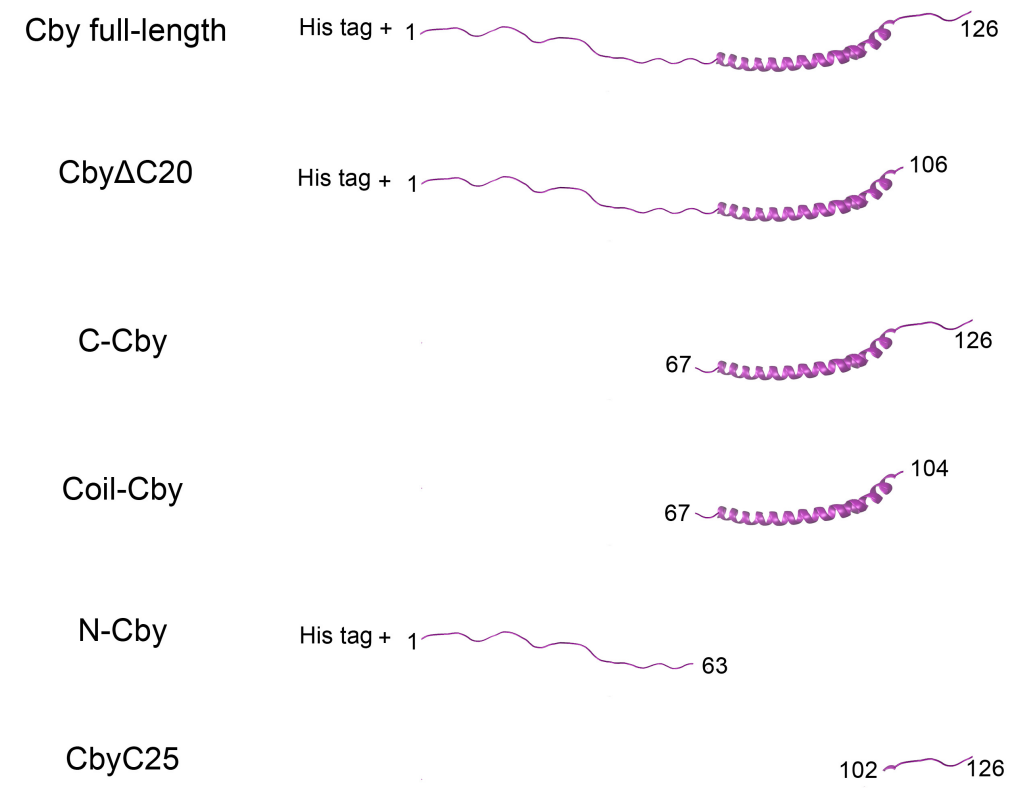

Figure 3.4 Cby constructs used in this study

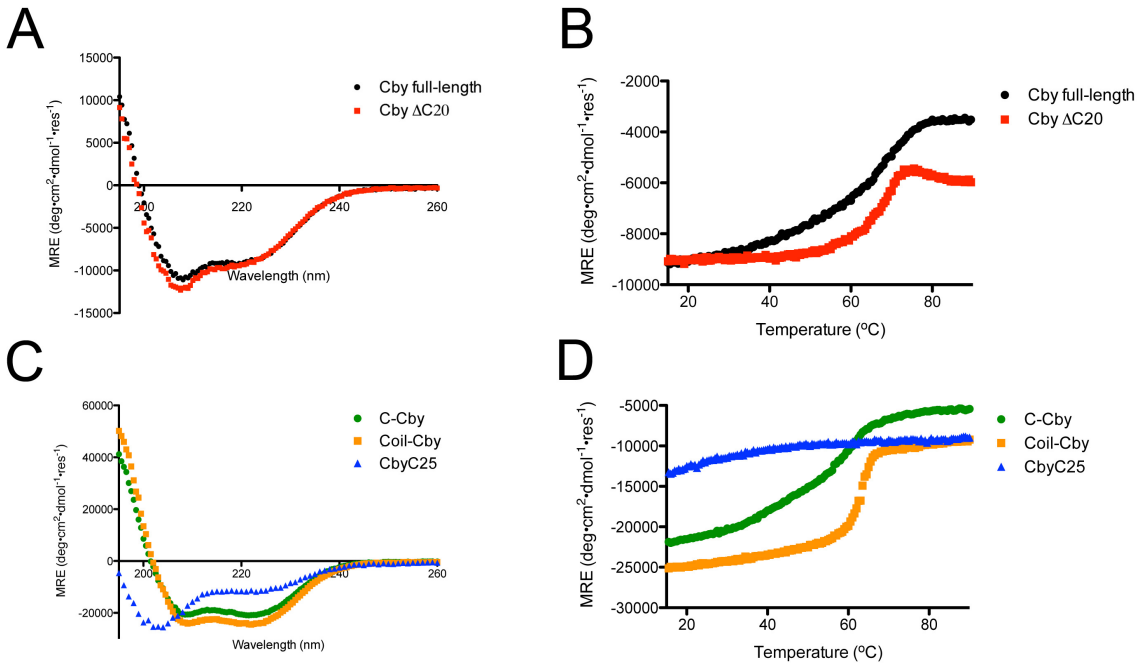

Figure 3.5 CD spectra and thermal melts of Cby constructs
A. CD spectra of full-length Cby and CbyΔC20. Displayed spectra are the average of 5 scans. **B.** Thermal melts of full-length Cby and CbyΔC20 monitored using CD at 222 nm. **C.** CD spectra of C-Cby, Coil-Cby and CbyC25. Displayed spectra are the average of 5 scans. **D.** Thermal melts of C-Cby, Coil-Cby and CbyC25 monitored using CD at 222 nm.

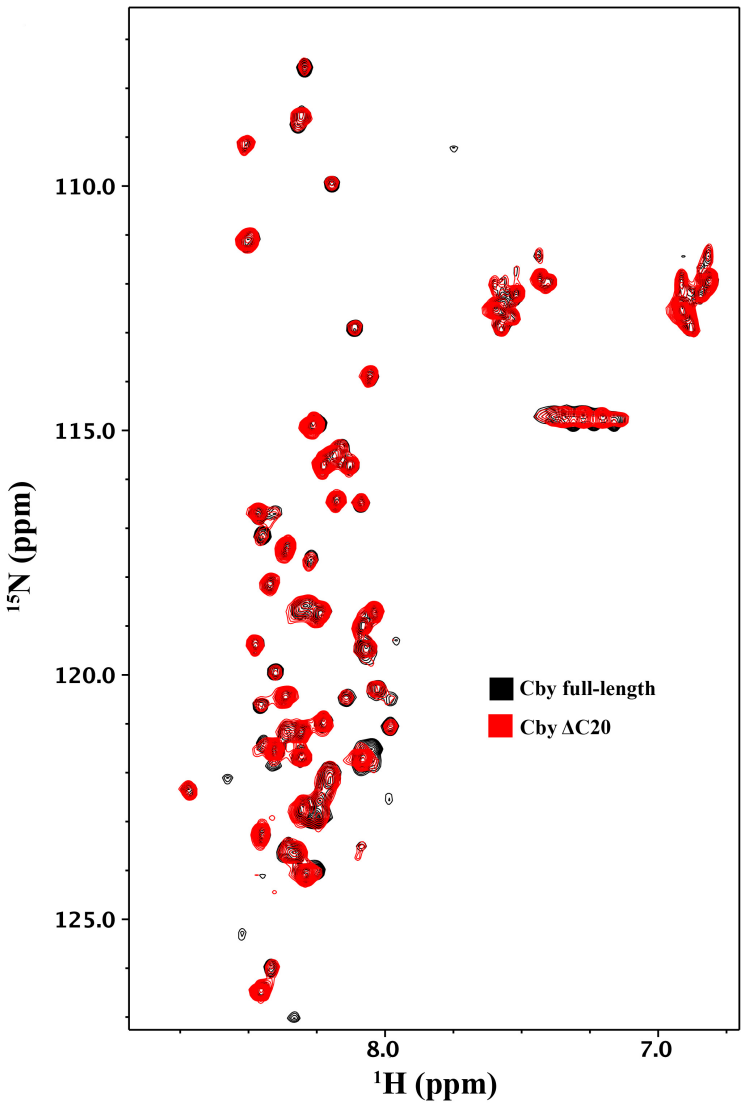

Figure 3.6 NMR spectra of full-length Cby and CbyΔC20
^{1}H-^{15}N HSQC NMR spectrum of full-length Cby (black) overlayed with a ^{1}H-^{15}N HSQC of CbyΔC20 (red) (spectra collected at 100 μM).

Next, we sought to characterize isolated C-terminal half of Cby in the absence of the disordered N-terminus. A CD spectrum reveals that C-Cby (residues 67-126) is largely helical (Figure 3.5 C). The deconvoluted procedure reports 64% helical, 3% strand and 33% disordered/turn. The $[\theta]_{222}/[\theta]_{208}$ ratio is ≈ 1, which is indicative of coiled-coil structure [45]. A thermal melt of C-Cby, using CD monitored at 222 nm, displays a profile similar to that of full-length Cby, where a broad transition is observed between 20 and 70 ^{o}C (Figure 3.5 D). Like full-length Cby, C-Cby could completely refold after thermal denaturation. A HSQC spectrum collected for isolated C-Cby only contains a few broad peaks, indicating that most of the NMR signals from the coiled-coil motif and C-terminal extension in this construct remain largely unobservable (Figure 3.7).

After extensive efforts, we managed to purify the coiled-coil domain of Cby (Coil-Cby, residues 67-104), despite its significantly lower solubility relative to the other constructs. A HSQC spectrum of Coil-Cby has no detectable peaks, while the deconvoluted CD spectrum returns 80% helical and 20% disordered/turn and the $[\theta]_{222}/[\theta]_{208}$ ratio ≈ 1 (Figure 3.5 C). Its thermal denaturation profile, like all Cby constructs comprising the coiled-coil domain, displays a sharp reduction in signal between 60-70 ^{o}C (Figure 3.5 D). Similar to CbyΔC20, Coil-Cby aggregated upon thermal denaturation.

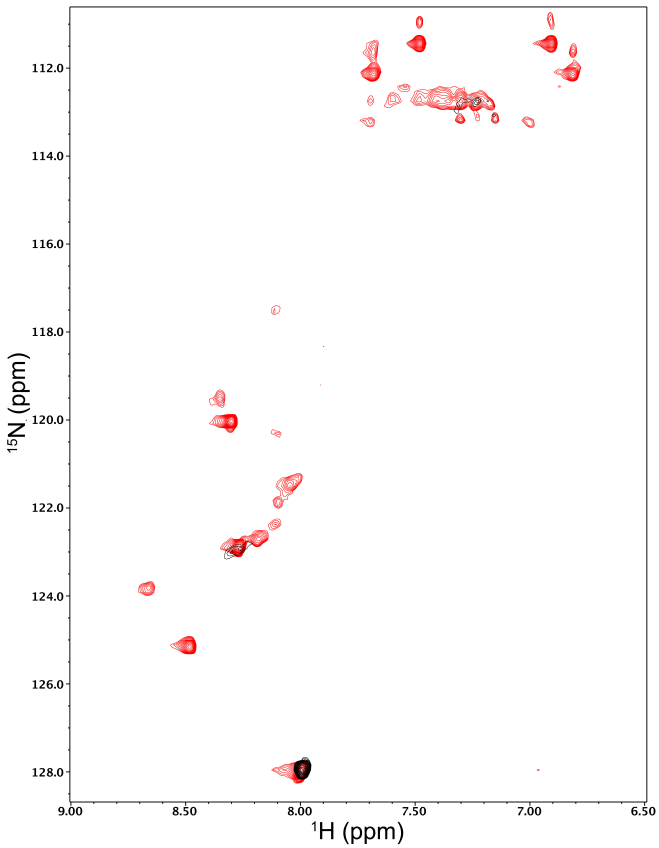

Figure 3.7 NMR Spectra of C-Cby
Overlay of ^{1}H-^{15}N HSQC spectra of C-Cby in the absence (black) and presence (red) of TC-1 at a 1:1.5 ratio (C-Cby 100 μM:TC-1 150 μM).

3.3.3 Disordered regions of Cby tune its binding affinity to TC-1

Focusing on the Cby/TC-1 interaction, we next investigated to what extent target recognition of Cby is modulated by specific structural elements, i.e., the coiled-coil domain, or the N- and C-terminal disordered regions. TC-1 functions as a positive regulator of Wnt signaling by competing with β-catenin in binding the C-terminal half of Cby [9]. Previous structural characterization of TC-1 by our lab established that the predominantly disordered TC-1 contains three regions with α-helical propensity in its C-terminal half and that these regions are responsible for mediating the interactions with Cby [8].

Upon titration of unlabelled CbyΔC20 to ^{15}N-labelled TC-1 (2:1), decreases in peak intensity were observed for residues within TC-1's C-terminal half (Figure 3.8 B). The peaks that displayed intensity losses matched the intensity losses observed when full-length Cby was titrated to ^{15}N-labelled TC-1 (Figure 3.8 A, C). A titration of the CbyC25 peptide, which comprises the C-terminal extension, to TC-1 did not result in any intensity changes (Figure 3.9 A). Together, these results suggest that the C-terminal extension is likely expendable for Cby's interaction with TC-1.

Next, the individual halves of Cby, N-Cby and C-Cby, were titrated with ^{15}N-labelled TC-1. As expected, titrating N-Cby did not induce any changes in the HSQC spectrum of TC-1 (Figure 3.9 B). Conversely, titrating C-Cby led to the broadening of most TC-1 amide resonances (Figure 3.10 A, B). The drops in peak intensities were most severe in the C-terminal half of TC-1, where many signals were broadened beyond

detection. Additionally, titration of unlabelled TC-1 to ^{15}N-labelled C-Cby led to the appearance of a number of peaks (Figure 3.7).

The greater intensity losses observed in the TC-1 spectrum upon titration with C-Cby suggest that C-Cby binds TC-1 with a higher affinity than the full-length protein. This was confirmed by ITC experiments, which revealed that C-Cby binds to TC-1 with a K_d of ~ 2 μM (Figure 3.10 C, Figure 3.11 A). On the other hand, the interactions between TC-1/full-length Cby and TC-1/CbyΔC20 are too weak to produce discernible enthalpy changes with the protein concentrations (which are limited by the proteins' solubilities) used in the ITC experiments (Figure 3.11 B, C).

Intriguingly, when Coil-Cby was added to TC-1 in a 2:1 ratio, no changes in the HSQC spectrum were observed (Figure 3.9 C). The lack of observed binding may be due to its potential aggregation at the concentration (~100 μM) used for these NMR experiments. Attempts to concentrate the protein to > 200 μM led to the observation of a gel-like precipitate, again highlighting the importance of disordered regions for the solubility of Cby.

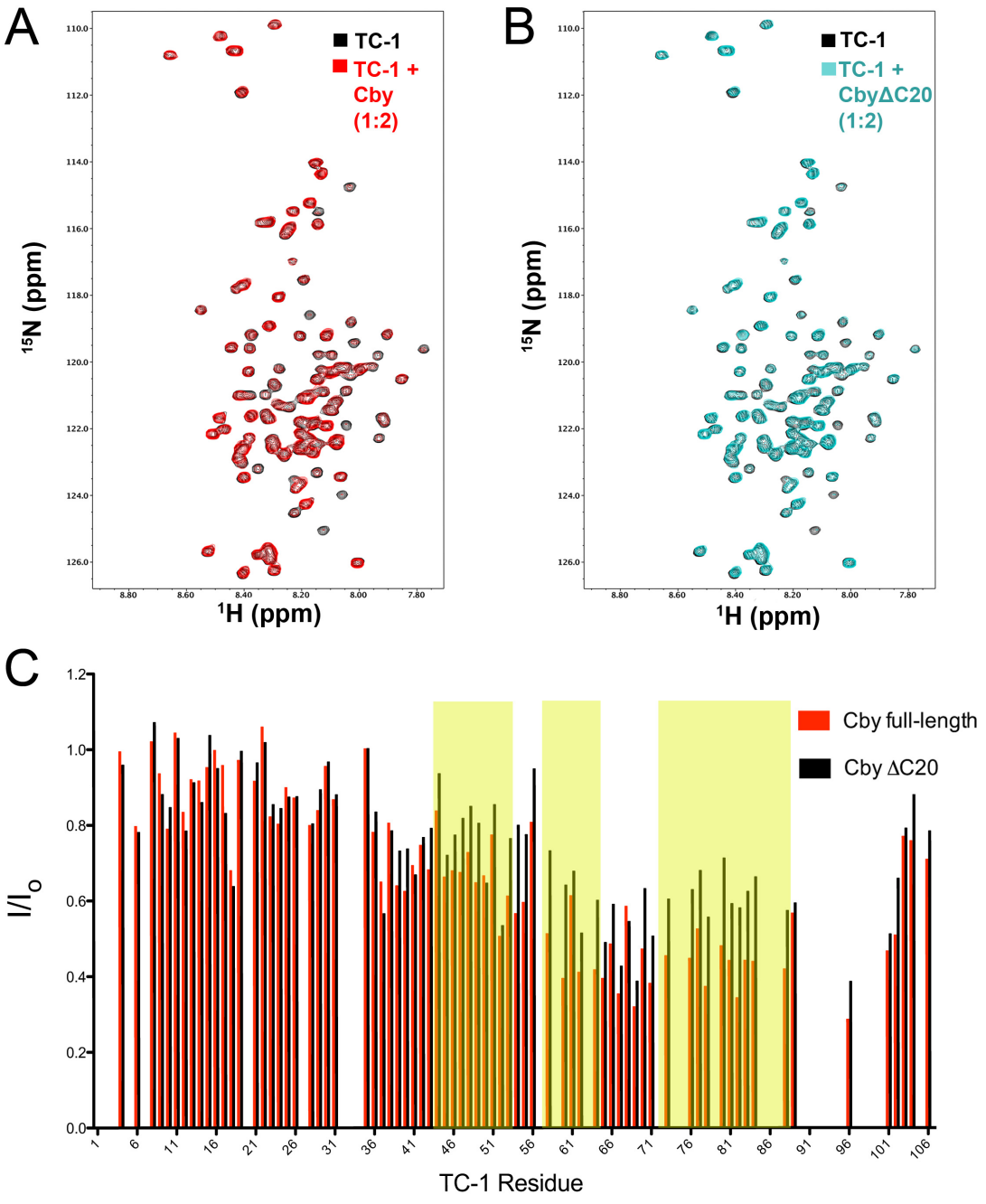

Figure 3.8 TC-1/Cby NMR titration experiments
A. Overlay of ^{1}H-^{15}N HSQC spectra of TC-1 in the absence (black) and presence (red) of full-length Cby at a 1:2 ratio (TC-1 60 μM:Cby 120 μM). **B.** Overlay of ^{1}H-^{15}N HSQC spectra of TC-1 in the absence (black) and presence (blue) of CbyΔC20 at a 1:2 ratio (TC-1 60 μM:CbyΔC20 120 μM). **C.** Intensity ratios (I/Io) for assigned TC-1 amide resonances in the presence (I) or absence (Io) of either full-length Cby or CbyΔC20. Yellow shaded areas correspond to the three regions on TC-1 with high-helical propensity as determined by chemical shift analysis [8].

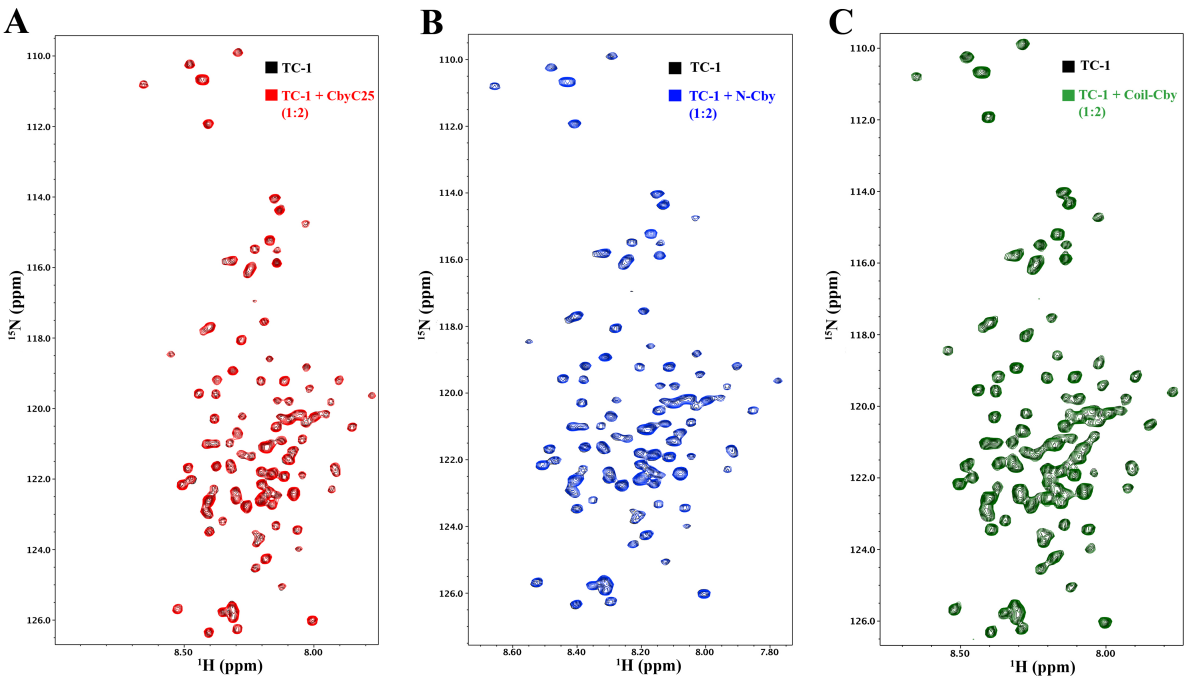

Figure 3.9 NMR titrations with TC-1/Cby constructs
A. Overlay of the ^{1}H-^{15}N HSQC spectra of TC-1 in the absence (black) and presence (red) of N-Cby at a 1:2 ratio (TC-1:N-Cby). **B.** Overlay of the ^{1}H-^{15}N HSQC spectra of TC-1 in the absence (black) and presence (red) of CbyC25 at a 1:2 ratio (TC-1:CbyC25). **C.** Overlay of the ^{1}H-^{15}N HSQC spectra of TC-1 in the absence (black) and presence (red) of Coil-Cby at a 1:2 ratio (TC-1:Coil-Cby).

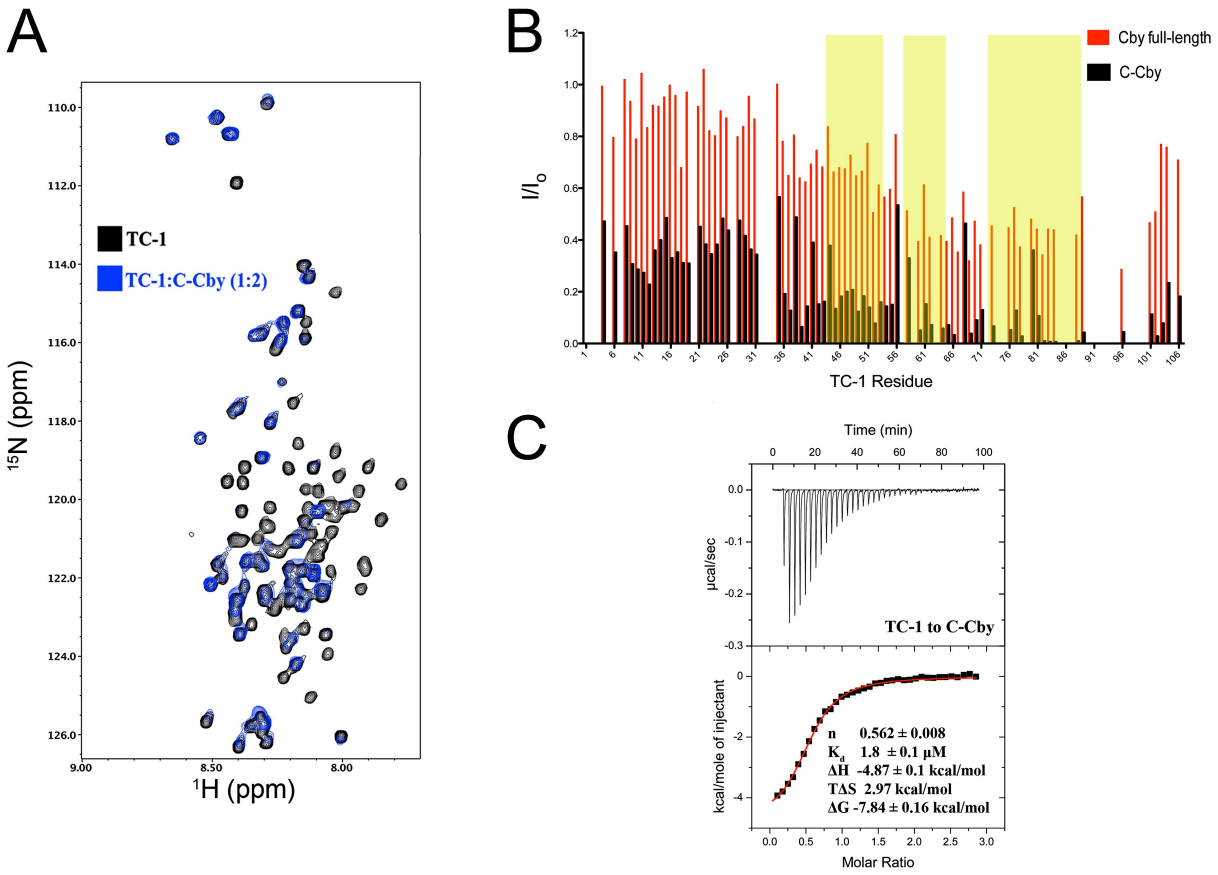

Figure 3.10 TC-1/C-Cby NMR and ITC binding experiments
A. Overlay of ^{1}H-^{15}N HSQC spectrum of TC-1 in the absence (black) and presence (blue) of full-length C-Cby at a 1:2 ratio (TC-1 50 µM:C-Cby 100 µM). **B.** Intensity ratios (I/Io) for assigned TC-1 amide resonances in the presence (I) or absence (Io) of either full-length Cby (as shown in Figure 3.8) or C-Cby. Yellow shaded areas correspond to the three regions on TC-1 with high-helical propensity as determined by chemical shift analysis[8]. **C.** An ITC thermal profile of TC-1 binding to C-Cby. Thermodynamic experimental values are displayed. K_d is the dissociation constant ΔH, ΔS and ΔG are the change in enthalpy, entropy and Gibbs free energy upon binding at T = 298 K, respectively.

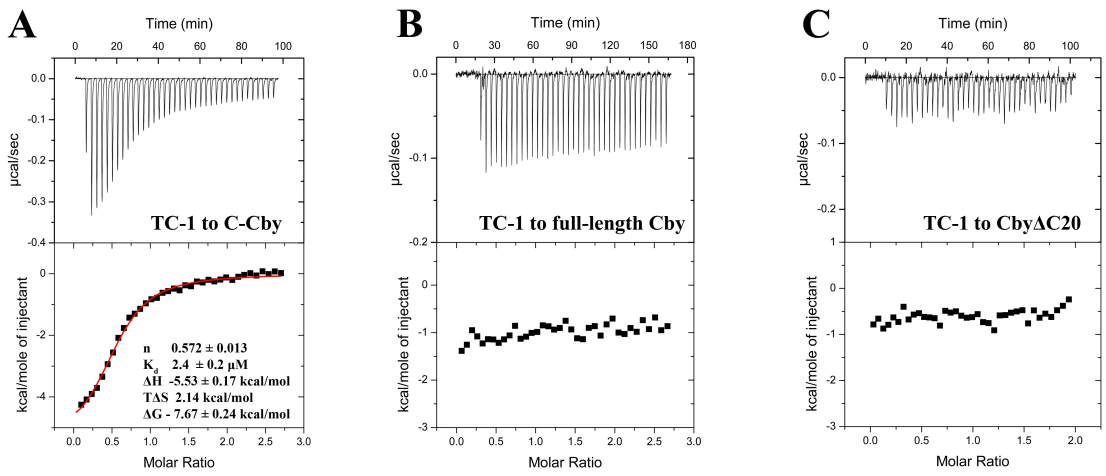

Figure 3.11 ITC thermograms for binding experiments between TC-1 and Cby constructs

A. A duplicate ITC thermal profile of TC-1 binding to C-Cby in 10 mM ammonium acetate. Thermodynamic experimental values are displayed. K_d is the dissociation constant ΔH, ΔS and ΔG are the change in enthalpy, entropy and Gibb free energy upon binding at T = 298.15 K, respectively. **B.** ITC thermal profile of TC-1 binding to full-length Cby in 10 mM sodium acetate, pH 5.0. **C.** ITC thermal profile of TC-1 binding to CbyΔC20 in 10 mM ammonium acetate, pH 5.0.

3.4 Discussion

The mapping of coiled-coil domains using NMR spectroscopy has proven to be a challenge for not only Cby, but also for other partially unstructured proteins such as CHOP, Par-4 and NA14 [31,32,33]. For those three proteins, the only observable HSQC peaks correspond to residues located in disordered regions. As demonstrated in this study, HDX-MS is a valuable alternative technique for deciphering which residues make up these coiled-coil domains.

Cby first exhibits HDX protection in large fragments comprised of residues 60-84 and 60-90. Our ability to set a defined boundary for the N-terminus of the coiled-coil is limited by the size of the peptic fragments produced during online digestion. Meanwhile, a peptic fragment comprising residues 85-90 displays further reduced HDX rates while residues 91-98 display virtually no deuterium uptake over the course of the experiment. These results align well with the predicted coiled-coil region, residues 68-102 [7].

The HDX data revealed a previously unrecognized structural feature, i.e., considerable disorder in the C-terminal extension of Cby (residues 102-126), where deuterium levels around 90% were observed for the earliest time point of t = 1 min. This behavior does not necessarily imply that the C-terminal extension is completely unfolded. Instead, it is more likely that this region exhibits rapid coil/helix fluctuations. Following the standard HDX model [46] one can estimate the average deuteration rate constant as $k_{HDX} = K_{op} \times k_{ch}$, where K_{op} is the coil/helix equilibrium constant, and $k_{ch} \approx 7$ min^{-1} is the "chemical" exchange rate constant at pH 5. An assumed value of $K_{op} = 0.3$ corresponds to a deuteration level of 90% for t = 1 min. Thus, our HDX data suggest that the residual

helicity of the C-terminal extension could be as high as 77% (considering that a coil/helix equilibrium constant of 23/77 yields K_{op} = 0.3). Although the C-terminal extension is not part of the coiled-coil domain, it is not visible in the HSQC spectra of full-length Cby or its C-terminal half (C-Cby). It is likely that the proximity of the C-terminal extension to the coiled-coil and the suggested coil/helix fluctuations collectively contribute to signal broadening of these residues.

Our NMR and CD spectroscopy experiments demonstrate that Cby's C-terminal extension is expendable for coiled-coil formation, in good agreement with a yeast two-hybrid assay that demonstrated full-length Cby could bind to a large Cby fragment (residues 60-112), where the C-terminal extension's last 14 residues are not present [16]. However, the absence of the C-terminal extension results in a reduction in Cby's solubility. Importantly, this extension plays a major functional role as it contains Cby's nuclear localization signal, residues 123-126, which binds to importin-α [5].

From our NMR experiments, Cby's coiled-coil domain mediates the interaction with TC-1. For the Cby/TC-1 interaction, no binding was observed between TC-1 and the CbyC25 peptide, while the CbyΔC20 construct was observed to bind TC-1 by NMR spectroscopy. Notably, while the coiled-coil is required for the Cby/TC-1 complex formation, we failed to detect interactions between Coil-Cby and TC-1 by NMR, possibly due to the aggregation of the former at high concentration. Despite remaining α-helical as shown by CD spectroscopy, the absence of both disordered ends on Coil-Cby drastically reduces the solubility of this domain.

The C-Cby construct bound to TC-1 with much greater affinity compared to full-length Cby. Our ITC data, based on the calculated molar ratio, suggests that C-Cby binds to TC-1 as a dimer. We speculate that the bound C-Cby dimer likely lies along the helical region of TC-1's C-terminal half. The difference in affinity for TC-1 between full-length and C-Cby may be due to a higher entropic cost of binding for full-length Cby compared to C-Cby. Alternatively, the disordered N-terminus of Cby may inhibit the interaction by acting as an entropic bristle, that is, an unstructured region that impedes surrounding macromolecules via random, thermally driven motions [47].

In summary, our HDX-MS data help characterize the structure and dynamics of the NMR-invisible C-terminal half of Cby. The data reveal that Cby is comprised of a disordered N-terminus, a short coiled-coil and an unstructured C-terminal extension. These three structural elements were assessed for their importance to Cby's interaction with the Wnt signaling enhancer TC-1. Our results also provide insight into how Cby's disordered regions and coiled-coil work in concert to assemble higher order protein complexes, such as the trimolecular Cby/14-3-3/β-catenin [6] or Cby/clusterin/NBPF1 complexes [15]. Cby's N-terminus comprises the binding motifs for a number of binding targets, including 14-3-3 protein and clusterin. In the free state, Cby's N-terminus may reduce the affinity for some binding targets that bind to its C-terminal half, as demonstrated in this work with TC-1. However, this inhibition may be abrogated if the N-terminus is present in a bound state. Such a mechanism may allow for cooperative, sequential formation of multi-molecular Cby complexes.

3.5 Acknowledgements

This work was supported by The Natural Sciences and Engineering Research Council of Canada (NSERC). An Ontario Graduate Scholarship was awarded to R.C.K.

3.6 References

1. Schepers A, Clevers H (2012) Wnt Signaling, Stem Cells, and Cancer of the Gastrointestinal Tract. Cold Spring Harbor Perspectives in Biology 4.

2. Polakis P (2012) Drugging Wnt signalling in cancer. Embo Journal 31: 2737-2746.

3. Clevers H, Nusse R (2012) Wnt/beta-Catenin Signaling and Disease. Cell 149: 1192-1205.

4. Takemaru KI, Yamaguchi S, Lee YS, Zhang Y, Carthew RW, et al. (2003) Chibby, a nuclear beta-catenin-associated antagonist of the Wnt/Wingless pathway. Nature 422: 905-909.

5. Li FQ, Mofunanya A, Fischer V, Hall J, Takemaru KI (2010) Nuclear-Cytoplasmic Shuttling of Chibby Controls beta-Catenin Signaling. Molecular Biology of the Cell 21: 311-322.

6. Li FQ, Mofunanya A, Harris K, Takemaru KI (2008) Chibby cooperates with 14-3-3 to regulate beta-catenin subcellular distribution and signaling activity. Journal of Cell Biology 181: 1141-1154.

7. Mofunanya A, Li FQ, Hsieh JC, Takemaru KI (2009) Chibby forms a homodimer through a heptad repeat of leucine residues in its C-terminal coiled-coil motif. Bmc Molecular Biology 10.

8. Gall C, Xu HY, Brickenden A, Ai XJ, Choy WY (2007) The intrinsically disordered TC-1 interacts with Chibby via regions with high helical propensity. Protein Science 16: 2510-2518.

9. Jung YS, Bang S, Choi K, Kim E, Kim Y, et al. (2006) TC1 (C8orf4) enhances the Wnt/beta-catenin pathway by relieving antagonistic activity of Chibby. Cancer Research 66: 723-728.

10. Chua EL, Young L, Wu WM, Turtle JR, Dong QH (2000) Cloning of TC-1 (C8orf4), a novel gene found to be overexpressed in thyroid cancer. Genomics 69: 342-347.

11. Xu HT, Liu Y, Liu SL, Miao Y, Li QC, et al. (2013) TC-1 (C8orf4) expression is correlated with differentiation in ovarian carcinomas and might distinguish

metastatic ovarian from metastatic colorectal carcinomas. Virchows Archiv 462: 281-287.

12. Zhang P, Cao HY, Bai LL, Li WN, Wang Y, et al. (2015) The high expression of TC1 (C8orf4) was correlated with the expression of beta-catenin and cyclin D1 and the progression of squamous cell carcinomas of the tongue. Tumor Biology 36: 7061-7067.

13. Su K, Huang LJ, Li WH, Yan XL, Li XF, et al. (2013) TC-1 (c8orf4) enhances aggressive biologic behavior in lung cancer through the Wnt/beta-catenin pathway. Journal of Surgical Research 185: 255-263.

14. Burke MC, Li FQ, Cyge B, Arashiro T, Brechbuhl HM, et al. (2014) Chibby promotes ciliary vesicle formation and basal body docking during airway cell differentiation. Journal of Cell Biology 207: 123-137.

15. Vandepoele K, Staes K, Andries V, Van Roy F (2010) Chibby interacts with NBPF1 and clusterin, two candidate tumor suppressors linked to neuroblastoma. Experimental Cell Research 316: 1225-1233.

16. Hidaka S, Konecke V, Osten L, Witzgall R (2004) PIGEA-14, a novel coiled-coil protein affecting the intracellular distribution of polycystin-2. Journal of Biological Chemistry 279: 35009-35016.

17. Mokhtarzada S, Yu C, Brickenden A, Choy WY (2011) Structural Characterization of Partially Disordered Human Chibby: Insights into Its Function in the Wnt-Signaling Pathway. Biochemistry 50: 715-726.

18. Killoran RC, Fan JS, Yang DW, Shilton BH, Choy WY (2015) Structural Analysis of the 14-3-3 zeta/Chibby Interaction Involved in Wnt/beta-Catenin Signaling. Plos One 10.

19. Dos Santos HG, Abia D, Janowski R, Mortuza G, Bertero MG, et al. (2013) Structure and Non-Structure of Centrosomal Proteins. Plos One 8.

20. Nido GS, Mendez R, Pascual-Garcia A, Abia D, Bastolla U (2012) Protein disorder in the centrosome correlates with complexity in cell types number. Molecular Biosystems 8: 353-367.

21. Anurag M, Singh GP, Dash D (2012) Location of disorder in coiled coil proteins is influenced by its biological role and subcellular localization: a GO-based study on human proteome. Molecular Biosystems 8: 346-352.

22. Galea CA, High AA, Obenauer JC, Mishra A, Park CG, et al. (2009) Large-Scale Analysis of Thermostable, Mammalian Proteins Provides Insights into the Intrinsically Disordered Proteome. Journal of Proteome Research 8: 211-226.

23. Flock T, Weatheritt RJ, Latysheva NS, Babu MM (2014) Controlling entropy to tune the functions of intrinsically disordered regions. Current Opinion in Structural Biology 26: 62-72.

24. Uversky VN (2013) The most important thing is the tail: Multitudinous functionalities of intrinsically disordered protein termini. Febs Letters 587: 1891-1901.

25. Hegde ML, Tsutakawa SE, Hegde PM, Holthauzen LMF, Li J, et al. (2013) The Disordered C-Terminal Domain of Human DNA Glycosylase NEIL1 Contributes to Its Stability via Intramolecular Interactions. Journal of Molecular Biology 425: 2359-2371.

26. Vuzman D, Levy Y (2012) Intrinsically disordered regions as affinity tuners in protein-DNA interactions. Molecular Biosystems 8: 47-57.

27. Trudeau T, Nassar R, Cumberworth A, Wong ETC, Woollard G, et al. (2013) Structure and Intrinsic Disorder in Protein Autoinhibition. Structure 21: 332-341.

28. Konrat R (2014) NMR contributions to structural dynamics studies of intrinsically disordered proteins. Journal of Magnetic Resonance 241: 74-85.

29. Kosol S, Contreras-Martos S, Cedeno C, Tompa P (2013) Structural Characterization of Intrinsically Disordered Proteins by NMR Spectroscopy. Molecules 18: 10802-10828.

30. Jensen MR, Ruigrok RWH, Blackledge M (2013) Describing intrinsically disordered proteins at atomic resolution by NMR. Current Opinion in Structural Biology 23: 426-435.

31. Rodriguez-Rodriguez M, Trevino MA, Laurents DV, Arranz R, Valpuesta JM, et al. (2011) Characterization of the structure and self-recognition of the human centrosomal protein NA14: implications for stability and function. Protein Engineering Design & Selection 24: 883-892.

32. Libich DS, Schwalbe M, Kate S, Venugopal H, Claridge JK, et al. (2009) Intrinsic disorder and coiled-coil formation in prostate apoptosis response factor 4. Febs Journal 276: 4134-4152.

33. Singh VK, Pacheco I, Uversky VN, Smith SP, MacLeod RJ, et al. (2008) Intrinsically disordered human C/EBP homologous protein regulates biological activity of colon cancer cells during calcium stress. Journal of Molecular Biology 380: 313-326.

34. Konermann L, Rodriguez AD, Sowole MA (2014) Type 1 and Type 2 scenarios in hydrogen exchange mass spectrometry studies on protein-ligand complexes. Analyst 139: 6078-6087.

35. Keppel TR, Howard BA, Weis DD (2011) Mapping Unstructured Regions and Synergistic Folding in Intrinsically Disordered Proteins with Amide H/D Exchange Mass Spectrometry. Biochemistry 50: 8722-8732.

36. Wales TE, Engen JR (2006) Hydrogen exchange mass spectrometry for the analysis of protein dynamics. Mass Spectrometry Reviews 25: 158-170.

37. Englander SW (2006) Hydrogen exchange and mass spectrometry: A historical perspective. Journal of the American Society for Mass Spectrometry 17: 1481-1489.

38. Zhu MM, Rempel DL, Du ZH, Gross ML (2003) Quantification of protein-ligand interactions by mass spectrometry, titration, and H/D exchange: PLIMSTEX. Journal of the American Chemical Society 125: 5252-5253.

39. Wales TE, Fadgen KE, Gerhardt GC, Engen JR (2008) High-speed and high-resolution UPLC separation at zero degrees Celsius. Analytical Chemistry 80: 6815-6820.

40. Whitmore L, Wallace BA (2004) DICHROWEB, an online server for protein secondary structure analyses from circular dichroism spectroscopic data. Nucleic Acids Research 32: W668-W673.

41. Abdul-Gader A, Miles AJ, Wallace BA (2011) A reference dataset for the analyses of membrane protein secondary structures and transmembrane residues using circular dichroism spectroscopy. Bioinformatics 27: 1630-1636.

42. Delaglio F, Grzesiek S, Vuister GW, Zhu G, Pfeifer J, et al. (1995) Nmrpipe - a Multidimensional Spectral Processing System Based on Unix Pipes. Journal of Biomolecular Nmr 6: 277-293.

43. Johnson BA (2004) Using NMRView to visualize and analyze the NMR spectra of macromolecules. Methods Mol Biol 278: 313-352.

44. Lupas A (1996) Prediction and analysis of coiled-coil structures. Computer Methods for Macromolecular Sequence Analysis 266: 513-525.

45. Lau SYM, Taneja AK, Hodges RS (1984) Synthesis of a Model Protein of Defined Secondary and Quaternary Structure - Effect of Chain-Length on the Stabilization and Formation of 2-Stranded Alpha-Helical Coiled-Coils. Journal of Biological Chemistry 259: 3253-3261.

46. Bai Y, Milne JS, Mayne L, Englander SW (1993) Primary structure effects on peptide group hydrogen exchange. Proteins 17: 75-86.

47. Hoh JH (1998) Functional protein domains from the thermally driven motion of polypeptide chains: A proposal. Proteins-Structure Function and Genetics 32: 223-228.

Chapter 4

4 Cby's coiled-coil domain: Differing binding modes to TC-1 and β-catenin

4.1 Introduction

The Wnt/β-catenin signaling pathway, activated by the Wnt family of cysteine-rich glycoproteins, is critical in embryonic development, stem cell control and adult tissue homeostasis [1,2,3]. Mutations to the Wnt genes as well as Wnt signaling components are associated with various human diseases, including cancer [4,5]. Activation of the pathway occurs when the Wnt proteins interact with the cellular receptors frizzled and lipoprotein receptor-related protein (LRP). Signaling is relayed and transduced to the transcriptional co-activator β-catenin where it translocates to the nucleus, interacts with the Tcf/Lef family of transcription factors and induces Wnt signaling target genes [6]. When the pathway is turned off, cytosolic β-catenin exists within a large protein complex, termed the destruction complex. This complex is comprised of scaffolding proteins (Axin, APC) and a collection of kinases (GSK3β, Ck1) that phosphorylate β-catenin [6]. Phosphorylated β-catenin is targeted for ubiquitination and subsequent degradation through the proteasome [7].

With aberrant Wnt signaling being implicated in a number of diseases, cellular regulation of the Wnt signaling cascade is vital. Regulation of the key player in the pathway, β-catenin, is a focal point, with a number of its binding partners influencing its phosphorylation, degradation, cellular localization and ability to interact with the Tcf/Lef transcription factors [8,9,10]. One such modulator is the protein Chibby (Cby), an antagonist of β-catenin-mediated signaling [11]. Cby's antagonism is achieved using two

mechanisms. First, it competes directly with the Tcf/Lef transcription factors for binding to β-catenin [11] and secondly, in conjunction with the 14-3-3 proteins, promotes the cytoplasmic sequestration of β-catenin [12,13]. These two modes of regulation effectively suppress Wnt signaling [13].

Cby is regulated by a small, disordered protein named thyroid cancer-1 (TC-1) [14]. The 106-residue TC-1 received its name when it was identified as a gene overexpressed in papillary thyroid cancer [15]. By binding directly to Cby, TC-1 effectively frees β-catenin to bind to the Tcf/Lef factors and induces transcription of Wnt genes [14].

Structurally, the 17.5 kDa Cby is partially disordered, comprising an intrinsically disordered N-terminal half, while its C-terminus harbours a coiled-coil motif [16,17]. These two structural halves of Cby are independently responsible for interacting with the protein's Wnt signaling binding partners. The disordered N-terminal half comprises Cby's 14-3-3 binding motif and nuclear exportation signal [13], while the C-terminus contains the binding sites for β-catenin [11] and TC-1 [14] as well as its nuclear localization signal [13]. Cby interacts with the last α-helix on β-catenin (termed the helix C) [18], whereas it binds to the C-terminal half of TC-1 [14,19].

The coiled-coil domain promotes the homo-dimerization of Cby and is predicted to range from residues 73-102 [16], which is confirmed in our hydrogen-deuterium exchange mass-spectrometry study discussed in Chapter 3. Some cell studies have demonstrated the importance of Cby's dimerization in Wnt signaling. By mutagenizing some of the core leucines (L77, L84, L91, L98) within the coiled-coil region to alanine,

Mofunanya *et al.* [16] demonstrated that Cby's dimerization could be disrupted. These engineered monomeric Cby mutants were incapable of binding to importin-α, the receptor responsible for Cby's nuclear localization. However, pull-downs showed that monomeric Cby retained the ability to interact with β-catenin and TOPFLASH assays, a reporter kit designed to monitor the activation of the Wnt signaling pathway in cultured cells [20], showed that these mutants could still repress β-catenin-mediated signaling. Conversely, although ITC experiments have shown that Cby interacts with TC-1 as a dimer (Chapter 3), whether or not monomeric Cby can interact with TC-1 is unknown.

NMR spectroscopy represents a valuable technique in the characterization of intrinsically disordered proteins [21,22]. However, analyzing the Cby/β-catenin interaction using NMR spectroscopy is challenging due to Cby's insolubility in buffers at physiological pH, where β-catenin is most stable [17]. Moreover, the majority of resonances in Cby's C-terminal half are severely broadened out to disappearance as the result of conformational exchange [17]. The large size of full-length β-catenin (88 kDa), along with its elongated shape [18], leads to a rapidly decaying NMR signal, making typical protein binding NMR experiments using labelled β-catenin unfeasible.

To further dissect Cby's interaction between its coiled-coil domain and β-catenin, a series of mutants were designed to either stabilize or destabilize the coiled-coil. The goal of these mutants was to increase Cby's solubility and to reduce the severe peak broadening observed in Cby's HSQC spectrum, enabling the Cby/β-catenin complex to be studied using NMR spectroscopy. A diagram of Cby's coiled-coil, represented as helical wheels, is displayed in Figure 4.1. Within the four heptad-repeats of this domain, there are four core leucines (L77, L84, L91, and L98) at position *d* and two asparagines

(N81, N88) are buried in the core at position *a*. To destabilize the coiled-coil, L84A/L98A (Cby-2A) and L77A/L84A/L91A/L98A (Cby-4A) mutants were generated. Conversely, to stabilize the coiled-coil, the two asparagines in the hydrophobic core of the domain, N81 and N88, were both mutated to leucine (Cby N81L/N88L). An additional construct comprising six mutations (Cby-6mut, N81L/N88L/L90R/L93R/I97R/L99E) was designed to strengthen the dimer interface while removing the hydrophobic patch on the coiled-coil surface and to promote the formation of an electrostatic bridge between residue E99 and K94.

Our findings demonstrate that the leucine to alanine mutants, Cby-2A and Cby-4A, have additional peaks in their ^{1}H-^{15}N HSQC spectra compared to Cby-WT but remain insoluble at pH ≥7. However, making these same mutations to recombinant constructs comprising only the C-terminal half of Cby (C-Cby residues 67-126) lead to drastically increased solubility as well as the appearance of the majority of NMR peaks. Critically, these C-Cby mutants retain binding to β-catenin as demonstrated by pull-down and NMR titration experiments.

These same mutants were tested for binding to TC-1. Our results demonstrate that the destabilizing Cby-2A mutant was incapable of interacting with TC-1. Additionally, although Cby N81L/N88L retained an interaction with TC-1, Cby-6mut did not. Collectively, the results suggest Cby interacts with TC-1 as a dimer, with key interacting residues present on the surface of the coiled-coil.

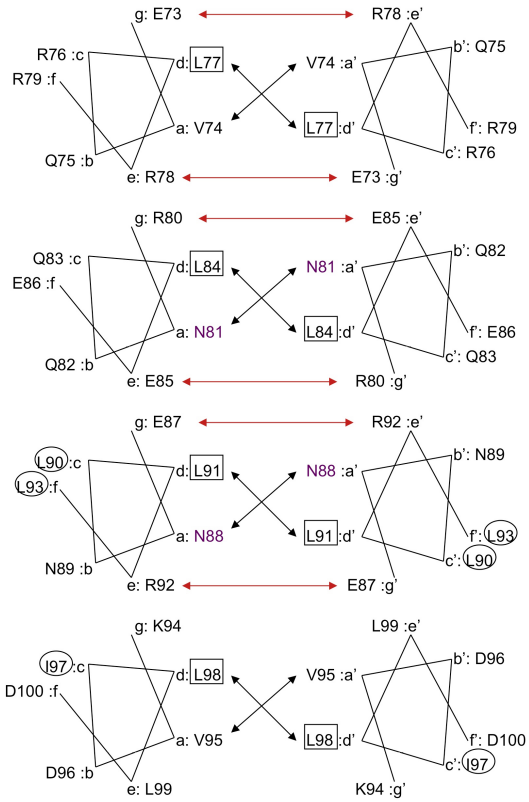

Figure 4.1 Schematic of Cby's coiled-coil, represented as helical wheels
Core leucines (position *d*) are boxed, core asparagines at position *a* are highlighted in purple, and surface-exposed hydrophobic residues are circled. Figure was taken from Supplementary Material provided in the published manuscript by Mokhtazarda *et al.* [17].

4.2 Materials and Methods

4.2.1 Mutagenesis, Expression and Purification of Recombinant Proteins

All Cby mutants were generated using the QuikChange Multi Site-Directed Mutagenesis Kit (Agilent Technologies). Each mutant was confirmed through DNA sequencing. Expression and purification of full-length Cby-WT, Cby-2A (L84A/L98A), Cby-4A (L77A, L84A, L91A, L98A), Cby N81L/N88L and Cby-6mut (N81L, N88L, L90R, L93R, I97R and L99E) were performed as previously described for Cby-WT [17]. Expression and purification of TC-1 was performed as described in [19]. The expression and purification protocols for C-Cby-WT, N81L/N88L, 6mut and Coil-Cby-WT (residues 67-102) (which are expressed as His-MBP fusions) are described in Chapter 3. The C-Cby-2A and C-Cby-4A mutants were found to be soluble after TEV cleavage in a buffer comprising 20 mM Tris, 50 mM NaCl, pH 7.5. C-Cby-2A and C-Cby-4A samples, were concentrated and exchanged into 20 mM Tris, 50 mM NaCl, 3 M guanidine-HCl, pH 7.5 and run through a Superdex 200 column (GE Healthcare) in the same buffer comprising 6 M guanidine-HCl. Pooled protein fractions were dialyzed into 50 mM sodium phosphate, pH 7.0.

The pET-28a expression vector for β-catenin, consisting of the first armadillo repeat to the C-terminal end (residues 138-781) and termed β-catR1C, was generously gifted from Dr. Wenqing Xu of the University of Washington [18]. The His-tagged proteins were induced for over-expression in *E. coli* BL21 (DE3) cells, in M9 medium, with 1 mM of IPTG upon reaching an $O.D._{600}$ of 0.7 at 37 °C. Cells were grown for 3 hours at 37 °C before harvesting. Cells were lysed and loaded onto Ni-NTA beads.

Subsequent eluates were incubated with His-tagged TEV overnight at room temperature. The cleavage mixture was then loaded onto Ni-NTA beads in 20 mM Tris, 50 mM NaCl pH 7.5, with the His-tagged cleaved β-catR1C collected in the flow-through.

β-catR10C (tenth armadillo repeat to the C-terminus; residues 531-781) was inserted for expression into a pDEST17 vector using Gateway Recombination Cloning Technology (Thermo Fisher Scientific). The His-tagged β-catR10C was grown in *E. coli* BL21 (DE3) pLysS cells at 37 °C in M9 medium. Upon reaching an $O.D._{600}$ of 0.7, overexpression was induced with 1 mM of IPTG at 22 °C. Lysed cells were loaded onto Ni-NTA beads and elutions were dialyzed into 50 mM sodium phosphate, pH 7.0. The His-tag was not cleaved for solubility purposes.

All proteins used in this work were analyzed on SDS-PAGE and electrospray ionization mass spectrometry for purity and to ensure they were the correct mass.

4.2.2 Circular Dichroism Spectropolarimetry

CD spectra and thermal melting curves were collected on a Jasco J-810 spectropolarimeter (Easton, MD). Spectra of full-length Cby-WT, Cby (N81L/N88L), Cby-6mut, Cby-2A and Cby-4A and C-Cby(N81L/N88L), C-Cby-6mut (at concentrations ranging from 0.15 mg/mL to 0.30 mg/mL) were collected in a 1 mm cuvette at 25°C in 10 mM sodium acetate, pH 5.0 with 5 accumulated scans each. Spectra for C-Cby-2A and C-Cby-4A were collected in 50 mM sodium phosphate, pH 7.0. The program CONTIN included in the DichroWeb online analysis software [23] was used to deconvolute the CD spectra. Deconvolution was performed using the SMP180 (optimized for 190-240 nm) reference set [24,25].

For the melting curves of all Cby constructs, the temperature was scanned from 20 °C to 95 °C, with the ellipticity monitored at 222 nm. Full-length and C-terminal half Cby-WT, Cby N81L/N88L and Cby-6mut were performed at a rate of 1 °C/min and full-length Cby-2A and Cby-4A were performed at 3 °C/min.

4.2.3 Pull-down Assays

For the MBP-Cby fusion pull-down assays, 30 μg of His-MBP fusions (Coil-Cby, C-Cby and all C-Cby mutants) in 500 μL were incubated with 30 μL of amylose resin for 1 hour in protein binding buffer (PBB) (20 mM Tris, 70 mM NaCl, pH 7.5) at room temperature. After washing with two individual 500 μL washes with PBB, 100 μg of β-catR1C in 500 μL was incubated with the resin in PBB for 45 minutes at room temperature. Beads were washed with 100 μL of PBB followed by an additional 75 μL wash of PBB. Bound proteins were eluted with 50 μL of PBB containing 100 mM maltose. 30 μL of the eluted fractions were run on SDS-PAGE.

4.2.4 NMR Spectroscopy

NMR experiments were performed on Varian Inova 600 MHz spectrometers equipped with xyz-gradient triple resonance probe at 25 ^{o}C. Samples contained 10% (v/v) D_2O and sodium 2, 2-dimethyl-2-silapentane-5-sulfonate (DSS) was added as an internal standard for chemical shift referencing. Buffers used for each experiment and protein concentrations used for titration experiments are described within the figure captions. NMR data were processed using NMRPipe [25] and analyzed using NMRView [26].

4.2.5 Peptide Synthesis

The Cby peptide comprising its C-terminal 25 residues (CbyC25) was purchased from and synthesized at the Tufts University Core facility. The peptide was dissolved in 20 mM Tris, 50 mM NaCl, pH 7.5 for ITC experiments.

4.2.6 Isothermal Titration Calorimetry

Using a VP-ITC instrument (MicroCal), 0.6 mM of the CbyC25 peptide was titrated from the syringe in 10 μL injections into the cell containing 20 μM β-catR1C. The titration experiment was run in 20 mM Tris, 50 mM NaCl, pH 7.5 at 25 ^{o}C.

4.3 Results

4.3.1 Design of Cby coiled-coil mutants and their effect on the protein's stability

CD spectra were collected for all mutants to assess their secondary structure content and thermal denaturation experiments were used to measure their stability (Figure 4.2 A-D). The results for the deconvoluted spectra of all mutants are displayed in Table 4.1. The WT, N81L/N88L and Cby-6mut constructs share similar percentages of α-helix, β-strand and turns-disorder secondary structures. Conversely, the Cby-2A and Cby-4A mutants have a reduced level of α-helical content and an increased level of β-strand content relative to Cby-WT.

Thermal melting curves were collected for each mutant using CD spectroscopy, monitored at 222 nm (Figure 4.2 B, D). Cby-WT, as previously demonstrated in Chapter 3, displays a gradual loss in signal over the 20 °C – 60 °C temperature range followed by a sharper loss of signal starting at approximately 60 °C, signifying the melting of the coiled-coil. Cby-6mut follows a similar pattern as the WT in the 20 °C – 60 °C, however, the continued loss of signal starting at 60 °C is much more gradual than the WT protein, suggesting that the coiled-coil domain is more stable. Additionally, like the WT protein, Cby-6mut is able to refold properly after its thermal denaturation (data not shown). Interestingly, the N81L/N88L mutant showed almost no change in signal at 222 nm, suggesting its structure is extremely stable. Indeed, a CD spectrum of Cby N81L/N88L taken at 80 °C shows a nearly identical curve to the protein at 25 °C (Figure 4.2 A, Table 4.1). As such, the L90R/L93R/I97R/L99E mutations in the Cby-6mut construct, which also contains the N81L/N88L mutations, likely destabilize the coiled-

coil of the Cby N81L/N88L mutant. Both the Cby-2A and 4A mutants, which lack a coiled-coil structure, showed little reduction in CD signal over the course of the thermal melt.

^{1}H-^{15}N HSQC spectra of these Cby mutants were collected. The Cby N81L/N88L and Cby-6mut spectra are very similar to that of Cby-WT (Figure 4.3 A, B), indicating that only resonances derived from Cby's N-terminus can be observed in these mutants. HSQC spectra of Cby-2A and Cby-4A show an increase in the number of observed peaks compared to Cby-WT (Figure 4.3 C). For the WT protein, ~ 61 amide resonances of 149 non-proline residues (includes His-tag) are detected. Conversely, ~ 101 resonances are observed in both Cby-2A and in Cby-4A. Despite the HSQCs of Cby-2A and Cby-4A having more peaks, only 68% of the expected number of peaks are observed, suggesting some self-association or conformational exchange may still be occurring. As well, although these new observed resonances are all expected to originate from Cby's C-terminus, it is unknown if some residues have multiple peaks originating from monomer and dimer species. While these two mutants display a similar number of resonances, the Cby-2A mutant's spectrum shows more peak crowding and line broadening compared to the Cby-4A mutant where the peaks are sharper. The Cby-4A mutant potentially shifts the monomer-dimer equilibrium more toward the monomeric state than Cby-2A.

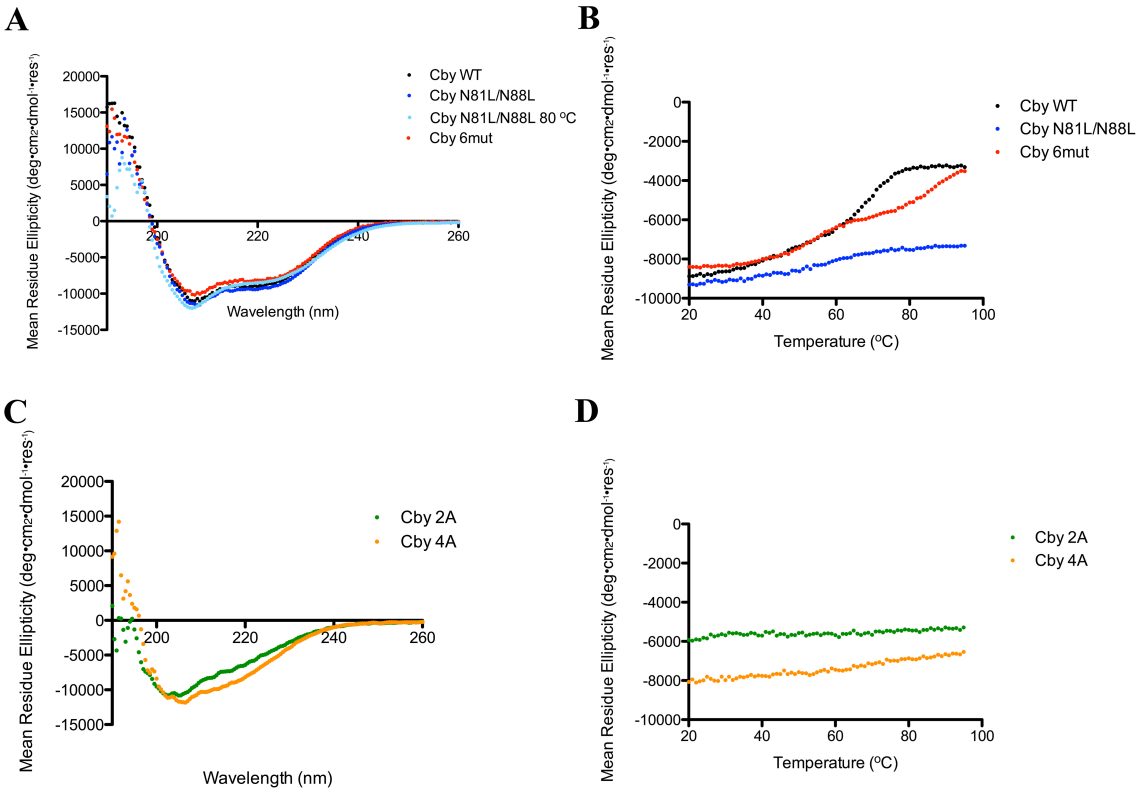

Figure 4.2 CD spectra and thermal melts of full-length Cby coiled-coil mutants
A. CD spectra of full-length Cby-WT, N81L/N88L and Cby-6mut at 25 °C and Cby N81L/N88L at 80 °C. Displayed spectra are the accumulation of 5 scans. **B.** Thermal melting curves of full-length Cby-WT, N81L/N88L and Cby-6mut using CD at 222 nm. **C.** CD spectra of full-length Cby-2A and Cby-4A. Displayed spectra are the accumulation of 5 scans. **D.** Thermal melting curves of full-length Cby-2A and Cby-4A using CD at 222 nm. All spectra collected in 10 mM sodium acetate, pH 5.0.

Table 4.1 Deconvoluted CD spectra of full-length Cby and C-terminal Cby coiled-coil mutants

Unless otherwise specified, all spectra were collected at 25 °C

		Helix	Strand	Turns/Disorder
Full-length Cby constructs	WT	26%	24%	50%
	N81L/N88L	29%	17%	54%
	N81L/N88L at 80 °C	32%	10%	58%
	6mut	24%	26%	50%
	2A	12%	32%	56%
	4A	17%	31%	52%
C-Cby constructs	N81L/N88L	60%	3%	37%
	6mut	50%	7%	43%
	2A	8%	36%	56%
	4A	18%	24%	58%

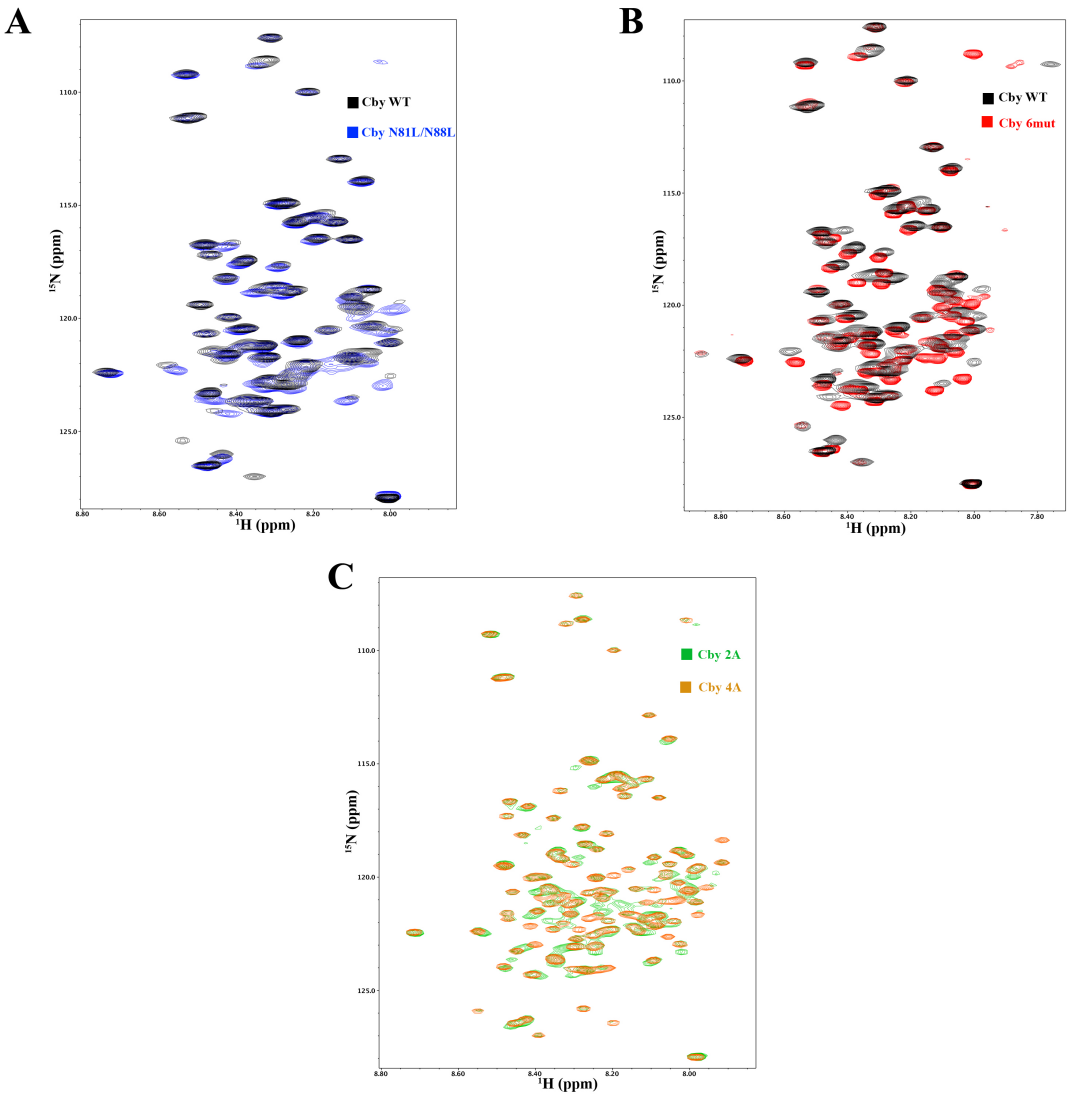

Figure 4.3 ^{1}H-^{15}N HSQC NMR spectra of full-length Cby-WT and coiled-coil mutants

A. Cby N81L/N88L (blue) overlayed with WT (black). **B.** Cby-6mut (red) overlayed with WT (black). **C.** Cby-2A (green) overlayed with Cby-4A (orange). All spectra were collected in 10 mM sodium acetate buffer, pH 5.0.

4.3.2 Interactions between TC-1 and Cby mutants

In Chapter 3, our ITC data suggested that TC-1 bound to dimeric Cby, however it is still unclear whether TC-1 can bind to monomeric Cby and which specific residues on Cby's coiled-coil mediate the interaction. Here we used NMR to investigate the interactions of TC-1 with the Cby-2A, Cby-6mut and Cby N81L/N88L mutants.

Decreases in peak intensities were observed predominantly in TC-1's C-terminal half upon titration of unlabelled Cby N81L/N88L to ^{15}N-labelled TC-1 (2:1) (Figure 4.4 A, B), similar to what has previously been observed in WT Cby titrations [19]. In contrast, titration of Cby-6mut to TC-1 did not lead to any substantial decreases in peak intensity (Figure 4.4 C, D). Collectively, the data demonstrates that although TC-1 maintained an interaction with the coiled-coil stabilized N81L/N88L mutant, the hydrophobic patch on the surface of the coiled-coil, which is mutated in Cby-6mut, may mediate Cby's interaction with TC-1. However, individual or a combination of mutations to residues in this hydrophobic patch (such as L90R, L93R, I97R, without N81 or N88 mutations) should be designed and tested to confirm their significance in TC-1 complex formation. Next, titration of Cby-2A to TC-1 did not produce any significant changes in peak intensities, suggesting that monomeric Cby is unable to bind to TC-1 (Figure 4.4 E, F).

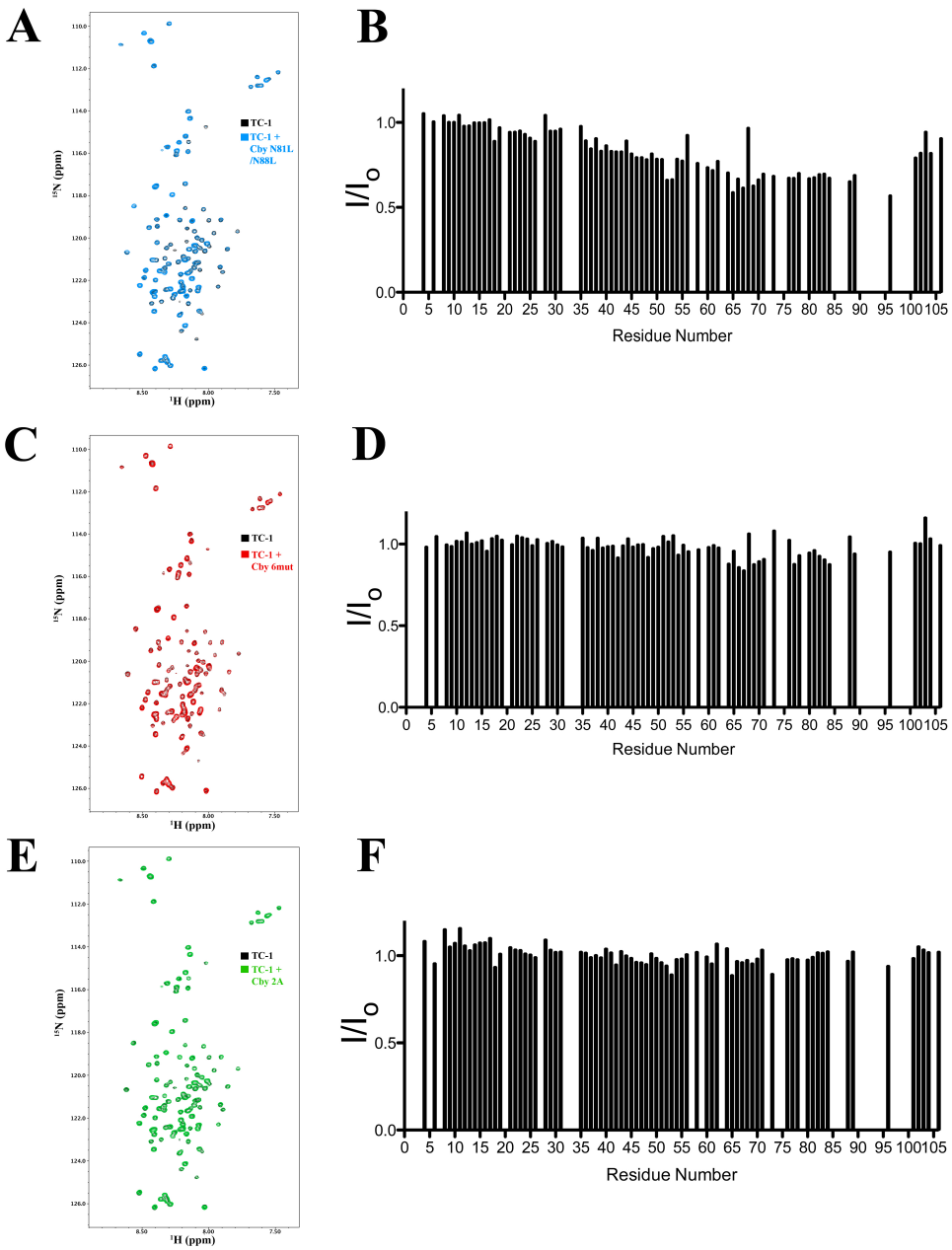

Figure 4.4 NMR titrations with TC-1 and Cby coiled-coil mutants
A. Overlay of ^{1}H-^{15}N HSQC spectra of TC-1 in the absence (black) and presence (blue) of Cby N81L/N88L at a 1:2 ratio (TC-1 60 μM: Cby 120 μM). **B.** Intensity ratios (I/I_o) for assigned TC-1 amide resonances in the presence (I) and absence (I_o) of Cby N81L/N88L. **C.** Overlay of HSQC spectra of TC-1 in the absence (black) and presence (red) of Cby 6mut at a 1:2 ratio (TC-1 35 μM: Cby 70 μM). **D.** I/I_o values for assigned TC-1 amide resonances in the presence (I) and absence (I_o) of Cby-6mut. **E.** Overlay of HSQC spectra of TC-1 in the absence (black) and presence (green) of Cby-2A at a 1:2 ratio (TC-1 60 μM: Cby 120 μM). **F.** I/I_o values for assigned TC-1 amide resonances in the presence (I) and absence (I_o) of Cby-2A. All spectra collected in 10 mM sodium acetate buffer, 50 mM NaCl, pH 5.0.

4.3.3 Structural analysis and stability of mutations to the coiled-coil of Cby in constructs lacking the disordered N-terminus

Characterizing the interaction between Cby and β-catenin using NMR spectroscopy is hindered by the two proteins' buffer incompatibility and by the peak broadening observed in Cby's C-terminal half. While more resonances are observed in the Cby-2A and 4A mutants' HSQCs, all coiled-coil mutations to full-length Cby discussed above are only soluble in buffers of low pH (pH 5) and ionic strength, while nearly full-length β-catenin (βcatR1C) is stable in buffers closer to pH 8 with 50-100 mM NaCl. Therefore, we sought to design the same set of mutations on a construct comprising the C-terminal half of Cby (C-Cby, residues 67-126), to see if the removal of Cby's disordered N-terminus may help stabilize these mutant proteins in a buffer compatible with β-catenin.

Like the full-length protein, CD spectra and thermal melting curves were collected for each C-Cby mutant (Figure 4.5, Table 4.1). As expected, the C-Cby N81L/N88L and 6mut mutants remain folded, containing much higher fractional α-helical content compared to the full-length mutants in 10 mM sodium acetate, pH 5. Additionally, the thermal melting profiles for these two mutants, measured at 222 nm, show very similar curves to what was observed in the full-length mutants. C-Cby N81L/N88L displayed very little reduction in signal over the course of the melt. Conversely, C-Cby-6mut showed a gradual reduction in signal from 20-65 °C, followed by a secondary phase of melting from 70-95 °C. Although C-Cby-6mut appears to be less thermally stable than C-Cby N81L/N88L, it is still remarkably more stable than what was observed for C-Cby-WT (see Chapter 3, Figure 3.5 D).

The C-Cby-2A and 4A mutants were found to be soluble in sodium phosphate buffer, pH 7 upon their refolding (as outlined in the Materials and Methods section). CD spectra of the C-Cby-2A and 4A mutants in 50 mM sodium phosphate, pH 7 show drastically reduced α-helical content and increased β-strand content, confirming the coiled-coil has been disrupted (Figure 4.5, Table 4.1).

The HSQCs of all C-Cby mutants were collected to determine whether they suffered the same severe line broadening as the C-Cby-WT (see Chapter 3, Figure 3.7). The C-Cby N81L/N88L and C-Cby-6mut HSQCs (Figure 4.6, A, B) show multiple weak and heavily crowded/clustered peaks characteristic of an oligomerized or aggregated protein. In contrast, the C-Cby-2A and 4A HSQCs, recorded in 50 mM sodium phosphate, pH 7, have sharp, dispersed peaks (Figure 4.6, C, D). Peak detection on the C-Cby-2A spectra counts ~ 50 resonances out of the 60 non-proline residues while C-Cby-4A has ~ 51 of 60 expected peaks. Similar to what was observed between the full-length Cby-2A and 4A HSQC spectra, C-Cby-4A has slightly sharper and less crowded peaks than C-Cby-2A.

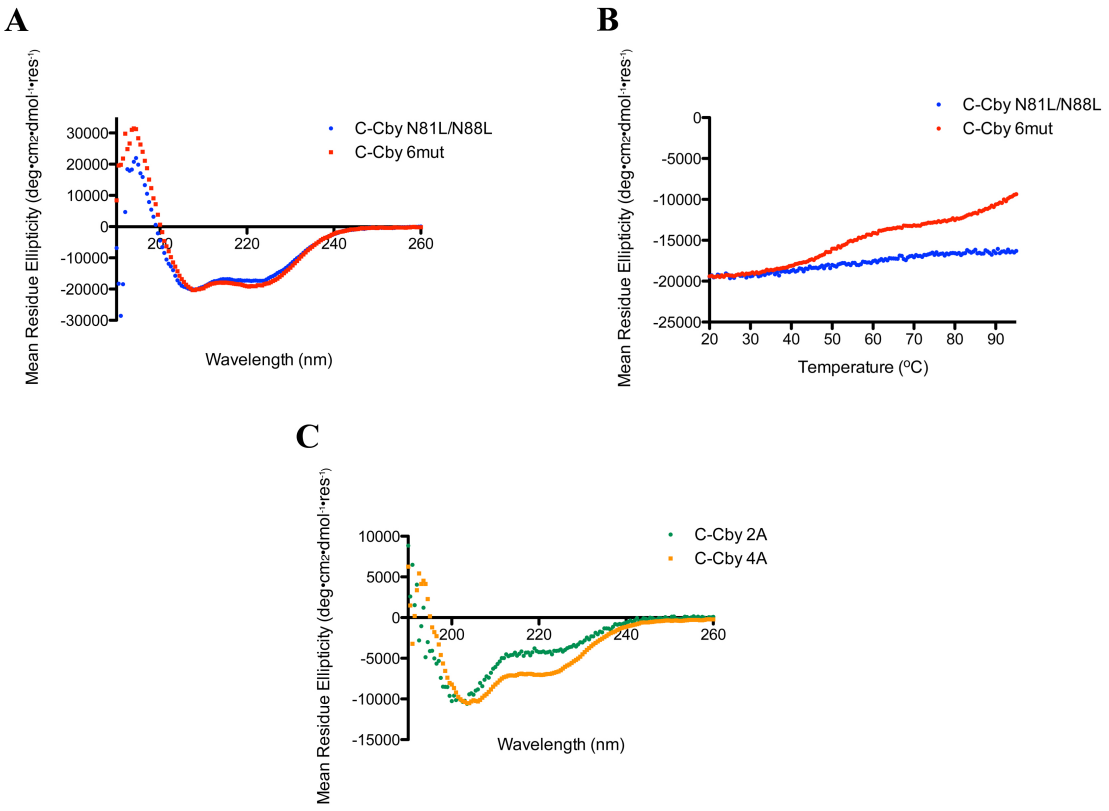

Figure 4.5 CD spectra and thermal melts of C-Cby coiled-coil mutants
A. CD spectra of C-Cby N81L/N88L and 6mut collected in 10 mM Na acetate, pH 5.0. Displayed spectra are the accumulation of 5 scans. **B.** Thermal melting curves of C-Cby N81L/N88L and C-Cby 6mut using CD at 222 nm, collected in 10 mM Na acetate, pH 5.0. **C.** CD spectra of C-Cby 2A and 4A collected in 50 mM sodium phosphate, pH 7.0. Displayed spectra are the accumulation of 5 scans.

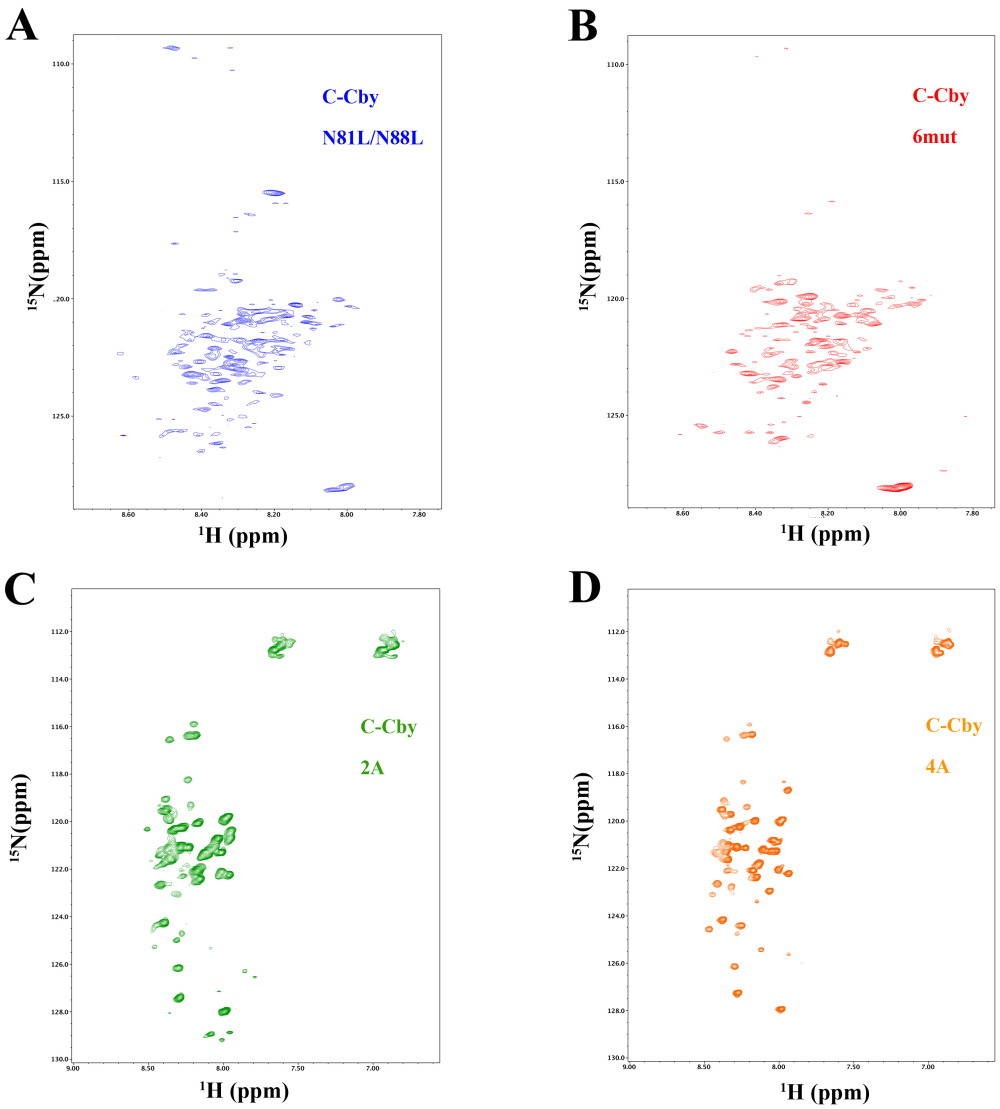

Figure 4.6 ^{1}H-^{15}N HSQC NMR spectra of C-Cby WT and C-Cby coiled-coil mutants **A.** C-Cby N81L/N88L. **B.** C-Cby-6mut. **C.** C-Cby-2A. **D.** C-Cby-4A. C-Cby N81L/N88L and 6mut were collected in 10 mM sodium acetate, pH 5.0 and C-Cby-2A and 4A were collected in 50 mM sodium phosphate, pH 7.0.

4.3.4 Cby's Interaction with β-catenin

Previous work has demonstrated the C-terminal half of Cby alone can bind to β-catenin [11]. Our hydrogen-deuterium exchange (HDX) mass spectrometry results, discussed in Chapter 3, revealed that Cby's C-terminal half contains the coiled-coil region and a disordered C-terminal extension ranging from residues 101-126. We investigated whether or not the coiled-coil region of Cby is sufficient for binding β-catenin. A pull-down experiment using amylose resin reveals that an MBP-fused Cby construct comprising Cby's coiled-coil domain (Coil-Cby, residues 67-104) retains the ability to bind β-catR1C, while MBP alone does not (Figure 4.7, A). Additionally, isothermal titration calorimetry (ITC) reveals that a synthetic peptide comprising Cby residues 102-126 shows no binding to β-catR1C (Figure 4.7, B). However, this ITC result does not rule out very weak binding between the C-terminal extension and β-catenin. Alternatively, the C-terminal extension may only participate in the interaction in the context of the full-length protein.

Next, we tested whether the C-Cby coiled-coil mutants could interact with β-catR1C using an MBP pull-down assay. Full-length Cby-2A and 4A have already been shown to bind to β-catenin using a similar assay using MBP-fusion Cby proteins [16]. Results of the assay confirm this, as C-Cby-2A pulled-down β-catR1C, while the C-Cby N81L/N88L and C-Cby-6mut mutations compromised Cby's interaction with β-catR1C (Figure 4.7, C).

With the C-Cby-2A construct able to bind to β-catR1C, along with it being soluble at physiological pH and having observable amide resonances in its ^{1}H-^{15}N HSQC

spectrum, we were able to test the binding of these two proteins using NMR spectroscopy. Titration of β-catR1C to C-Cby-2A at a 0.3:1 ratio showed peak intensity loss for some residues, confirming the binding result of the pull-down assay (Figure 4.8).

Using NMR spectroscopy to assess the binding between β-catenin and C-Cby-2A from β-catenin's perspective is challenging due to the large size of β-catR1C (~ 70 kDa). Therefore, as initial work, we attempted to use a smaller β-catenin construct comprising armadillo repeat 10 to the C-terminus (β-catR10C, 28 kDa), which still contains Cby's proposed binding site, helix C on β-catenin [18]. Unfortunately, the HSQC of β-catR10C displays less than half of the expected number of amide resonances expected, many of which are weak, crowded and dispersed over a narrow ^{1}H chemical shift range (Figure 4.9, A). In a previous study, NMR titration experiments by Xing *et al*. [18] were designed to assess whether the disordered C-terminal end of β-catenin interacted with β-catenin's armadillo repeats or disordered N-terminal tail. To do so, they expressed and purified the ^{15}N-labelled C-terminal tail (residues, 697-781) of β-catenin and titrated an unlabelled construct comprising the armadillo repeats (1-686) (Figure 4.9, B). The group's collected HSQC spectrum of the C-terminal tail looks extremely similar to what we observe in the β-catR10C spectrum, suggesting that no resonances from the armadillo repeats in β-catR10C are observed. Importantly, a CD spectrum of β-catR10C demonstrates the protein is folded (deconvolution of spectrum: 33% α-helix, 21% β-strand, 46% turns/disordered) (Figure 4.9, C). An even smaller β-catenin construct, perhaps with a truncated C-terminal tail, may be required to assess the complex from β-catenin's perspective.

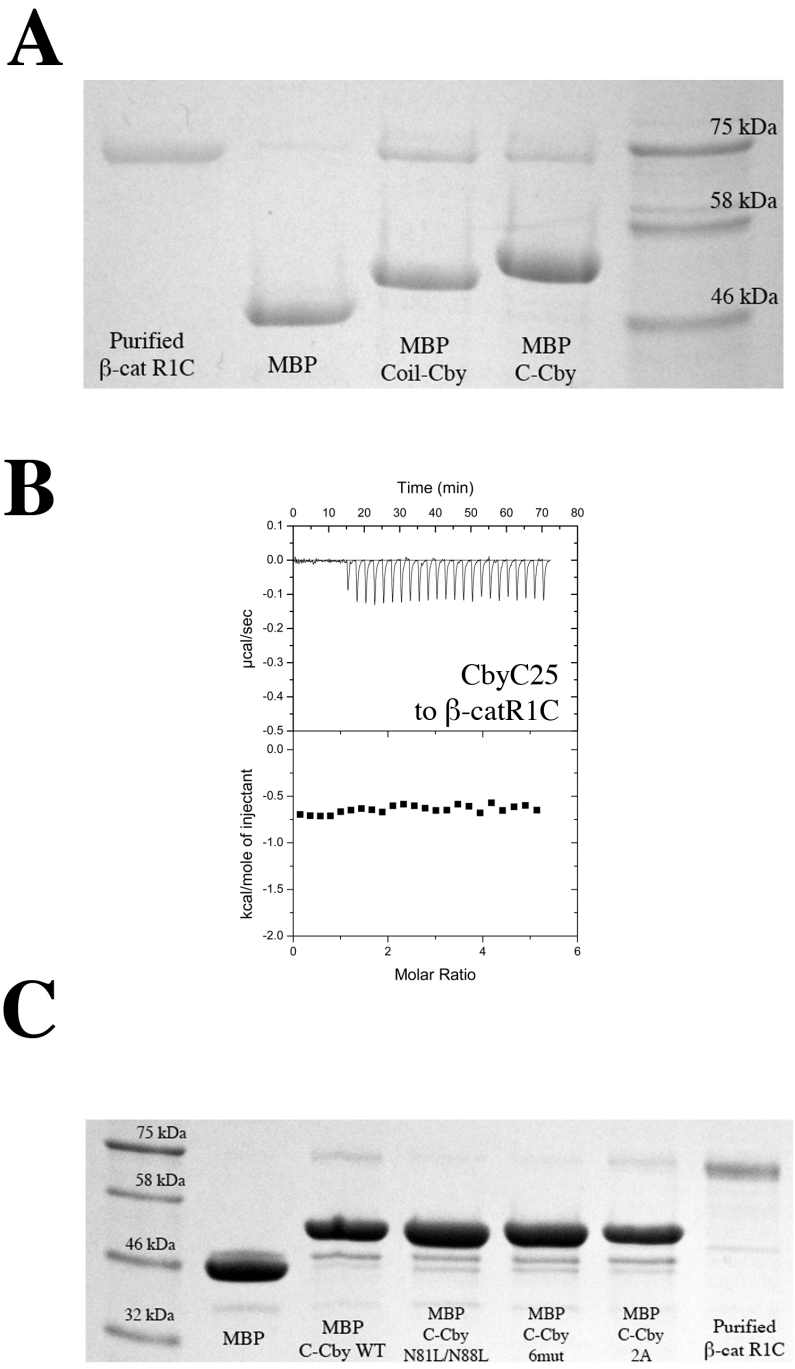

Figure 4.7 Cby binding to β-catenin using pull-down assays and ITC
A. Binding of Cby constructs (C-Cby, Coil-Cby) evaluated by an *in vitro* pull-down assay. **B.** ITC profile of the CCby25 peptide titrated to β-catR1C. **C.** Binding of C-Cby-WT and mutants evaluated by an *in vitro* pull-down assay.

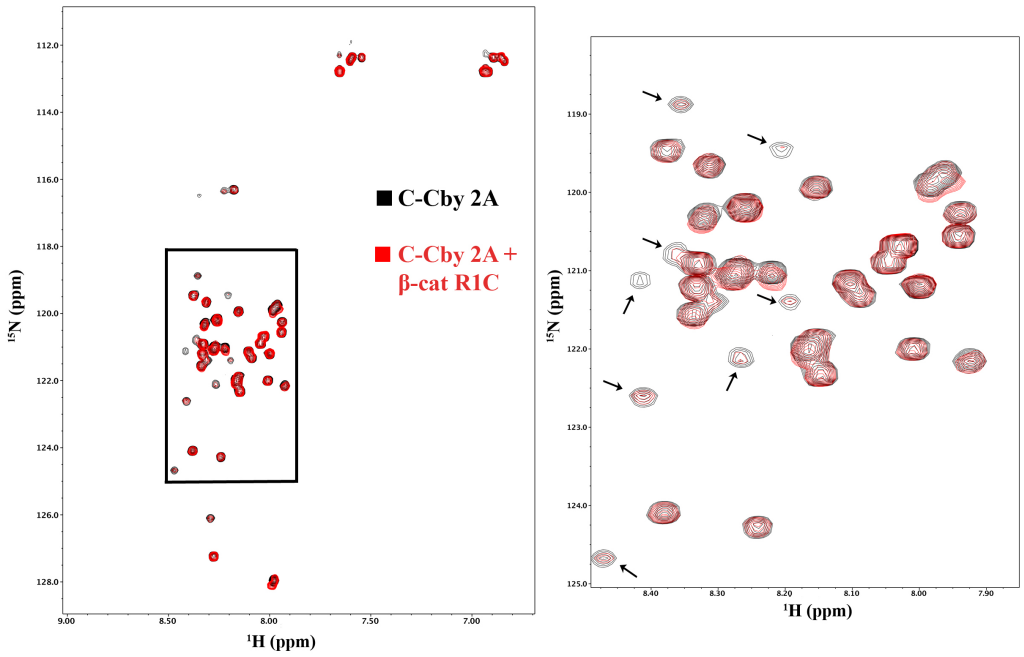

Figure 4.8 NMR titration experiment with C-Cby-2A and β-catenin
On left: ^{1}H-^{15}N HQSC of C-Cby 2A (black) overlayed with C-Cby 2A in the presence of β-catR1C (red) at a 1:0.3 molar ratio (C-Cby 2A: β-catR1C, 45 μM: 15 μM. On right: Zoomed in segment that is boxed in on the left spectrum. Arrows point to peaks with greatest losses in intensity.

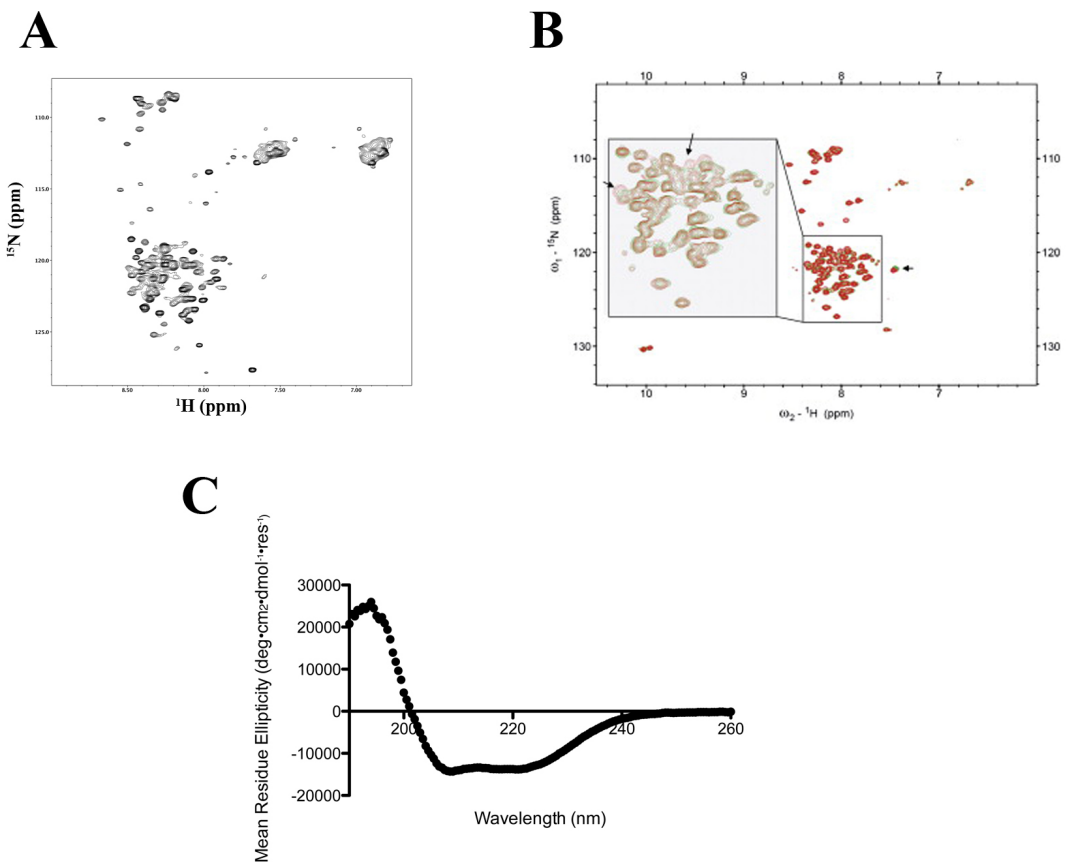

Figure 4.9 Characterization of β-catR10C
^{1}H-^{15}N HSQC spectrum of His-tagged β-catR10C in 50 mM sodium phosphate, pH 7.0. **B.** ^{1}H-^{15}N HSQC spectrum of C-terminal β-catenin (residues 687-781) in 20 mM Tris, 100 mM NaCl, 2mM DTT, pH 7.5 collected and reported by Xing *et al*. [18]. **C.** CD spectrum (5 accumulated scans) of His-tagged β-catR10C in 50 mM sodium phosphate, pH 7.0.

4.4 Discussion

Attempts to analyze the structural mechanisms by which Cby achieves its antagonistic role in the Wnt signaling pathway remain hindered by the protein's insolubility. Additionally, characterizing the protein using NMR spectroscopy is hampered by the invisibility of peaks in its C-terminal half, likely due to conformational exchange [17]. In this work, we have attempted to use two mutagenesis strategies to generate recombinant Cby that is soluble in buffers closer to physiological pH, and that may promote the appearance of C-terminal peaks in ^{1}H-^{15}N HSQC spectra. The first strategy was to stabilize the coiled-coil through mutation of core asparagines (Cby N81L/N88L), followed by the removal of hydrophobic residues on the surface of the coiled-coil (Cby-6mut, N81L/N88L/L90R/L93R/I97R/L99E). While both of these mutants led to a more stabilized coiled-coil relative to WT, both proteins remained insoluble at physiological pH and did not produce additional peaks in their HSQC spectra. The second strategy involved breaking the coiled-coil domain using core leucine to alanine mutations that have previously been found to produce monomeric Cby. While these Cby-2A (L84A/L98A) and 4A (L77A/L84A/L91A/L98A) mutants successfully disturbed the coiled-coil and produced additional resonances in their HSQC spectra, they remained highly insoluble. However, by utilizing the same 2A and 4A mutations to the C-terminal half of Cby (C-Cby), we obtained a soluble Cby construct that could be used to study the Cby/β-catenin complex using NMR spectroscopy.

While TC-1 and β-catenin both interact with Cby's coiled-coil domain [11,14], their modes of interaction may be different. With TC-1, it appears to preferentially bind to dimeric Cby as it fails to interact with the monomeric mutant, Cby-2A. In order to

bind to dimeric Cby, TC-1 would have to interact with the surface of the coiled-coil. Indeed, while TC-1 maintained an interaction with the N81L/N88L Cby mutant, this binding was abolished with Cby-6mut, which has three hydrophobic residues on the surface of the coiled-coil mutated to arginine (L90R, L93R, I97R). Critically, the design of Cby mutants with mutations to solely L90, L93 and/or I97R (no mutations to the core asparagines, N81L/N88L) should be made to confirm their importance in the TC-1 interaction. Conversely, β-catenin was able to bind to monomeric C-Cby-2A as demonstrated in a pull-down assay and NMR titration experiment, but was unable to interact with C-Cby N81L/N88L and C-Cby-6mut in our pull-down assay.

The differing modes of interaction in the Cby/TC-1 and Cby/β-catenin complexes may be critical to Cby's regulation in Wnt signaling. If β-catenin exclusively binds to monomeric Cby, then TC-1 will not only antagonize Cby by competing with β-catenin for binding to Cby's C-terminal half, but may also keep Cby in a dimeric state.

Of note, it is important to point out that being restricted to utilizing pull-down assays to characterize the Cby/β-catenin complex is the result of the severe insolubility of Cby, hindering our ability to quantitatively assess the strength of the interactions between these Cby mutants and β-catenin. While β-catenin can bind to monomeric Cby, it's of interest to determine whether it binds to the surface exposed residues of Cby's coiled-coil or its core residues. Also, it is unknown if Cby's C-terminal extension plays a role in the interaction. Our NMR titration experiment using ^{15}N-labelled C-Cby-2A and unlabelled β-catR1C showed reduced peak intensities for a number of residues. Backbone chemical shift assignment of the ^{1}H-^{15}N HSQC spectrum of C-Cby-2A will be critical to determine

which residues undergo peak intensity loss and may help in identifying the residues that specifically bind to β-catR1C. Notably, our purification yields only ~ 0.4 mg per L of growth in M9 medium, therefore a large scale growth will be required to obtain a sufficiently high concentration for 3D NMR experiments.

Although C-Cby-2A can help provide molecular details of the Cby/β-catenin complex, it is unfortunate that the full-length Cby-2A remains insoluble, as the role of Cby's N-terminus in the interaction, if any, cannot be determined. Although the N-terminal half of Cby cannot bind to β-catenin on its own, it may still form subsequent secondary contacts with β-catenin after the C-terminal half of Cby interacts. Such a mechanism is observed in another inhibitor of β-catenin called ICAT (inhibitor of β-catenin and Tcf4) [27,28]. ICAT consists of an α-helical N-terminal half and a disordered C-terminal half. ICAT's antagonism is achieved when its N-terminal helical bundle anchors itself into armadillo repeat 12, followed by its unstructured C-terminal half interacting around repeats 5-9. ICAT's C-terminal half cannot bind to β-catenin alone, however, and its N-terminal helical half, although able to bind on its own, cannot inhibit Tcf4 binding [29]. As such, the N-terminal half of ICAT must first anchor to β-catenin, enabling its C-terminal half to subsequently bind and mask the Tcf4 binding site (armadillo repeats 2-10). Seeing as Cby's C-terminal half anchors to the helix C (and possibly armadillo repeat 12) of β-catenin, it is possible Cby's unstructured N-terminus is utilized to mask the Tcf4 binding site.

4.5 References

1. Nusse R, Varmus H (2012) Three decades of Wnts: a personal perspective on how a scientific field developed. EMBO J 31: 2670-2684.

2. Cadigan KM, Peifer M (2009) Wnt signaling from development to disease: insights from model systems. Cold Spring Harb Perspect Biol 1: a002881.

3. Niehrs C (2012) The complex world of WNT receptor signalling. Nat Rev Mol Cell Biol 13: 767-779.

4. Freese JL, Pino D, Pleasure SJ (2010) Wnt signaling in development and disease. Neurobiol Dis 38: 148-153.

5. Baron R, Kneissel M (2013) WNT signaling in bone homeostasis and disease: from human mutations to treatments. Nat Med 19: 179-192.

6. Clevers H, Nusse R (2012) Wnt/beta-catenin signaling and disease. Cell 149: 1192-1205.

7. Aberle H, Bauer A, Stappert J, Kispert A, Kemler R (1997) beta-catenin is a target for the ubiquitin-proteasome pathway. EMBO J 16: 3797-3804.

8. Kikuchi A (2000) Regulation of beta-catenin signaling in the Wnt pathway. Biochem Biophys Res Commun 268: 243-248.

9. Kim W, Kim M, Jho EH (2013) Wnt/beta-catenin signalling: from plasma membrane to nucleus. Biochem J 450: 9-21.

10. Jamieson C, Sharma M, Henderson BR (2012) Wnt signaling from membrane to nucleus: beta-catenin caught in a loop. Int J Biochem Cell Biol 44: 847-850.

11. Takemaru K, Yamaguchi S, Lee YS, Zhang Y, Carthew RW, et al. (2003) Chibby, a nuclear beta-catenin-associated antagonist of the Wnt/Wingless pathway. Nature 422: 905-909.

12. Li FQ, Mofunanya A, Harris K, Takemaru K (2008) Chibby cooperates with 14-3-3 to regulate beta-catenin subcellular distribution and signaling activity. J Cell Biol 181: 1141-1154.

13. Li FQ, Mofunanya A, Fischer V, Hall J, Takemaru K (2010) Nuclear-cytoplasmic shuttling of Chibby controls beta-catenin signaling. Mol Biol Cell 21: 311-322.

14. Jung Y, Bang S, Choi K, Kim E, Kim Y, et al. (2006) TC1 (C8orf4) enhances the Wnt/beta-catenin pathway by relieving antagonistic activity of Chibby. Cancer Res 66: 723-728.

15. Chua EL, Young L, Wu WM, Turtle JR, Dong Q (2000) Cloning of TC-1 (C8orf4), a novel gene found to be overexpressed in thyroid cancer. Genomics 69: 342-347.

16. Mofunanya A, Li FQ, Hsieh JC, Takemaru K (2009) Chibby forms a homodimer through a heptad repeat of leucine residues in its C-terminal coiled-coil motif. BMC Mol Biol 10: 41.

17. Mokhtarzada S, Yu C, Brickenden A, Choy WY (2011) Structural characterization of partially disordered human Chibby: insights into its function in the Wnt-signaling pathway. Biochemistry 50: 715-726.

18. Xing Y, Takemaru K, Liu J, Berndt JD, Zheng JJ, et al. (2008) Crystal structure of a full-length beta-catenin. Structure 16: 478-487.

19. Gall C, Xu H, Brickenden A, Ai X, Choy WY (2007) The intrinsically disordered TC-1 interacts with Chibby via regions with high helical propensity. Protein Sci 16: 2510-2518.

20. Molenaar M, van de Wetering M, Oosterwegel M, Peterson-Maduro J, Godsave S, et al. (1996) XTcf-3 transcription factor mediates beta-catenin-induced axis formation in Xenopus embryos. Cell 86: 391-399.

21. Jensen MR, Ruigrok RW, Blackledge M (2013) Describing intrinsically disordered proteins at atomic resolution by NMR. Curr Opin Struct Biol 23: 426-435.

22. Konrat R (2014) NMR contributions to structural dynamics studies of intrinsically disordered proteins. J Magn Reson 241: 74-85.

23. Whitmore L, Wallace BA (2004) DICHROWEB, an online server for protein secondary structure analyses from circular dichroism spectroscopic data. Nucleic Acids Res 32: W668-673.

24. Abdul-Gader A, Miles AJ, Wallace BA (2011) A reference dataset for the analyses of membrane protein secondary structures and transmembrane residues using circular dichroism spectroscopy. Bioinformatics 27: 1630-1636.

25. Delaglio F, Grzesiek S, Vuister GW, Zhu G, Pfeifer J, et al. (1995) NMRPipe: a multidimensional spectral processing system based on UNIX pipes. J Biomol NMR 6: 277-293.

26. Johnson BA (2004) Using NMRView to visualize and analyze the NMR spectra of macromolecules. Methods Mol Biol 278: 313-352.

27. Graham TA, Clements WK, Kimelman D, Xu W (2002) The crystal structure of the beta-catenin/ICAT complex reveals the inhibitory mechanism of ICAT. Mol Cell 10: 563-571.

28. Daniels DL, Weis WI (2002) ICAT inhibits beta-catenin binding to Tcf/Lef-family transcription factors and the general coactivator p300 using independent structural modules. Mol Cell 10: 573-584.

29. Tago K, Nakamura T, Nishita M, Hyodo J, Nagai S, et al. (2000) Inhibition of Wnt signaling by ICAT, a novel beta-catenin-interacting protein. Genes Dev 14: 1741-1749.

Chapter 5

5 Summary and Perspectives

The Wnt signaling antagonist Chibby (Cby) acts on the transcriptional co-activator β-catenin, preventing its interaction with the Tcf/Lef transcription factors and in concert with the 14-3-3 proteins, promotes β-catenin's cytoplasmic sequestration [1,2]. The structural mechanisms by which Cby interacts with the Wnt signalling components 14-3-3 and β-catenin remain elusive, largely due to recombinant Cby's insolubility, as well as its partially disordered structure. Cby harbours a coiled-coil domain in its C-terminal half while its N-terminal half is unstructured. These individual halves of Cby contain binding motifs for the Wnt signalling components 14-3-3, β-catenin and the Cby antagonist, TC-1. Cby's N-terminal half contains a 14-3-3 binding motif, whereas its C-terminal half is responsible for binding to β-catenin and TC-1.

Cby has proven to be a challenge to work with using NMR spectroscopy, a valuable and powerful tool in the analysis of disordered proteins. In addition to Cby requiring low pH (~ 5) and ionic strength to remain soluble, residues within in its C-terminal half experience severe line broadening in the protein's ^{1}H-^{15}N HSQC spectra [3]. This line-broadening, likely due to conformational exchange of Cby's coiled-coil, not only hinders characterizing Cby by itself, but also the analysis of its protein-protein interactions. Despite these challenges, the work in this thesis provides molecular insights into the protein's interactions with the Wnt signalling components 14-3-3, β-catenin and TC-1.

5.1 Characterizing the Cby/14-3-3 Interaction

Upon phosphorylation by the kinase Akt, Cby forms a complex with 14-3-3 to facilitate the nuclear export of β-catenin, thereby suppressing Wnt signalling [3]. Using a combination of X-ray crystallography, NMR spectroscopy and isothermal titration calorimetry, the molecular details of the Cby/14-3-3ζ interaction were revealed. Using a synthetic phosphorylated Cby peptide comprising Cby's 14-3-3 binding motif, the crystal structure of the 14-3-3ζ/phosphorylated Cby complex was solved. In addition to the canonical 14-3-3 binding mode observed in the solved crystal structure, NMR spectroscopy and ITC experiments showed that residues flanking Cby's 14-3-3 binding motif are important to the interaction. First, ITC experiments using phosphorylated Cby peptides of different lengths demonstrated that flanking residues contribute to the binding affinity. Second, upon completion of the backbone resonance assignment of 14-3-3ζ, NMR titration experiments revealed that residues outside of 14-3-3's conserved binding cleft, namely a flexible loop consisting of residues 203-210, are involved in the Cby interaction. While the structural characterization of the complex focused on the ζ isoform of 14-3-3, ITC experiments showed that Cby binds to all seven 14-3-3 human isoforms.

The vast majority of 14-3-3 complexes solved by X-ray crystallography are limited to using phosphorylated peptides. While this may be due to the technical challenges of crystallizing protein-protein complexes, the majority of 14-3-3 binding partners are thought to be partially disordered [4] and may therefore be non-crystallizable. To date, there is only one structure of a nearly full-length binding partner (Serotonin N-acetyltransferase or AANAT) in complex with 14-3-3 [5]. The

AANAT/14-3-3 complex structure reveals secondary binding contacts (contacts outside of the 14-3-3 binding groove, and outside of the binding partner's 14-3-3 binding motif) between AANAT and 14-3-3. Similar to what was observed in the 14-3-3/Cby complex, other structural studies looking at 14-3-3 binding partners, such as integrin [6], have demonstrated that residues flanking their 14-3-3 binding motifs contribute to their interactions with 14-3-3. Our completion of the 14-3-3ζ backbone assignment may aid in unveiling secondary contacts between 14-3-3 and binding partners that lack discernible electron density due to their dynamics in their co-crystallized structures, or for complexes that are extremely challenging to crystallize.

5.2 Elucidating the structural elements of Cby and their interplay in target recognition

Previous structural analyses of Cby using NMR spectroscopy suffered from severe line broadening within the protein's C-terminal half, hindering the characterization of its coiled-coil domain. In our study described in Chapter 3, we used hydrogen-deuterium exchange mass spectrometry (HDX-MS) as a complementary technique to examine the structural properties of Cby. Our results reveal three individual structural elements on Cby, its disordered N-terminus, the coiled-coil domain and a C-terminal unstructured extension consisting of the last ~ 25 residues. A series of truncation constructs were designed to assess the roles each structural element plays in the overall stability of Cby as well as their role in binding to the Cby antagonist TC-1. CD and NMR data showed that Cby maintains a coiled-coil structure upon deletion of either disordered region. Additionally, NMR and ITC binding experiments demonstrate that the Cby and TC-1 interaction is retained upon deletion of either the N-terminal half or C-

terminal extension, highlighting that the coiled-coil domain is vital to complex formation. Moreover, Cby appears to bind to TC-1 as a dimer. Interestingly, the C-terminal half of Cby alone binds to TC-1 with significantly greater affinity compared to the full-length protein. Our results suggest that Cby's flanking disordered regions affect the stability of the coiled-coil domain and its ability to target binding partners, potentially due to a higher entropic cost of binding.

5.3 Differing binding modes for the Cby/TC-1 and Cby/β-catenin complexes

A study by Mofunanya *et al.* [7] demonstrated that alanine substitutions to two or more of the four critical leucines within Cby's core of its coiled-coil domain (L77, L84, L91, L98) were sufficient for eliminating the dimerization of Cby. Moreover, these Cby mutants retained the ability to interact with β-catenin and repress β-catenin-mediated Wnt signalling. Our work described in Chapter 4 focused on determining whether these Cby mutants could be utilized to study the Cby/β-catenin complex using NMR spectroscopy, with the expectation that the disrupted coiled-coil may improve the solubility of Cby and lead to the appearance of C-terminal residue peaks in the protein's C-terminal half. Our findings show that two Cby mutants with alanine substitutions (L84A/L98A, or 2A, and L77A/L84A/L91A/L98A, or 4A) disrupt the coiled-coil in the full-length Cby, but remain highly insoluble in buffers close to physiological pH. However, when the same mutations were made to a Cby construct comprising its C-terminal half alone (C-Cby, residues 67-126), the mutants were found to be soluble at physiological pH. Additionally, the majority of peaks are visible in the C-Cby 2A and 4A ^{1}H-^{15}N HSQC.

An NMR titration experiment found that the C-Cby 2A construct binds to β-catenin as evidenced by drops in peak intensity for some resonances.

Additional mutants were designed along Cby's coiled-coil and tested for binding to TC-1. It was found that mutating surface exposed hydrophobic residues to arginines effectively abolished Cby's interaction with TC-1. With Cby binding to TC-1 as a dimer, it is reasonable to assume residues on the surface of the coiled-coil would mediate the interaction with TC-1.

5.4 Future Directions and Perspectives

5.4.1 Characterizing the 14-3-3/Cby interaction in the context of full-length Cby

The Cby/14-3-3 interaction has been extensively studied using synthetic phosphorylated Cby peptides. However, questions remain as to how the complex is formed when full-length Cby is bound. First, as the 14-3-3 dimer is able to bind to two Cby molecules at the same time, it is of interest to find out if two bound Cby proteins could still form a coiled-coil when bound to 14-3-3. The mechanisms for protein interactions involving unstructured proteins has largely fallen under a now out-dated paradigm of disorder-to-order transitions, as a growing amount of evidence reveals that disordered proteins may remain highly dynamic or "fuzzy" in their bound states [8]. Thus, although the C-terminal ends of each Cby molecule exit the 14-3-3 binding cleft at opposing ends of the 14-3-3 dimer, there could be sufficient length and flexibility in Cby's unstructured N-terminus for the coiled-coil to still form. Determining the particular binding orientation and stoichiometry necessary for the Cby/14-3-3 interaction

is critical towards the understanding of Cby-mediated β-catenin cytoplasmic sequestration.

Several obstacles must be overcome to study this interaction. First, the *in vitro* phosphorylation of Cby by the kinase Akt must be done in an Akt-active buffer, and one which will not cause Cby to aggregate. As such, successful phosphorylation may require an MBP or GST fusion Cby protein. Alternatively, a recently developed methodology allows the incorporation of phosphoserine into proteins *in vivo* in *E. coli* [9]. This powerful new tool was established by engineering the translational machinery in bacteria to enable phosphoserine to be integrated into proteins. This developing method has effectively been used to over-express several phosphorylated proteins [9,10,11]. The second major hurdle will be finding a compatible buffer for 14-3-3 and phosphorylated Cby.

5.4.2 Cby's Disordered Ends Modulate Target Binding and Applicability of HDX-MS to Other Protein Studies

An intriguing result from our NMR and isothermal titration calorimetry experiments in Chapter 3 showed that the C-terminal half of Cby bound to TC-1 with significantly greater affinity than the full-length protein. This suggest that the free unstructured N-terminal domain may auto-inhibit (potentially as an entropic bristle [12]) Cby's binding targets from interacting with the coiled-coil domain. This begs the question that if Cby's N-terminus is already bound to a protein, for example 14-3-3, whether this auto-inhibition may be relieved, allowing the C-terminus to bind to client proteins with high affinity. This mechanism would allow for sequential binding events, and would demonstrate cooperativity between Cby's structural halves.

As demonstrated in our HDX-MS experiment on Cby, this technique may be useful in characterizing and mapping of coiled-coil domains in other partially disordered proteins. Like Cby, NMR studies involving the coiled-coil containing proteins CHOP [13], Par-4 [14] and NA14 [15] have been troubled by line broadening for residues within their coiled-coils. HDX-MS can provide details on the size and dynamics of their respective coiled-coil domains.

5.4.3 Monomeric Cby and its interaction with β-catenin

As C-Cby 2A is soluble and its peaks are present in the protein's HSQC spectrum, backbone assignment of this construct, followed by titration experiments may help in deciphering which residues within the coiled-coil are responsible for binding to β-catenin.

Despite the challenges in characterizing the β-catenin/Cby interaction, it has been speculated that Cby may antagonize β-catenin in a similar fashion to ICAT [16]. In the bound state, an α-helical bundle located in ICAT's N-terminus anchors within armadillo repeats R10-R12 of β-catenin and likely interacts with helix C on β-catenin as well [16,17,18]. ICAT's disordered N-terminus then wraps around armadillo repeats R5-R9. The disordered C-terminus is responsible for displacing the Tcf/Lef transcription factors whose binding sites extend along repeats R2-R10 [17,19]. This mode of action has been referred to as an "anchor-and-kick" mechanism [16]. Intriguingly, despite the disordered C-terminal domain of ICAT burying 1700 Å of surface into β-catenin, and forming similar contacts in repeats R5-R9 as those seen in APC, Tcf and Lef, it is unable to interact with β-catenin in the absence of the N-terminal helical bundle [19]. Moreover, while the N-terminal α-helical bundle of ICAT alone maintains binding to β-catenin, it is incapable of displacing the Tcf/Lef transcription factors [17]. With regards to the β-

catenin/Cby interaction, Cby's C-terminal coiled-coil domain is responsible for binding to the helix C of β-catenin and can bind independently of its N-terminal half. Conversely, its disordered N-terminus does not bind to β-catenin alone.

While ICAT and Cby may share similar modes of antagonism, Cby's dimerization represents an additional layer of complexity. Mutations to monomerize Cby retain the ability to bind to β-catenin, however whether Cby can interact in a dimeric state and what effect this may have on its effectiveness as a Wnt signaling antagonist must still be elucidated.

5.5 Conclusion

The coexistence of intrinsic disorder and coiled-coil domains is found throughout the proteome. Elucidating the structural mechanisms by which Cby interacts with itself, β-catenin, 14-3-3 and TC-1 not only provides insight into its role as an antagonist in the Wnt signalling pathway, but offers increased understanding of how dual-module proteins consisting of intrinsic disorder and coiled-coil domains function as hubs in signalling cascades linked to human disease.

5.6 References

1. Takemaru K, Yamaguchi S, Lee YS, Zhang Y, Carthew RW, et al. (2003) Chibby, a nuclear beta-catenin-associated antagonist of the Wnt/Wingless pathway. Nature 422: 905-909.

2. Li FQ, Mofunanya A, Harris K, Takemaru K (2008) Chibby cooperates with 14-3-3 to regulate beta-catenin subcellular distribution and signaling activity. J Cell Biol 181: 1141-1154.

3. Mokhtarzada S, Yu C, Brickenden A, Choy WY (2011) Structural characterization of partially disordered human Chibby: insights into its function in the Wnt-signaling pathway. Biochemistry 50: 715-726.

4. Johnson C, Crowther S, Stafford MJ, Campbell DG, Toth R, et al. (2010) Bioinformatic and experimental survey of 14-3-3-binding sites. Biochem J 427: 69-78.

5. Obsil T, Ghirlando R, Klein DC, Ganguly S, Dyda F (2001) Crystal structure of the 14-3-3zeta:serotonin N-acetyltransferase complex. a role for scaffolding in enzyme regulation. Cell 105: 257-267.

6. Bonet R, Vakonakis I, Campbell ID (2013) Characterization of 14-3-3-zeta Interactions with integrin tails. J Mol Biol 425: 3060-3072.

7. Mofunanya A, Li FQ, Hsieh JC, Takemaru K (2009) Chibby forms a homodimer through a heptad repeat of leucine residues in its C-terminal coiled-coil motif. BMC Mol Biol 10: 41.

8. Sharma R, Raduly Z, Miskei M, Fuxreiter M (2015) Fuzzy complexes: Specific binding without complete folding. FEBS Lett 589: 2533-2542.

9. Park HS, Hohn MJ, Umehara T, Guo LT, Osborne EM, et al. (2011) Expanding the genetic code of Escherichia coli with phosphoserine. Science 333: 1151-1154.

10. Rogerson DT, Sachdeva A, Wang K, Haq T, Kazlauskaite A, et al. (2015) Efficient genetic encoding of phosphoserine and its nonhydrolyzable analog. Nat Chem Biol 11: 496-503.

11. George S, Aguirre JD, Spratt DE, Bi Y, Jeffery M, et al. (2016) Generation of phospho-ubiquitin variants by orthogonal translation reveals codon skipping. FEBS Lett 590: 1530-1542.

12. Hoh JH (1998) Functional protein domains from the thermally driven motion of polypeptide chains: a proposal. Proteins 32: 223-228.

13. Singh VK, Pacheco I, Uversky VN, Smith SP, MacLeod RJ, et al. (2008) Intrinsically disordered human C/EBP homologous protein regulates biological activity of colon cancer cells during calcium stress. J Mol Biol 380: 313-326.

14. Libich DS, Schwalbe M, Kate S, Venugopal H, Claridge JK, et al. (2009) Intrinsic disorder and coiled-coil formation in prostate apoptosis response factor 4. FEBS J 276: 3710-3728.

15. Rodriguez-Rodriguez M, Trevino MA, Laurents DV, Arranz R, Valpuesta JM, et al. (2011) Characterization of the structure and self-recognition of the human centrosomal protein NA14: implications for stability and function. Protein Eng Des Sel 24: 883-892.

16. Graham TA, Clements WK, Kimelman D, Xu W (2002) The crystal structure of the beta-catenin/ICAT complex reveals the inhibitory mechanism of ICAT. Mol Cell 10: 563-571.

17. Daniels DL, Weis WI (2002) ICAT inhibits beta-catenin binding to Tcf/Lef-family transcription factors and the general coactivator p300 using independent structural modules. Mol Cell 10: 573-584.

18. Xing Y, Takemaru K, Liu J, Berndt JD, Zheng JJ, et al. (2008) Crystal structure of a full-length beta-catenin. Structure 16: 478-487.

19. Tago K, Nakamura T, Nishita M, Hyodo J, Nagai S, et al. (2000) Inhibition of Wnt signaling by ICAT, a novel beta-catenin-interacting protein. Genes Dev 14: 1741-1749.

Curriculum Vitae

RYAN KILLORAN
Department of Biochemistry, University of Western Ontario, London, ON

EDUCATION
University of Western Ontario, London, ON
Ph.D. in Biochemistry – Expected completion: August 2016
2011-2016
Supervisor: Dr. Wing-Yiu Choy

Queen's University, Kingston, ON
B.Sc. in Biochemistry
2007-2011

TEACHING ASSISTANT EXPERIENCE
Biochemistry 3390
Design and mark assignments, hold office hours, run tutorials
2012-2016

Biochemistry 2288
Mark assignments, proctor exams
2015

Biochemistry 2280
Proofread exams, administrative exam preparations
2014

PUBLICATIONS
Killoran, R.C., Sowole, M.A., Halim, M.A., Konermann, B.H. and Choy W.Y. 2016. Conformational characterization of the intrinsically disordered protein Chibby: Interplay between structural elements in target recognition. Protein Science, doi:10.1002/pro.2936

Killoran, R.C., Fan, J., Yang, D., Shilton, B.H. and Choy W.Y. 2015. Structural Analysis of the 14-3-3ζ/Chibby Interaction Involved in Wnt/B-catenin Signaling. Plos One, 10(4):e0123934.

Khan, H., Killoran, R.C., Brickenden, A., Fan, J., Yang, D. and Choy, W.Y. 2015. Molecular effects of cancer-associated somatic mutations on the structural and target recognition properties of Keap1. Biochemical Journal, 467(1):141-51

Cino, E.A., Killoran, R.C., Kartunnen, M., Choy, W.Y. 2013. Binding of disordered proteins to a protein hub. Nature Scientific Reports, 3:2305. doi: 10.1038/srep02305

AWARDS
Ontario Graduate Scholarship
2012, 2014, 2015

Western Graduate Research Scholarship
2011-2016

Principal's Scholarship, Queen's University
2007, 2008